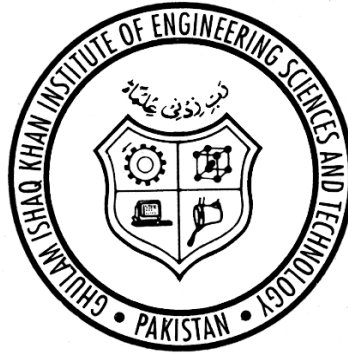


Study of β -decay half-lives measurement and microscopic calculations



Mavra Ishfaq

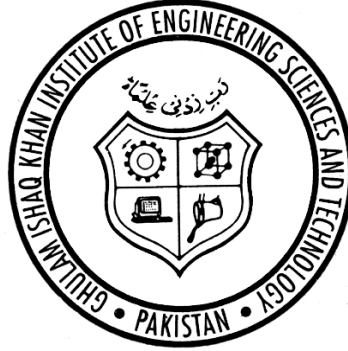
PhD Dissertation

Ghulam Ishaq Khan Institute of Engineering Sciences and Technology
Faculty of Engineering Sciences

March 2019

Study of β -decay half-lives measurement and microscopic calculations

PhD Dissertation



Mavra Ishfaq

ES-1517

In Partial Fulfillment
of the Requirements for the Degree of
Doctor of Philosophy (PhD) in
Engineering Sciences
(Computational Nuclear Astrophysics)

Ghulam Ishaq Khan Institute of Engineering Sciences and Technology

March 2019

Disclaimer

I hereby state that this dissertation is my own unique work and has not been submitted to any institution for assessment purpose. To the best of my knowledge, this dissertation contains no material previously published by other person expect for which the due acknowledgement has been made.

Mavra Ishfaq

March 2019

Author's Declaration

I Mavra Ishfaq hereby state that my PhD thesis titled "Study of β -decay half-lives measurement and microscopic calculations" is my own work and has not been submitted previously by me for taking any degree from Ghulam Ishaq Khan Institute of Engineering Sciences and Technology, or any where else in the country/World.

At any time if my statement is found to be incorrect even after my Graduate the University has the right to withdraw my PhD degree.

Mavra Ishfaq

March 2019

Plagiarism Undertaking

I solemnly declare that research work presented in the thesis titled "Study of β -decay half-lives measurement and microscopic calculations," is solely my research work with no significant contribution from any other person. Small contribution wherever taken has been duly acknowledged and that complete thesis has been written by me.

I understand the zero tolerance policy of the HEC and Ghulam Ishaq Khan Institute of Engineering Sciences and Technology, towards plagiarism. Therefore I as an Author of the above titled thesis declare that no portion of my thesis has been plagiarized and any material used as reference is properly cited.

I undertake that if I am found guilty of any formal plagiarism in the above titled thesis even after award of PhD degree, the University reserves the rights to revoke my PhD degree and that HEC and the University has the right to publish my name on the University Website on which names of students are placed who submitted plagiarized thesis.

Signature

Mavra Ishfaq

Certificate

It is certified that Ms. Mavra Ishfaq has completed her dissertation entitled "Study of β -decay half-lives measurement and microscopic calculations," under my supervision. This dissertation is found acceptable for the partial fulfilment of the requirements for the degree of Doctor of Philosophy (PhD) in Engineering Sciences (Computational Nuclear Astrophysics)

Signature

Dr. Jameel-Un Nabi (Supervisor)

Professor (Pro-Rector (Academics))

Faculty of Engineering Sciences

GIK Institute, Topi, Swabi

Certificate of Approval

This is to certify that the research work presented in this thesis, entitled "Study of β -decay half-lives measurement and microscopic calculations" was conducted by Miss. Mavra Ishfaq under the supervision of Prof. Dr. Jameel-Un Nabi. No part of this thesis has been submitted anywhere else for any other degree. This thesis is submitted to the Faculty of Engineering Sciences in partial fulfillment of the requirements for the degree of Doctor of Philosophy in Field of Computational Nuclear Astrophysics, Ghulam Ishaq Khan Institute of Engineering Sciences and Technology

Mavra Ishfaq

Signature: _____

Examination Committee:

External Examiner I

Signature: _____

External Examiner II

Signature: _____

Internal Examiner:

Signature: _____

Prof. Dr. Jameel-Un Nabi (Supervisor)

Signature: _____

Prof. Dr. Hassan Sayyad (Dean)

Signature: _____

Dedication

To The Almighty The Most Beneficent The Most Merciful

Acknowledgements

On the big day of my life, I want to thank all those who contributed in my success. First of all I am extremely grateful to Almighty Allah, for giving me the strength and perseverance to complete my Ph.D. studies. I would like to thank my supervisor, Prof. Dr. Jameel-Un Nabi (Pro-Rector Academics, GIKI), for proposing interesting thesis project and for his continuous support and enthusiasm toward it. I am grateful to him for expanding my knowledge of physics, both from the academic point of view, but surely also from a human perspective. During my research work, I found him wholehearted and helpful. I found him a very good supervisor and indomitable researcher. He made my debut in the Physics of the Heavens (stars) and the nucleus. Whenever I was in trouble he always suggest a wise solution. Without his kind support I was not able to finish this work.

I am thankful to Prof. Dr. M. Hassan Sayyad (Dean, FES), Prof. Dr. Ghulam Shabbir (Dean Graduate Studies), Prof. Dr. Habib-Ullah Jamal, Prof. Dr. Sirajul Haq, Prof. Dr. Irgaziev Bakhadir, Dr. M. Zahir Iqbal, Dr. Tahseen Amin, Dr. Muhammad Fayaz, and Dr. Muhammad Majid for their kind interaction and valuable suggestions during the course and research work. I am thankful to all the faculty members for their full cooperation in this regard. I will never forget the encouraging and sincere help of Mr. Munir Ahmed. He gave me a lot of suggestions and guidance during this work. I am also really indebted to Prof. Ismail Boztosun, Dr. Haris Djapo, Dr. Canel Eke (Akdeniz University, Antalya, Turkey), for their support, suggestions and collaborations for β decay half-life measurement during my foreign one year research stay at Akdeniz University, Turkey. I am also grateful to Prof. Sabin Stoica, Prof. Mihail Mirea and (Horia Hulubei Foundation, Magurele, Romania) for their fruitful discussions first for the calculations of Phase space factors and then half-life calculation.

All my love and thanks goes to my loving parents, my sweet sister Sobia Ashfaq (Principal GGHS, Muridke), beloved brothers Mr. Faiz-Ul Hassan (Elite Force) and Mr. Ali Faisal (CSP) for their prayers, sincere help, continuous motivation and bearing with me during

the challenges. I am also pleased for my friends and colleagues, especially Miss Zermina Shafique, Miss Farah Naz, Miss Nazia Nasr, Mr. Kabir, Mr. Kaleem, Mr. Muneem khan, Mr. Asim Ullah and Miss Huma for their encouragement and prayers. I am immensely grateful to all sincere friends for their support and prayers, which are a constant source of strength for me. Finally I acknowledge the GIK Institute for providing me platform to complete this studies, and financial support by Higher Education Commission (HEC), Pakistan for giving me fully funded scholarship for my Ph.D. studies. Thanks to Scientific and Technological Research Council of Turkey (TUBITAK) for one year research support in Turkey, also Pakistan Science Foundation (PSF) for providing grant for our joint project with TUBITAK Turkey, this was really a great award for me.

Mavra Ishfaq

March 2019

In the name of Allah, the most merciful and the most compassionate.

”He created the heavens and the earth with truth. He wraps the night around the day and wraps the day around the night, and has made the Sun and Moon subservient, each one running for a specified term. Is He not indeed the Almighty, the Endlessly Forgiving?”

Al-Quran (Surah Az-Zumar 5)

Contents

List of Tables	xv
List of Figures	xviii
List of Symbols and Abbreviations	xxii
Abstract	xxiii
1 Nuclear β-Decay	1
1.1 Introduction	1
1.2 Nucleon Decay	3
1.3 β -Decay	4
1.3.1 β^+ -Decay	5
1.3.2 β^- -Decay	5
1.3.3 <i>Electron Capture</i>	7
1.4 β -Decay Transition Types	7
1.4.1 <i>Fermi Transitions</i>	8
1.4.2 <i>Gamow-Teller Transitions</i>	8
1.5 Allowed and Forbidden Transitions	9
1.5.1 <i>Half-Lives, Reduced Transition Probabilities and ft Values</i>	9
1.5.2 <i>Matrix Elements for Fermi and Gamow-Teller Transitions</i>	11
1.5.3 <i>Phase Space Factors</i>	13
1.5.4 <i>Combined β^+ and Electron Capture Decays</i>	15

1.5.5	<i>Decay Q-Values</i>	16
1.5.6	<i>Partial and Total Decay Half-lives; Decay Branchings</i>	16
1.6	Rare Decay Modes	17
1.6.1	<i>Bound State β-Decay</i>	17
1.6.2	<i>Double β-Decay</i>	18
2	Photon Activation Analysis	19
2.1	Radiation Spectroscopy	21
2.1.1	<i>Photon Spectrometry</i>	21
2.1.2	<i>Scintillation Detectors</i>	22
2.1.3	<i>Semiconductor Detectors</i>	22
2.2	Basic Instrumentation for Photon Counting Electronics	23
2.2.1	<i>Nuclear Instrumentation Module</i>	25
2.2.2	<i>Preamplifier</i>	25
2.2.3	<i>Spectroscopy Amplifier</i>	26
2.2.4	<i>Pulse-Height Analyzer and Analog-To-Digital Converter</i>	27
2.2.5	<i>Multichannel Analyzer</i>	28
2.2.6	<i>High Voltage Power Supply</i>	29
2.2.7	<i>Digital Signal Processing</i>	29
2.3	Pulse-Height Spectrum	30
2.3.1	<i>Photoelectric Effect</i>	30
2.3.2	<i>Compton Scattering</i>	31
2.3.3	<i>Pair Production</i>	32
2.4	Principle Devices	34
2.4.1	<i>Clinical Linear Accelerator</i>	34
2.4.2	<i>High Purity Germanium Detector</i>	36
3	The pn-QRPA Theory and Formalism	38

3.1	Introduction	38
3.2	Assumptions and Model Formalism	40
3.3	Model Description and Parameters	40
3.4	Quasi-Particle Transitions	48
3.5	Extension of the pn-QRPA model	52
3.5.1	<i>Even Even Nuclei</i>	53
3.5.2	<i>Odd A Nuclei</i>	53
3.5.3	<i>Odd-Odd Nuclei</i>	55
3.6	Calculation of Stellar β -Decay and Positron Capture Rates	57
4	Analysis of β-Decay Half-life of ^{44}Sc	60
4.1	Introduction	60
4.2	Measurement of β -Decay Half-life	61
4.2.1	<i>Experiment</i>	62
4.3	Calculation of Half-life	64
4.4	Comparison between Measured and Calculated Results	69
4.5	Summary	75
5	Implications of pn-QRPA Model Parameters on β-Decay Half-lives	76
5.1	Implications of Pairing Correlations on Terrestrial Half-lives	76
5.1.1	<i>Terrestrial Half-lives Calculation for fp-Shell Nuclei</i>	78
5.1.2	<i>Pairing Gaps Effect on GT Strength, Terrestrial Half-lives</i>	80
5.2	Summary	84
5.3	Newly Calculated Phase Space Factor	85
5.3.1	<i>For β^+/Electron Capture-Decay</i>	86
5.3.2	<i>For β^--Decay</i>	98
5.4	β -Decay Half-life Calculation	108
5.4.1	<i>Parameters used for Calculation</i>	109

5.4.2	<i>Comparison between Measured and Calculated Half-lives</i>	110
5.5	Summary	114
5.6	Gamow-Teller Strength Distributions and Stellar Rates for ^{76}Ge , ^{82}Se	116
5.6.1	<i>Parameters used for the Calculation of Gamow-Teller Strength and Stellar Rates</i>	117
5.6.2	<i>Results and Discussion</i>	123
5.7	Summary	128
6	Summary, Conclusions and Future Work	129
6.1	Conclusions and Summary	129
6.2	Future Work	131
	Bibliography	132

List of Tables

4.1	Comparison of γ -ray energies obtained in the present measurement by average the results of before and after calibration with values found in the literature (NUDAT)	71
4.2	Measured half-life for this work (TW) with associated error in comparison with literature (NUDAT) half-life, error and calculated half-life using half-life . . .	73
4.3	Measured half-life for this work (TW) in comparison with literature (NUDAT) and calculated half-life using pn-QRPA	73
5.1	Measured [73] and pn-QRPA calculated half-lives using the $Emp-1$ and $Emp-2$ schemes. Half-lives are stated in units of s and pairing gaps in units of MeV	80
5.2	Comparison between pn-QRPA calculated Gamow-Teller strength distributions using different values of pairing gaps: $\Delta_{nn}^{(Emp-1)}$, $\Delta_{pp}^{(Emp-1)}$ and $\Delta_{nn,pp}^{(Emp-2)}$. Shown were the calculated pairing gaps (in MeV), total Gamow-Teller strength, centroid values and cut off energy (in MeV) using the pn-QRPA($Emp-1$) and pn-QRPA($Emp-2$) scheme for selected nuclei.	81
5.3	Comparison between experimental [73], pn-QRPA $^{(Emp-1)}$, pn-QRPA $^{(Emp-2)}$, FRDM model [89] and EQRPA model (with and without pn pairing) [79] calculated half-lives. Q_β values were taken from Ref. [73] and given in units of MeV . All half-lives were given in units of s	82

5.4	Calculated phase space of β^+ -decay (BP) compared with previous calculations. The value of maximum β -decay energy was taken from [108] for pure Fermi transitions. The last two columns show present calculated results.	89
5.5	Calculated phase space of β^+ -decay (BP) for heavy nuclei compared with the ones calculated by using recipe of [97].	90
5.6	State-by-state comparison of calculated PSF (for β^+ /EC-decay) using recipe of [97] and current prescription (TW). Shown also were the daughter energy levels, nuclear matrix elements NME, Q values, partial half-lives (PHL) for β^+ /EC-decay and branching ratio $I_{(\beta^+/EC)}$ of the selected nuclei.	92
5.7	Same as Table 5.6 but for ^{56}Ni depicting highest PD among all selected cases	92
5.8	Calculated phase space factors F_{EC} for electron capture (assuming exchange corrections to be equal to 1). The value of maximum β -decay energy was taken from [108] for pure Fermi transitions. The electron densities, their ratios, and the binding energies ϵ were also provided for the orbitals $1s_{1/2}$ and $2s_{1/2}$, including those given in [96]. Binding energies were given in units of keV . . .	97
5.9	Calculated phase space factors F_{EC} for electron capture, with Q -values from [107].	98
5.10	State-by-state comparison of calculated PSF (for β -decay) using recipe of [97] and current prescription (TW). Shown also were the daughter energy levels, nuclear matrix elements NME, Q values, partial half-lives (PHL) and branching ratio $I_{(\beta^-)}$ for β^- -decay of the selected nuclei.	104
5.11	Comparison of measured, calculated half-lives and percentage deviation (PD) for positron decay of selected nuclei.	111
5.12	Same as Table. 5.6 but for β^- -decaying nuclei.	112
5.13	Measured and calculated total GT strength and centroid values for ^{76}Ge and ^{82}Se along β -decay direction. For references see text.	123

5.14 Ratio of calculated positron capture to β -decay rates as a function of stellar temperature and density. 127

List of Figures

Chapter 1

1.1 β -stable nuclei in Z - N plane [2].	1
1.2 Nuclear β^- , β^+ and EC decay in the impulse approximation, where only one nucleon takes part in the weak decay process and the remaining A - 1 nucleons are spectators. The initial and final states Ψ_i and Ψ_f are nuclear A-body states with strong two-nucleon interactions. At the weak-interaction vertices the anti lepton lines are drawn as going backwards in time. The strength of the point like effective weak interaction vertex is given by the Fermi constant G_F [7]. . .	6
1.3 Number of emitted electrons as a function of the electron energy e for $E_0 = 6$. For β^\pm decay $Z = 20$; 'Z = 0' marks the case with the Fermi function omitted [7]	15

Chapter 2

2.1 NaI(Tl) and Ge spectrum of ^{133}Ba , ^{137}Cs and ^{60}Co [26]	23
2.2 Typical NIM-based electronic setup	25
2.3 Schematic of analog to digital conversion [29]	27
2.4 A typical MCA card [29]	29
2.5 DSP module (ORTEC)	30
2.6 The importance for these three major phenomenons at different gamma ray energies for different absorber material has been illustrated [32].	34

2.7	Depletion region generates in Ge crystal when applied to reverse biasing. Electron-hole pair are drawn away from junction resulting depletion of charge carriers [36].	36
2.8	Electronic block diagram of high resolution γ -ray spectrometry system [36] . .	37

Chapter 3

3.1	In a nucleus the nucleons distributions among single-particle orbits ; (a) with no pairing correlations (the simplest shell model), (b) with pairing correlations. (c) Ground-state wave function in pn-QRPA. The line connecting circles, which denotes q-p denotes angular momentum coupling of the proton-neutron pair. Both pairs have similar J^π spin-parity [45].	42
3.2	For parent nucleus containing odd nucleon, an example of (q-p) and QRPA phonon transitions. The (q-p) are represented by cross and phonons by an oval symbol with two crosses in it. (a) Transitions from the even-proton odd-neutron parent nucleus to the odd-proton even-neutron daughter nucleus. (b) Transitions from the ground-state of an odd.odd nucleus, which is described by a proton-neutron (q-p) pair state, to a two-proton (q-p) state in the even-even daughter nucleus [45].	50

Chapter 4

4.1	Philips SLI-25 clinical linear electron accelerator of Elekta TM Synergy. . . .	62
4.2	The diagrammatic view for creation of photon beam for the cLINAC employed in present experiment.	63
4.3	HPGe detector setup used in this work.	65
4.4	The functions used for fitting procedure during the analysis.	70
4.5	^{44}Sc spectrum without any subtraction which was irradiated for three days of counting. Labeled peaks were based on energy calibration.	71

4.6	Evolution of the spectra between ΔT time interval for the peak 271 keV of isomeric transition decay set (from 271 keV level) of ^{44}Sc	73
4.7	Evolution of the spectra between ΔT time interval for the peak 1157 keV of positron decay set (from ground state) of ^{44}Sc	74

Chapter 5

5.1	Dependence of pn-QRPA calculated half-lives on pairing gaps using the $Emp-1$ scheme for the three cases analyzed in previous works [41, 92]. The pairing gaps are given in units of MeV.	100
5.2	Same as Fig. 5.1 but employing $Emp-2$ scheme.	101
5.3	Calculated GT strength distributions for ^{46}Cr , ^{50}Fe and ^{54}Ni using pn-QRPA $^{(Emp-1)}$ and pn-QRPA $^{(Emp-2)}$ schemes.	102
5.4	Calculated Gamow-Teller strength distributions for ^{62}Zn , ^{66}Ge and ^{70}Se using pn-QRPA $^{(Emp-1)}$ and pn-QRPA $^{(Emp-2)}$ schemes.	103
5.5	Ratios R between experimental [107] and calculated half-lives undergoing β^+ decay for selected cases. Full lines: theoretical half-lives calculated within the (TW) recipe. Dotted lines: theoretical half-lives calculated with the (GM) recipe of Ref. [97].	114
5.6	Same as Fig. 5.5 but for selected β^- decay cases.	115
5.7	Present calculated cumulative $B(\text{GT}_-)$ distribution for the ground state of ^{76}Ge compared with experimental data [140] and the Ha and Cheoun [123] calculation.	121
5.8	Same as Fig. 1 but for ^{82}Se	122
5.9	This work calculated β -decay and positron capture rates for ^{76}Ge compared with other calculations as a function of stellar temperatures for a fixed stellar density $\rho = 10^{9.6} \text{ g cm}^{-3}$. For explanation of legends see text.	124
5.10	Same as Fig. 5.9 but for ^{82}Se	125

5.11 Same as Fig. 5.9 but as a function of stellar density at a fixed temperature of $T_9(\text{K}) = 10$	126
5.12 Same as Fig. 5.11 but for ^{82}Se	127

List of Symbols and Abbreviations

EC	Electron Capture
s-process	Slow Neutron Capture Process
r-process	Rapid Neutron Capture Process
p-process	Proton Capture Process
rp-process	Rapid Proton Capture Process
RPA	Random Phase Approximation
LSSM	Large Scale Shell Model
DQRPA	Deformed Quasiparticle Random Phase Approximation
pn-QRPA	Proton-Neutron Quasiparticle Random Phase Approximation
HFB	Hartree-Fock-Bogoliubov
BCS	Bardeen-Cooper-Schrieffer
GT Transitions	Gamow Teller Transitions
q-p	Quasi-Particle
p-p	Particle-Particle
p-h	Particle-Hole
p-n	Proton-Neutron
P_n	Probabilities of β -Delayed Neutron Emission

Abstract

Major processes (e.g. presupernova evolution in massive stars, supernova explosions, rp , r , s processes) taking place in astrophysical environment consists of unstable nuclei and decay spontaneously. There is a need to determine the accurate value of half-life of these unstable nuclei. The reliability of the half-life value is one of the key factors to calculate weak interaction rates in the stellar environment. Many experimentalists and theorists paid attention in this direction to perform reliable measurements as well as calculations. Present work is believed to contribute in this direction, to calculate half-life in more delicate and reliable manner, by implementing both approaches (experimental and theoretical model). The experimental part was performed at FEN Faculty, Physics Department Akdeniz University, Antalya Turkey.

The β decay half-life of ^{44}Sc was measured by photon activation analysis (PAA) and later calculated by proton neutron quasiparticle random phase approximation (pn-QRPA). As a result of this experiment, the obtained spectra were analyzed by MAESTRO and ROOT package. The photonuclear reaction is produced using a clinical linear accelerator (cLINAC) which generate bremsstrahlung photon beam to activate the desired sample. One aspect of this analysis is the comparison of measured results by PAA and those calculated by pn-QRPA. A decent comparison between measured and calculated results with literature value is established.

Accurate value of phase space factor (PSF) is a prerequisite for the calculation of half-life. In my second analysis I report a new recipe for the calculaton of PSF. This work is

being done in collaboration with the Romanian Collaborators (Horia Hulubei Foundation, Magurele, Romania). To obtain the electron/positron wave function, a code is developed by solving the Dirac equation with a nuclear potential derived from a realistic proton density distribution in the nucleus. For the electron capture (EC) process, it is found that the screening effect has a notable influence on the computed PSF values especially for light nuclei. Further the calculated PSFs are utilized for calculation of β -decay half-lives for fp -shell and heavier nuclei of astrophysical interest. This investigation also explores the improvement in calculated β -decay half-lives, using a given set of nuclear matrix elements, employing the recently introduced prescription for calculation of phase space factors PSFs.

The role of proton neutron residual interaction for the calculation of beta decay half-life is also explored. The proton neutron residual interaction is another important feature influencing the calculated β -decay half-lives and is studied in my third part of the work. Pairing gaps may have effect on calculated half-lives and is being studied in current investigation.

Gamow-Teller (GT) strength distribution may have implications on stellar weak rates and associated nucleosynthesis in stellar environment. GT strength for β -decay of medium mass nuclei for supernovae core collapse are calculated. The calculated GT strength distribution, stellar weak rates employing deformed pn-QRPA formalism in comparison with shell model and experimentally extracted GT strengths is presented.

It is expected that the current study of β -decay half-life measurement and developed theoretical techniques may contribute to a reliable estimation of half-life values both under terrestrial and stellar conditions. Consequently this work may contribute towards a better understanding of astrophysical processes.

List of Publications

- J.-U. Nabi and **M. Ishfaq**. "Gamow-Teller strength distributions and stellar weak interaction rates for ^{76}Ge and ^{82}Se using the deformed pn-QRPA model" *Astrophysics and Space Science* 2016, (2016) 361:245.
- S. Stoica, M. Mirea, O. Niuescu, J.-U Nabi and **M. Ishfaq**. "New Phase Space Calculations for β -Decay Half-Lives" *Advances in High Energy Physics*, 2016, Article ID 8729893.
- J.-U Nabi, **M. Ishfaq**, M. Boyukata, and M. Riaz. "Nuclear structure properties and stellar weak rates for ^{76}Se : Unblocking of the Gamow-Teller strength" *Nuclear Physics A* 966 (2017) 1-19.
- **M. Ishfaq**, J.-U Nabi, O. Niuescu, M. Mirea, and S. Stoica. "Study of the Effect of Newly Calculated Phase Space Factor on β -Decay Half-Lives" *Advances in High Energy Physics*, 2019, Article ID 5783618.
- **M. Ishfaq**, H. Djapo, C. Ertugay, I. Boztosun, J.-U. Nabi. "Study of half life measurement and Gamma-Transitions for ^{44}Sc using Photo-Nuclear Reaction" *ALKU Fen Bilimleri Dergisi* (2019): 117-124.
- **M. Ishfaq**, J.-U Nabi. "On the role of pairing correlations in calculation of β -decay half-lives within QRPA formalism" *Brazilian Journal of Physics*, Manuscript Number, BJPH-D-18-00636. (Under Review)
- **M. Ishfaq**, C. Eke, I. Boztosun, "A comparative study on the self attenuation correction factors by using HPGe and NaI(Tl) spectrometers" *International Journal of Sustainable Energy and Environmental Research*, 366-567-1-RV. (Under Review)
- C. Eke, **M. Ishfaq**, "Natural radionuclides activity concentrations and dose evaluations in tobacco samples", *International Journal of Environmental Science and Technology*, JEST-D-18-01650. (Under Review)

Chapter 1

Nuclear β -Decay

1.1 Introduction

A very narrow band of stable nuclei appeared on the Z-N plane is shown in Fig. 1.1. Rest occurred naturally unstable and becomes stable via various decay processes [1]. Such decays take place in the form of radioactivity by the emission of radiation i.e, α , β and γ radiations to become stable.

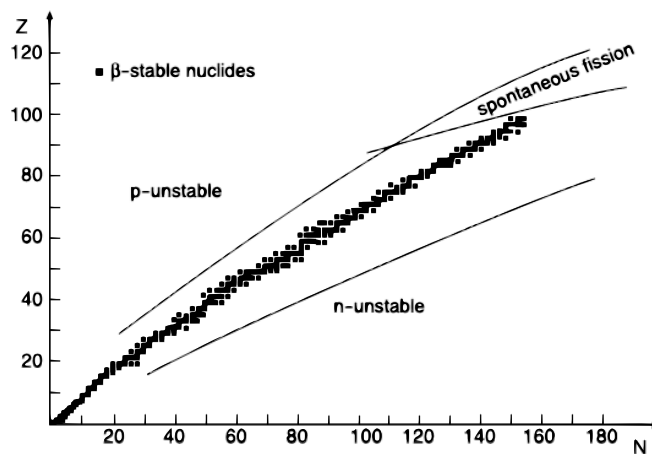


Figure 1.1: β -stable nuclei in Z - N plane [2].

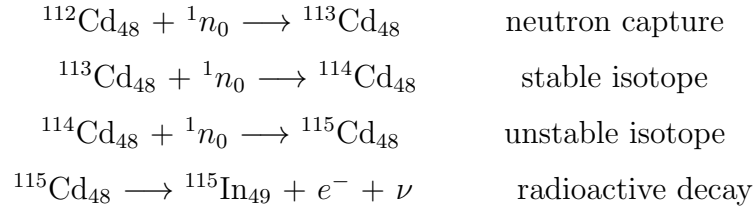
β -decay occurs within those sets of isobars (nuclei without change of mass number A

with the change in Z and N number) whose neighboring nucleus possess smaller masses [3]. One of the manifestations for radioactivity is due to weak interactions and associated decays occur due to the weak forces. Thus weak interactions are responsible for the β -decay, and considered to be lengthy decay time compared with the rapid proton capture process. The nucleonic composition comprised of "up and down quarks". Thus weak force allows the transformation of one type of quark to the other by the conversion of W boson. Which leads to the production of positron/neutrino or electron/antineutrino pair, familiar as β^+ and β^- -decay respectively. Majority of the nuclei subjected to the β -decay are supposed to be very lengthy i.e, of the range of thousands of years. Due to weak interactions these decays regulates the conversion of one nucleus to the other. The β -decays are believed to emit strong ionizing radiations.

Isotopes of Fe and Ni comprised of the paramount binding energy per nucleon and thus are the most stable nuclides. Due to large Coulomb repulsion, binding energy is smaller in heavy mass nuclei as compared with the lighter ones. The formation of heavy elements in stellar environment plays key role to understand the nucleosynthesis. In the mid of twentieth century, stellar nucleosynthesis and supernovae explosion were considered principle source of these elements [4]. Light elements like hydrogen, helium, deuterium, lithium were produced in the big bang nucleosynthesis. According to the big bang theory, temperature in the early universe was so high such that fusion reactions could possible easily. This results in the formation of following elements: hydrogen, deuterium, helium, lithium and trace amounts of beryllium. Every nuclear fusion converts hydrogen into helium in stellar core. Fusion reaction is the only reaction which takes place in stars less massive than Sun. In stars more massive than Sun but less massive than $8M_{\odot}$ further conversion reactions takes place in successive stages of stellar evolution. In very massive stars this chain of reaction continues till production of iron. Elements heavier than iron cannot be formed through fusion because extensive amount of energy is required. Majority of the elements heavier than iron originates from supernova. In supernova explosion neutron capture reaction takes place leading to form

heavy elements.

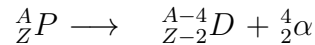
Elements heavier than iron formed by neutron capture and decays rapidly to the next isotope and some unstable elements decay by radioactivity such as,



Among all these reactions, last one denotes radioactivity. Which plays decisive role for the understanding of unstable nuclei of an element. Some common decay modes will be discussed in the following section.

1.2 Nucleon Decay

This decay takes place when parent nucleus emits a nucleon. Among various types of nucleon decay, α decay is one of the common decays in nature producing spontaneous fission. Other decay modes for nucleon emission includes neutron, proton emission, among all these decays neutron emission decay occurs rarely so having specific name as 'exotic decay modes'. The α decay will be discussed here shortly. In an α decay, a parent nucleus losses an α particle equals in weight of a helium nucleus, following is the equation explaining α decay,



Where ' P ' and ' D ' stands for parent and daughter nucleus respectively. Keeping aside some exceptions, it is quite evident that such phenomenon occurs only in regions of heavy masses ($A \simeq 150$), where Q -value for α emission becomes significantly positive [5].

$$Q_\alpha = (m_P - m_D - m_\alpha)c^2 = T_D + T_\alpha \quad (1.1)$$

Eq. (1.1) shows Q -value or binding energy relation between parent, daughter and emitted α particle, m stands for mass while T is the kinetic energy for the element. It is evident while studying α decay cases that penetration ability plays vital role on the decay rate of the nucleus. However, theoretical observation has been proved in favor of the observations concluded by Geiger-Nuttal law, which shows the relationship between experimental half-lives and unstable α nucleus.

$$\log T_{1/2} = a + \frac{b}{\sqrt{T_\alpha}}. \quad (1.2)$$

One can conclude from above relation that α half-lives are extremely sensitive to the T_α (kinetic energy of α particle).

1.3 β -Decay

In the era of nuclear physics nuclear β -decay plays vital role for the understanding of nuclear structural properties. In this section, we briefly describes about β -decay processes, its various types and associated phenomenon. Nuclear β -decay is a kind of radioactive decay. In such radioactive decay a fast energetic beta ray in the form of electron or positron releases from the atomic nucleus. Leading to charge changing transitions for transformation of one nucleus to another. As a by-product of this decay a neutrino or antineutrino are also released. The beta particle and antineutrino do not exist in the nucleus prior to the beta decay. These are created just as a result of such decaying processes.

The nuclear binding energy is related to the probability of an unstable nuclei to a particular decay mode. The β -decay deals with nucleon in nucleus resulting the conversion of one nucleus to the other because of weak interaction. This decay has following two types;

1.3.1 β^+ -Decay

The β^+ -decay also known as positron emission. We need to describe the phenomenon about weak interaction conversion of one nuclei to the other. In which atomic number decreases by one in the resulting element as compared with the decaying element, with the emission of a e^+ (positron) and an ν_e (electron neutrino). More evident from Eq. (1.3).

$${}^A_Z P_N \longrightarrow {}^A_{Z-1} D_{N+1} + e^+ + \nu_e + Q_{\beta^+}, \quad (1.3)$$

and

$$Q_{\beta^+} = M[{}^A_Z P] - (M[{}^A_{Z-1} D] + 2m_e c^2). \quad (1.4)$$

These decays occur generally in neutron deficient nuclei. Here Q_{β^+} is the Q -value for β^+ -decay. From Eq. (1.3) it is clear that in β^+ -decay, the conversion of a proton to neutron along creation of a e^+ (positron) and an ν_e (electron neutrino) takes place. As it is well known that the mass of neutron is greater than the proton which becomes hurdle for the β^+ -decay to occur in isolated proton because of large energy requirements. This decay can happen only when binding energy of resulting nucleus has larger binding energy than decaying nucleus. The difference of these energies utilizes for conversion of proton to neutron, positron, neutrino and their kinetic energies.

1.3.2 β^- -Decay

Unlike β^+ -decay, the nucleus converts into other possessing an increases in atomic number by one magnitude, with the emission of e^- (electron) and $\bar{\nu}_e$ (electron antineutrino). These decays mostly occur in proton deficient nuclei. The equation for β^- -decay is:

$${}^A_Z P_N \longrightarrow {}^A_{Z+1} D_{N-1} + e^- + \bar{\nu}_e + Q_{\beta^-} \quad (1.5)$$

Q_{β^-} is Q -value for this decay. Q -value can be described by the following relation,

$$Q_{\beta^-} = M[{}^A_Z P] - (M[{}^A_{Z+1} D]) \quad (1.6)$$

Eq. (1.5) explains β^- -decay process. Here A & Z , are atomic mass and atomic number respectively. This decay occurs due to the interconversion of negatively ionized down quark to the positively ionized up quark with emission of the W -boson; and W -boson consequently decays to e^- and $\bar{\nu}_e$ such,

$$d \longrightarrow u + e^- + \bar{\nu}_e \quad (1.7)$$

In these decays, the real element changes to a chemically altered element via a phenomenon known with the name of nuclear transmutation. In 1934 Fermi introduced a theory about β -decay known as Fermi's golden rule [6].

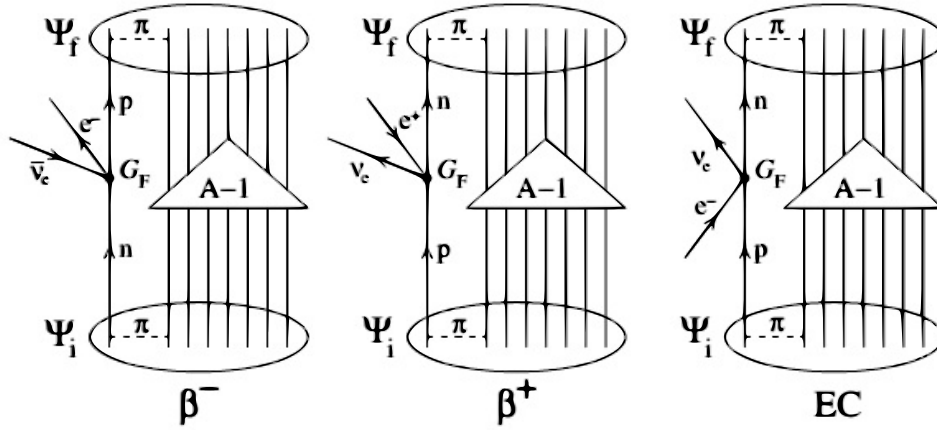
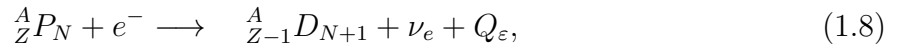


Figure 1.2: Nuclear β^- , β^+ and EC decay in the impulse approximation, where only one nucleon takes part in the weak decay process and the remaining $A - 1$ nucleons are spectators. The initial and final states Ψ_i and Ψ_f are nuclear A -body states with strong two-nucleon interactions. At the weak-interaction vertices the anti lepton lines are drawn as going backwards in time. The strength of the point like effective weak interaction vertex is given by the Fermi constant G_F [7].

1.3.3 *Electron Capture*

For the first time, theory about Electron Capture (EC) process was described by Gian-Carlo Wick, in (1934) and later developed by Hideki Yukawa and others. There is a strong possibility of β -decay to take place if mass of parent nucleus is greater than daughter nucleus. If energy difference of the decaying and resulting nuclei is smaller than $2m_0c^2$ (where m_0 is the rest mass of e^-), then the shell e^- (electron) captured by the nucleus might take place instead of the β^+ -decay [5]



and Q -value of the EC decay is given by following relation,

$$Q_\epsilon = (M_X - M_Y - B)c^2, \quad (1.9)$$

here B stands for the binding energy of devoured electron (e^-), which is usually an 'S' electron (e^-) coming from a tightly bound state (K or L). A secondary procedure happens just after the EC (like X-ray or Auger electron emission), stimulated due to the vacancy creation in the atomic shell.

1.4 β -Decay Transition Types

On the basis of J (angular momentum) and S (total spin) of emitted radiation β -decay could be further classified. Since the momentum conservation (total angular, orbital and spin angular momentum) is a vital condition for β -decay, it occurs through various quantum level transition to different values of J (nuclear angular momentum) or S (spin) states, and familiar with the name of Fermi and Gamow-Teller transitions. Which will be discussed in the succeeding section. When particles of an element bear ($J=0$) zero angular momentum, decay type will known as allowed otherwise forbidden. The rare decay modes are familiar

as double β -decay and bound state decay.

1.4.1 *Fermi Transitions*

The spin (S) of emitted particles S=0 are anti-parallel as a result of β -decay, are called Fermi decay [8]. Means decay process having zero units of orbital angular momentum with parallel spin known as allowed Fermi decay. So, no nuclear spin with $\Delta J = |J_i - J_f| = 0$ in Fermi decay. For non-relativistic limit of fermi transitions the nuclear part of the operator is as follows,

$$U_F = G_V \sum \tau_{\alpha\pm}. \quad (1.10)$$

Here G_V stands for weak vector coupling constant and τ_{\pm} for isospin raising and lowering operators and α runs for total neutrons & protons of a particular nucleus.

1.4.2 *Gamow-Teller Transitions*

When spin of emitted particles (as a result of β -decay process) say electron and antineutrino aligned parallel to one another $S=1$, in such situation system undergoes GT (Gamow-Teller) transition. For an allowed Gamow-Teller decay, the negatively charged electron and antineutrino carry unit 1 value for total angular momentum, hence J_i and J_f should be coupled through a vector bearing length 1: $\vec{J}_i = \vec{J}_f + \vec{1}$. It can be possible only when $\Delta J = 0$ or 1 (except for $J_i = 0$ and $J_f = 0$, in such condition only Fermi transition can take part [8]). For allowed Fermi transitions, the initial and final states followed an allowed GT (Gamow-Teller) decay have same parity. Following the condition $\Delta\pi = (-1)^J$, here (π) shows parity of the system. Nuclear part of such transitions could be explained by the following relation:

$$U_{GT} = G_A \sum \sigma_{\alpha} \tau_{\alpha\pm}. \quad (1.11)$$

In Gamow-Teller transitions G_A is weak axial vector coupling constant, σ denotes pauli spin matrices while other terms carry ordinary meanings.

1.5 Allowed and Forbidden Transitions

Allowed β -decay transitions are frequent occurring decay among all others. However, one more possibility while discussing β transitions for condition $\Delta J > 1$ or with the opposite parities for initial and final states, classified as forbidden transitions. To accomplish parity transition, the e^- and ν must be ejected with odd orbital angular momentum of the nucleus. Forbidden decays with limit $J = 1$ are known as First-Forbidden (FF) decays. Like allowed transitions, Fermi type decays also have, e^- and ν spin anti parallel to one another ($S=0$). For First Forbidden decays selection rules are $\Delta J = 0, 1, 2$.

Although the mechanism for β -decay is well understood, but it's very hard to generate a reasonable quantitative description about β -decay. Solution about quantum many body problem always be a challenge in almost every branch of physics. However, significant contribution has been made by using the concepts of proton-neutron quasiparticle random phase approximation (pn-QRPA) model, first introduced by Halbleib and Sorensen [9]. Charge changing transition like $(A, Z) \longrightarrow (N \mp 1, Z \pm 1)$ could introduced with the help of pn-QRPA model. Details about this model will be discussed in the succeeding chapters.

1.5.1 Half-Lives, Reduced Transition Probabilities and ft Values

The transition probability T_{fi} for β -decay can be calculated by the well known Fermi's golden rule about (time-dependent) perturbation theory. Half-life is correlated to it as

$$t_{1/2} = \frac{\ln 2}{T_{fi}}. \quad (1.12)$$

The resulting expression is given by

$$t_{1/2} = \frac{k}{f_0(B_F + B_{GT})}, \quad (1.13)$$

where the constant 'k' is [10]

$$k = \frac{2\pi^3 \hbar^7 \ln 2}{m_e^5 c^4 G_F^2} \quad (1.14)$$

integral for phase space (f_0) factor contains lepton kinematics, while B_F is Fermi and B_{GT} is GT (Gamow Teller) reduced transition probabilities. These transition probabilities could be broken into factors as

$$B_F = \frac{g_V^2}{2J_i + 1} |M_F|^2, \quad (1.15)$$

$$B_{GT} = \frac{g_A^2}{2J_i + 1} |M_{GT}|^2. \quad (1.16)$$

Here in Eqs. (1.15 and 1.16) angular momentum of the initial nuclear state is denoted by J_i , the term g is devoted for coupling constants while matrix elements are presented by M quantities. The term $f_0 t_{1/2}$ is known by ' ft ' value of an allowed β -decay transition. It relies significantly on the nuclear structure, which restrained with the reduced matrix elements. Also it had been symbolized with comparative half-life in literature [11] or by reduced half-life [12, 13]. The $g_V = 1.0$ factor is estimated value of vector coupling constant for weak interactions, estimated with the help of standard model's hypothesis CVC (conserved vector current). The $g_A = 1.25$ factor stands for axial-vector coupling constant for weak interactions, and the standard model hypothesis PCAC (partially conserved axial-vector current) has been employed to estimate its numerical value. In nuclei, the numerical value of g_A is affected by the many-nucleon correlations; a value after reduction 20-30 % is used sometimes. The free-nucleon value is accurate enough for current applications.

The parity, non-conserving nature in weak interactions has been reflected by the existence

of both the axial-vector and vector coupling constants in expression for half-life, Eq. (1.13). The axial-vector and vector parts contains opposite symmetry of space inversion, namely as (for axial-vector part) $A(-r) = +A(r)$ and (for vector part) $V(-r) = -V(r)$. In case of leptonic current the contravention about the parity conservation rule is maximal, and amplitudes of weak interaction from the contribution of leptons contain the following combination as $V - A$, a uniform dissection between the contributions from the vector and the axial-vector. The similar behavior occurs for the hadrons at quark level. In the case of hadronic current the contribution of axial-vector renormalizes because of colour forces between quarks, and combination $V - (g_A/g_V) A = V - 1.25 A$ is recovered. This structure of weak charged currents (vector-minus-axial-vector) is sign for the (left-handedness) about the weak interactions. Due to very large length of ft values these are generally demonstrated by $\log ft$ values, defined by

$$\log ft = \log_{10}(f_0 t_{1/2}[s]). \quad (1.17)$$

For the demonstration in logarithmic environment it is necessary to express the half-life (on right-hand side) as dimensionless quantity because of the dimensionless property of f_0 . Given the value for $\log ft$, the half-life could be defined as

$$t_{1/2} = \log^{\log ft - \log f_0} s \quad (1.18)$$

1.5.2 *Matrix Elements for Fermi and Gamow-Teller Transitions*

In the Eqs. (1.15 and 1.16) the transition probabilities possesses the matrix elements for Fermi as MF [6] and MGT for the GT (Gamow-Teller) transitions [14]. The nuclear wave functions for initial and final states in them carried the information about nuclear structure. In the operator sense, in case of Fermi is just 1 (unit operator) and for GT operator is σ (Pauli spin) operator. These are the simply scalar and axial-vector operators which could be established. Theoretically such operators could be extracted just as limiting expressions

of a proper relativistic treatment. For the representation of the occupation number, the Fermi and GT (NME) nuclear matrix elements could be written as

$$M_F = (\varepsilon_f J_f \parallel 1 \parallel \varepsilon_i J_i) = \delta_{j_i j_f} \sum_{ab} M_F(ab) (\varepsilon_f J_f \parallel [c_a^\dagger \tilde{c}_b]_0 \parallel \varepsilon_i J_i), \quad (1.19)$$

$$M_{GT} = (\varepsilon_f J_f \parallel \sigma \parallel \varepsilon_i J_i) = \sum_{ab} M_{GT}(ab) (\varepsilon_f J_f \parallel [c_a^\dagger \tilde{c}_b]_1 \parallel \varepsilon_i J_i), \quad (1.20)$$

where the reduced single-particle (ME) matrix elements are

$$M_F(ab) = (a \parallel 1 \parallel b) = \delta_{ab} \hat{j}_a = (n_a l_a j_a \parallel 1 \parallel n_b l_b j_b) = \delta_{n_a n_b} \delta_{l_a l_b} \delta_{j_a j_b} \hat{j}_a, \quad (1.21)$$

$$M_{GT}(ab) = \frac{1}{\sqrt{3}} (a \parallel \sigma \parallel b) = \frac{1}{\sqrt{3}} (n_a l_a j_a \parallel \sigma \parallel n_b l_b j_b) = \sqrt{2} \delta_{n_a n_b} \delta_{l_a l_b} \hat{j}_a \hat{j}_b (-1)^{l_a + j_a + \frac{3}{2}} \left\{ \begin{matrix} \frac{1}{2} & \frac{1}{2} & 1 \\ j_b & j_a & l_a \end{matrix} \right\}. \quad (1.22)$$

It could be noted that 'a' is proton index for β^- -decay while 'b' is a neutron index, whereas for (EC) electron capture and β^+ -decay 'a' acts as neutron index and consequently 'b' behaves like a proton index. For the single-particle matrix elements the symmetry properties are as follows

$$M_F(ba) = M_F(ab), \quad (1.23)$$

$$M_{GT}(ba) = (-1)^{j_a + j_b + 1} M_{GT}(ab). \quad (1.24)$$

The GT single-particle matrix elements are independent of n for $\Delta n = 0$ and they follows the selection rule $\Delta l = 0$.

1.5.3 Phase Space Factors

Half-Life in Eq. 1.13 carries the phase space factor (PSF) as integrated leptonic phase space, sometimes it is known as Fermi integral. The PSF for both types of β -decay (β^\pm) is,

$$f_0^\mp = \int_1^{E_0} F_0(\pm Z_f, \epsilon) p \epsilon (E_0 - \epsilon)^2 d\epsilon, \quad (1.25)$$

Term F_0 is known to be Fermi function

$$\epsilon \equiv \frac{E_e}{m_e c^2}, E_0 \equiv \frac{E_i - E_f}{m_e c^2}, p \equiv \sqrt{\epsilon^2 - 1}. \quad (1.26)$$

with emission of electron and positron the total energy is demonstrated by E_e , while energies for initial and final nuclear states are E_i and E_f . The PSF for (EC) is

$$f_0^{EC} = 2\pi \cdot (\alpha Z_i)^3 (\epsilon_0 + E_0)^2, \quad (1.27)$$

where

$$\epsilon_0 = \frac{m_e c^2 - \beta}{m_e c^2} \approx 1 - \frac{1}{2} (\alpha Z_i)^2. \quad (1.28)$$

The binding energy of electron in an atomic 1s orbital is symbolized by β while α is a fine-structure constant, $\alpha \approx \frac{1}{137}$.

It can be noted that Eq. 1.28 is basically not a good approximation because it assumes the simple non-relativistic s-electron wave function. The approximation is valid when $\alpha Z_i \ll 1$, and occurs for the light nuclei; $Z_i < 40$ is a thumb rule.

The additional improvements rises through the finite nuclear size and nuclear charge screening by the atomic electrons for low decay energies. The PSFs are the functions of nuclear energy difference (E_0) in Eqs. (1.25) and (1.27). The three-body state is the final state for β^\pm -decay. Its complex kinematics reflects in the intricate E_0 reliance of f^\pm , specifically shown in Eqs. (1.31). In the case of EC the final state is a two-body state, while

for emitted neutrino, momentum & energy conservation results in definite energy. Which is depicted in the simple PSF $f_{(EC)}$ with the parabolic dependence on E_0 . The Fermi function acts as correction factor which considers the Coulomb interaction between the final nucleus and the emitted lepton. In β^+ and β^- decay final state consists of daughter nucleus and two leptons. Because of the three-body state, thus the momentum and energy for final state leptons do not uniquely determine by the momentum and energy conservation. The number dn_e of e^- in an energy interval $(\epsilon, \epsilon + d\epsilon)$ divided by $d\epsilon$ as a function of the electron energy ϵ is given by

$$\frac{dn_e}{d\epsilon} = F_0(\pm Z_f, \epsilon) p \epsilon (E_0 - \epsilon)^2, \quad (1.29)$$

and is familiar by the shape function for allowed β -decay; and an integrand of Eq. (1.25). In a β -decay process the maximum energy E_0 of an electron is known as endpoint energy. In β^+ -decay positive nuclear charge accelerates the incoming negative electrons thus passing their energy distribution towards larger energies, and oppositely in β^- -decay. The Fermi function F_0 in Eq. (1.25) could be rewritten analytically in a nonrelativistic approximation familiar with the name of Primakoff-Rosen approximation [15]:

$$F_0(Z_f, \epsilon) \approx \frac{\epsilon}{p} F_0^{PR}(Z_f), \quad F_0^{PR}(Z_f) = \frac{2\pi\alpha Z_f}{1 - e^{-2\pi\alpha Z_f}}. \quad (1.30)$$

This approximation, is quite smart unless the Q -value of decay is very small. It directs to the PSF as

$$f_0^\mp \approx \frac{1}{30} (E_0^5 - 10E_0^2 + 15E_0 - 6) F_0^{PR}(\pm Z_f), \quad (1.31)$$

This expression is very easy to implement by using pocket calculators for the evaluations of β -decay half-lives.

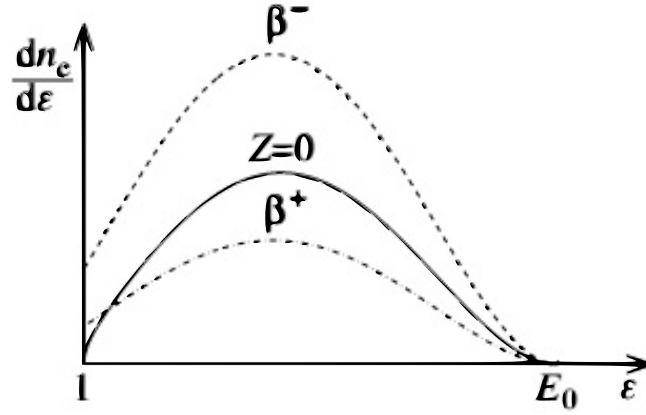


Figure 1.3: Number of emitted electrons as a function of the electron energy e for $E_0 = 6$. For β^\pm decay $Z = 20$; 'Z = 0' marks the case with the Fermi function omitted [7]

1.5.4 Combined β^+ and Electron Capture Decays

In both processes electron capture and β^+ -decay reduce the nuclear charge number by '1'. They could compete and co-exist in the de-excitation of the nuclear state. The combined effect of these modes could be obtained by the addition of the decay rates T_{fi} (probability of transition per unit time)

$$T_{fi}^+ = T_{fi}^{\beta^+} + T_{fi}^{EC}. \quad (1.32)$$

Following Eq. (1.12) leads that the total decay half-life of a combination of β^+ and (EC) transitions, denoted by β^+/EC is described by

$$f_0 t_{1/2} = [f_0^+ + f_0^{EC}] t_{1/2} = \frac{k}{B_F + B_{GT}}. \quad (1.33)$$

For energies $E_0 > 2$ the relation $f_0^+ \gg f_0^{EC}$ is valid, and half-life of a β^+/EC transition is determined by the β^+ -decay. Shortly, a full account about all allowed β -decay transitions is as follows

$$f_0 t_{1/2} = \frac{k}{B_F + B_{GT}}, f_0 = \begin{cases} f_0^- & \text{for } \beta^- \text{ decay,} \\ f_0^+ + f_0^{EC} & \text{for } \beta^+ / EC \text{ decay} \end{cases} \quad (1.34)$$

1.5.5 Decay Q -Values

The Q -value of nuclear β -decay has been introduced in previous sections (the total kinetic energy (K.E) of the final state leptons). These following useful links connects Q -value to the energy difference $\Delta E = E_i - E_f = E_0 m_e c^2$ of the initial and final nuclear states:

$$E_0 = \frac{Q_{\beta^-} + m_e c^2}{m_e c^2}, \quad (1.35)$$

$$E_0 = \frac{Q_{\beta^+} + m_e c^2}{m_e c^2} = \frac{Q_{EC} - m_e c^2}{m_e c^2}, \quad (1.36)$$

$$E_0 = \frac{Q_{EC} - m_e c^2}{m_e c^2}. \quad (1.37)$$

The β^+ endpoint energy is expressed in terms of $Q_{EC} = Q_{\beta^+} + 2m_e c^2$. An endpoint energy E_0 extracted from Eqs. (1.35), (1.36) and (1.37) could be employed in Eqs. (1.25), (1.27) or (1.31) for the computation of respective PSFs. A β -decay half-life could be then computed straightforwardly if the densities of one-body transition ($\varepsilon_f J_f \parallel [c_a^\dagger \tilde{c}_b]_{0,1} \parallel \varepsilon_i J_i$) are known.

1.5.6 Partial and Total Decay Half-lives; Decay Branchings

A nuclear state could undergoes β -decay to more than one final state. The transition probabilities are additive, as they are in electromagnetic decay. The β -decay probability to a given final state ' k ' corresponds to a partial decay half-life $t_{1/2}^k$. The total decay half-life $t_{1/2}$ is described by

$$\frac{1}{t_{1/2}} = \sum_k \frac{1}{t_{1/2}^k} \quad (1.38)$$

The partial half-life (PHL) is acquired from total half-life by employing the branching probability. It can be obtained from the measured decay branching by using the relation $B^{(k)} = (\text{experimental decay branching to final state 'k' in } \%) / 100$. The PHL is hence obtained by dividing the total half-life by the branching probability, i.e.

$$t_{1/2}^{(k)} = \frac{t_{1/2}}{B^{(k)}} \quad (1.39)$$

1.6 Rare Decay Modes

1.6.1 Bound State β -Decay

The process in which electrons fails to attain the necessary amount of energy (13.6 eV) to knock out the proton & as a result stay attached with the atom is called bound state β -decay. Only little number of neutrons decays (almost 4 over a million) hence known as "two body decays", also electron (e^-), proton (e^+) and antineutrino $\bar{\nu}_e$ are generated through this process [16].

The neutron decay energy is carried off by antineutrino in such beta decay process. In completely ionized atoms just like electrons (e^-) to fail from knock out and emitted through nucleus to the low lying atomic bound states. In case of neutral atoms it is prohibited to fully filled low lying bound states by (e^-) electrons. Bound state β -decay was first estimated by Daudel, Jean, and Lecoin in 1947 [17]. While Jung et al [18] first observed such incident in fully ionized atoms for $^{163}\text{Dy}^{66+}$ in (1992). The neutral atom of ^{163}Dy is stable and completely ionized $^{163}\text{Dy}^{66+}$ undergoes β -decay into the L and K shells with a half-life of 47 days. Other probability for completely ionized atom, undergoes greatly accelerated β -decay. Neutral atom of ^{187}Re undergo β -decay with a half-life of 42×10^9 years, but for completely

ionized $^{187}\text{Re}^{75+}$ value shortened from 10^9 to 32.9 years [19].

1.6.2 *Double β -Decay*

One type of the β -decay have characteristic of changing two units of charge in decaying element and known to be as double β -decay. Such process is complex decay and not easy to study because of very longer half life. The nuclei which could undergo both beta and double β -decay, the double β -decay process seems impossible to observe. While for nuclei in which β -decay is forbidden but double β -decay is allowed it can be observed by measuring half life [20]. Therefore, such decay could be studied only in β stable nuclei. Likewise in simple beta decay, 'A' number remains same. Generally in double β -decay two electrons and two antineutrinos are emitted. If ejected neutrinos are of the nature of own antiparticles (Majorana particles) this decay specified as neutrinoless double β -decay.

Chapter 2

Photon Activation Analysis

There are many analytical techniques in the field of nuclear physics among all others, activation analysis is the only one based on nuclear reaction. Radiations of very high energy are focused over the material of sample under investigation, and a nucleus in that sample might absorb these radiations partially. Therefore as a result of such absorption that nucleus is excited to higher energy state, and decays by emitting a photon or nuclear particle. In most cases the resulting nucleus is of radioactive nature and hence emission of delayed radiations takes place. Such radiations could be measured by employing suitable radiation detectors. With the help of assessment over detected particles count rate and energy, both types of analysis (quantitative and qualitative) could be performed for the sample material under investigation. To induce the activation process in the sample target, large number of neutral particles like (photons or neutrons) and also charged ones including heavy particles, deuterons, protons and tritons could be employed.

In almost all cases, from the reactors for nuclear research, thermal neutrons are employed for the activation procedure, and such method provides very high analytical sensitivity. The photonuclear reaction induced the photon activation in the target nucleus. Such activation inductions are supposed to occur at very high energies generally and must be 10 MeV or above not below than this limit. Elemental data about photonuclear reactions recommend

the activation energy of 30 MeV about the interfering reactions and analytical sensitivity. Which is the perfect energy by employing microtrons or high power linear accelerators (bremsstrahlung sources). The suitable parameters for irradiation are 30 MeV energy of electron at mean electron beam current of 100-150 μA . By the implementation of appropriate spectrometers say, high purity germanium detectors (HPGe) attached with complete suitable electronics system for the pulse processing, spectrum of emitted photon γ could be measured.

In 1934 Chadwick and Goldhaber [22] performed the photonuclear experiments for the first time in the history. By noticing the emission of radionuclides via process of photodisintegration when deuterium was bombarded by high energy γ rays (photons). The analytical application of photodisintegration makes photonactivation analysis an up to date method of activation over others like Neutron activation and activation with charged particles. The very first report over its analytical application with the help of γ induced photoactivation introduced in 1954 [23]. In the same year betatron application in PAA was also reported by Basile et al [24]. In the beginning for the radiation counting Geiger Muller (GM) counter were applicable. With the passage of time scintillation spectrometry replaced the GM counters usually by scintillator (Thallium activated, sodium iodide crystal) NaI(Tl). These scintillators are being used now a days for the identification of light elements like Carbon, Oxygen, Nitrogen and Fluorine etc.

Such spectrometers could be employed for the γ spectrometry and hence this was the beginning of the instrumental PAA. Since in the early 1960s, there was a dramatic development in the field of γ -ray spectroscopy when Ge based detectors along multichannel analyzer (MCA) were introduced. For the data processing purpose computer based system adjacent to whole setup was also familiar at that time. Large number of materials were investigated by the implementation of PAA technique because it is a complementary approach over neutron activation analysis (NAA). The principle devices for the implementation of PAA will be discussed briefly in the following sections.

2.1 Radiation Spectroscopy

Before the construction of energy discriminating devices, following the discrete measurements for analytes with the help of neutron detection or gas counters, the dissociation from the target sample of constituents was very important. After the invention of photon spectrometers and their availability such gadgets have been applied for the analysis by activation since many of the resulting nuclide from nuclear activation process ejects distinguished spectra of photons including X and γ radiations which could be discriminated very easily. Therefore analysis of the multielement type became easy and possible.

2.1.1 *Photon Spectrometry*

Two fundamental principles namely, detection through semiconductor crystals and by scintillators have been in practical use for counting photon. In both mentioned types for detection, photons are transformed to electric pulses whose heights are dependent quasi linearly on the absorbed quanta energies, in the range of (5-3000 keV) in PAA. The next step is then the amplification of pulses, reshaping and discrimination on the basis of their heights by employing electronic gadgets. Which will be discussed individually in the following parts. The processing regarding spectra are processes by a computer system. For summary, the mandatory parts for the activation analysis of the photon spectrometry are as follows:

1. Detector; Semiconductor crystal, scintillation crystal along photomultiplier, including voltage supply.
2. Preamplifier; Charge sensitive or voltage, plus power supply.
3. A spectroscopy amplifier; along pileup rejector, baseline restorer and shaping unit of pulse.
4. ADC; Analog-to-digital converter.
5. Pulse-height analyzer along data storage and data output unit, coupled with the data dumping device i.e, computer. Some other hardware setups are also required for specified

procedures only, but this was the basic instrumentation. At present time analog based electronics is being replaced by the digital systems. Signals are digitized from preamplifier directly in such systems. And the rest shaping processes for pulse are done with the help of digital processing algorithms.

2.1.2 *Scintillation Detectors*

During the fundamental processes like photoelectric effect, Compton scattering and pair production absorption of radiations with high energies results the production of light flashes due to generation of secondary electrons. Which is also familiar with the name of radio-luminescence measured and analyzed by the implementation of suitable detectors attached to monitor the pulse processing electronics. Hofstadter and McIntyre [25] revealed in their principle work about theory and practice of inorganic scintillators, that sodium iodide single crystal (thallium activated) were most suitable scintillators for the γ detection. Due to the absorption of γ photons or X rays flashes of light are generated. Such flashes are created photoelectrons in a photocathode. The electrons are run toward the photomultiplier connected with the operating voltage of 1 kV. The emission of secondary electrons are amplified and further processed to the electronic system of spectrometer. Until now for the analysis of light elements the scintillation detectors are being used.

2.1.3 *Semiconductor Detectors*

One of the major advantage of semiconductor detectors over scintillation crystals is their excellent power of spectral resolution, which is clear from Fig. 2.1. There are many materials tested regarding the high resolution but single crystal high purity germanium found superior over all others. Although cooling problem create complications for the handling of such detectors (mostly liquid nitrogen used) to address the cooling issue. For the first time development of lithium drifted germanium detectors with the help of drift process, was performed by different working groups in the early 1960s [27]. The working principle of

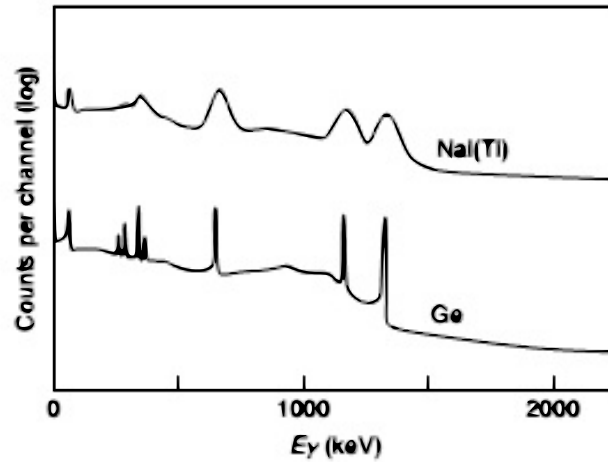


Figure 2.1: NaI(Tl) and Ge spectrum of ^{133}Ba , ^{137}Cs and ^{60}Co [26]

semiconductor detectors is comparable to proportional gas counter or ionization chamber.

Radiations are allowed to enter the single crystal generally germanium or silicon electrically isolated attached to an operating voltage. These radiation ejects photon and if these photons interact with detector material as a result of photoelectric effect and interaction processes the product electrons generate a great number of pairs of electrons and holes. Such generation of electron and hole pairs continue till the electrons lose whole of their energies and become unable for the creation of more charge carriers. The resulting pairs of charges rely exclusively on the incident radiation energy not on its kind. Hence for the case of scintillation detectors the height of the resulting pulse is proportional to the energy of the incident photon within the detector crystal.

2.2 Basic Instrumentation for Photon Counting Electronics

The fundamental parts for operation control electronic, data acquisition, signal processing includes detector connected with bias supply, preamplifier, spectroscopy amplifier, analog to digital converter (ADC) and pulse height analyzer with the single or multichannel operation.

Regarding the spectrometer performance, the premier cause for the deterioration are the noise of the electronic system and variability of pulse amplifying units. So, much attention needs to be paid over this issue. Further, the time in which a system processes only one signal becomes unable to accept other called dead time causes counting loss must be handled properly. For fixing the dead time issue there are various techniques at large count rates [28] but usually best scheme is to avoid to exceed specific count rate which relies over the integral performance of the spectrometer.

Such analog gadget components are handy and accessible in a number of different ways, enabling system to customize the particular needs of utility and depending upon available budget. For example, with basic capabilities low-end amplifiers are available but with demand from user about count rate or high resolution needs may refer to amplifiers having Pileup Rejection/ Live Time Correction (PUR/LTC) quality and both Gaussian, triangular shaping. Likewise ADC either be cheap Wilkinson ADC or speedy Fixed Dead Time (FDT) according to user's demand. In recent past Digital Signal Processor (DSP) substitute the analogue to digital converter (ADC) and amplifier devices with electronics having digital signal processing. The purpose of these electronic machines is to gather electrons originate from signal and processing the signals to categorize them on the base of height and energy. This complete process consist of these following steps. Production of electrons burst as a result of photon interaction with detector crystal. Bias voltage remove electrons from crystal. These electrons will generate current which results in the formation of signal pulse. Size of this signal could be increased with the help of preamplifier. Shape and intensity of the pulse is enhanced with amplifier. Conversion of pulse intensity into numerical value is performed by ADC. These numerical values then forwarded to MCA. To visualize and perform basic analysis of spectrum by using software for spectrum analysis a computer is also used.

2.2.1 *Nuclear Instrumentation Module*

The industry for nuclear electronics has standardized the power supply voltages, signal definitions and dimensions of fundamental nuclear instrumentation modules (NIM) started in 1960s. This standardization offers user capacity to exchange modules, flexibility to change modules, flexibility and reshaping or expansion of counting systems, with the change in counting applications and grow.



Figure 2.2: Typical NIM-based electronic setup

2.2.2 *Preamplifier*

Photons (produced as a result of irradiation) interact with detector crystal and as a result of this interaction created charge is collected by means of preamplifier. In addition it also provide match in between low impedance for coaxial cable to amplifier and high impedance of detector, which may be places at large distances from preamplifier. Recent Ge detectors are furnished with charge sensitive preamplifiers and RC-feedback. Having different operational modes: voltage, current, charge sensitive. In common practice charge-sensitive preamplifiers are employed. For increasing the performance preamplifier should be placed at or near the

detector. A produced output voltage pulse is proportional to input charge in charge-sensitive preamplifiers. When Coaxial Ge detector is employed for high throughput applications, transistor reset preamplifier (TRP) is preferred over RC feedback preamplifier. High cost for TRP is justified with high capacity of energy rate.

The basic role of preamplifier is modify the coupling of detector output to the rest of spectrometer. More it facilitates with the exact analog conversion of electrons burst, which produced as a result of radiation energy absorption in the detector, to a pulse which could be transmitted to the measurement system quite easily. The other job of preamplifier is about its pulse entrance unit, to reduce the noise sources, which could effect the energy resolution ability of the spectrometer significantly. In summary it is employed to obtain precise, reproducible, stable and undisturbed signal as output from the detector system.

2.2.3 *Spectroscopy Amplifier*

The primary purpose for amplifier is to change the output signal from the preamplifier to the most suitable form for the subsequent step of analog to digital (ADC) convert signal input.

Following are the key required features.

1. Amplification: for preamplifier the amplification level kept constant and the output level of spectroscopy for amplifier could be set as to regulate the energy range for processing.
2. Baseline restoring: For providing a reference level the baseline level of output for each pulse must be restored to analyze the pulse height and digitization.
3. Pulse shaping: Energy resolution system requires a quasi Gaussian shaped amplifier output signal with adjustable half width, for various reasons in a standard γ ray spectroscopy $4 \mu s$ is the ideal option. In order to avoid the interference of sequential pulses with the previous ones a pileup rejection system is introduced. The subsequent signals behaves inhibited automatically until the recovery of the output signal to baseline level. In short linear amplifiers in spectroscopic systems are utilized to transform the signals coming from

the preamplifier, perfect Gaussian shaped, free of noise signals whose heights should be proportional to the energy of photon incident to the detector. Such signals must arise over a stable and adjustable baseline.

2.2.4 *Pulse-Height Analyzer and Analog-To-Digital Converter*

In order to follow the radiations spectral distribution a pulse height discriminatory gadget is needed. These days its two types are being used, named as single channel analyzer (also known as differential pulse height discriminator), which is employed for the data output device trigger through signals whose heights fall within the adjustable channel (also known as window), between two pulse heights level, mostly employing an anti coincidence mechanism. While working by using Single channel analyzer, the signals from the outside of the channel are discarded.

The conversion module ADC considered as heart of gamma spectrometer. It changes the information gathered in analog format signal from pulse chain to digital form which can be saved and processed by computer. For every pulse in analog format collected by ADC, a number is produced which has direct relation with amplitude (height) of that signal.

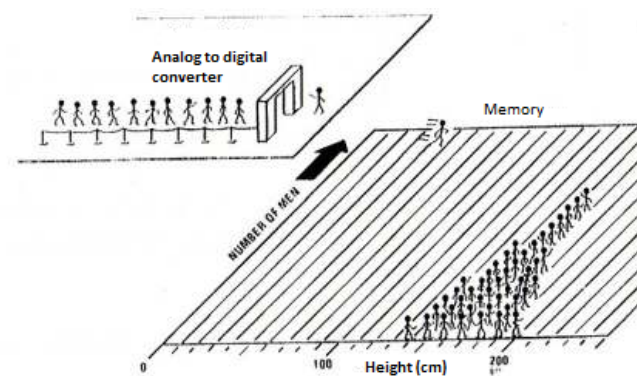


Figure 2.3: Schematic of analog to digital conversion [29]

Such devices are used for light elements (C, N, O, F) analysis for PAA.

In the case of more than one pulse height needs to be measured a multichannel analyzer system have to be employed. Which consists on following components;

1. Analog to digital converter (ADC) a device used for the quantizing and digitization which regulates every incoming signal along specific amplitude channel.
2. A memory device (data storage), to trace the pulses in number falling in each of the amplitude channels.
3. A device for the display which permits the immediate visual inspection of the data collected.
4. data output facility which have capability to allow instant processing of data, data storage of any carrier.

2.2.5 Multichannel Analyzer

Most important unit for experimental measurements is multichannel analyzer MCA. It works for some necessary functions of accumulating data, to furnish with visual monitor, creating output in final results form or for later analysis of data. It consists of basically ADC, memory, display and control logic. It collects information about all ranges voltage pulses at once and show this data with real time. The ADC counter number is variable and must be stored for later analysis, information about storage process is described in the following way: The ADC counter contents is employed as to recognize a counter of MCA. Contents are increased by "1" for this counter (or channel). In gamma ray spectroscopy a MCA containing 4096, 8192 or 16384 channels is employed. Every channel has ability to save minimum 106 pulses. Number of counts (or different channels contents) as a function of these channel numbers are known as pulse height spectrum for both digital or analogue representation. Acquisition modes for data analysis may be of following types: Pulse Height Analysis (PHA) Multi-input PHA. In PHA operating mode, series of pulses generated from radiation detector are applied to the input of MCA. Amplitudes of these pulses are proportional with the incident radiation energies which are absorbed by detector. A MCA employing multi-input

PHA permits simultaneous collection and reserving multiple spectra. With the help of Multiplexer it is generally accomplished and can be employed for applications of low count rate/low resolution counting. Every input of detector leads to the same ADC, but a separate unit of memory is chooses by routing bits. For less to medium count rates, multiplexer facilitate a cheap way to gather data from different detectors at same time.

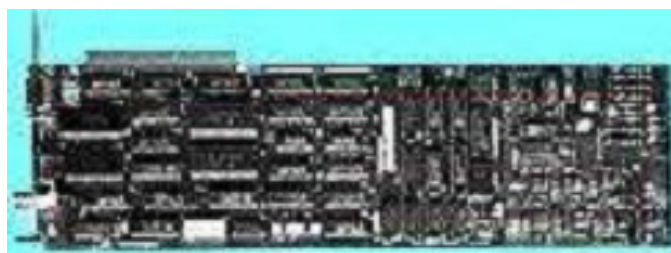


Figure 2.4: A typical MCA card [29]

Modern multichannel are integrated via standard PC, either through universal serial bus input, plug in card or through external unit connection. The number of channels are of choice generally starting with 2^8 to 2^{15} (256 to around 34000). The data range for output of ADC needs to be adjust accordingly.

2.2.6 High Voltage Power Supply

Power supply component with high voltage provides the mandatory high voltage to detector. And required voltages to other remaining units of the system. These components are commonly capable to provide upto 5000 V. Normally HPGe detectors needs about 3000 V.

2.2.7 Digital Signal Processing

Analog amplifiers for shaping and amplification is an old technology today Digital Signal Processing (DSP) is being applied for high performance based gamma spectrometers. So, with the use of this technology spectrum shaping functions are performing in digital domain

rather with analog approach. It filters and proceeds the pulses employing fast speed digital computations rather than utilization of time varying pulses of voltage in analog region.

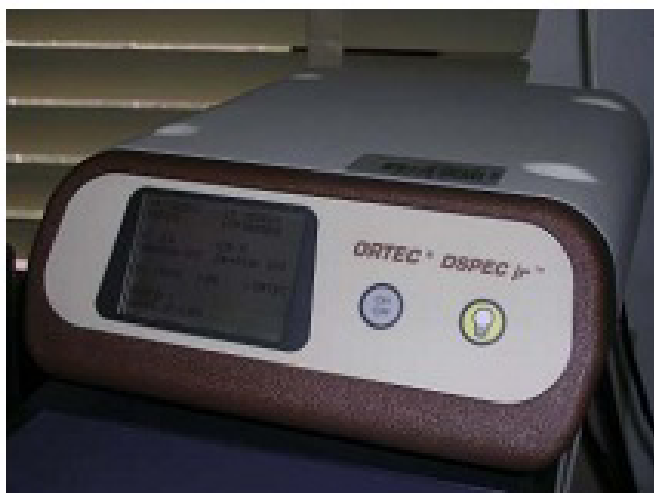


Figure 2.5: DSP module (ORTEC)

2.3 Pulse-Height Spectrum

For the detection of photons there are three fundamental processes which could be differentiate as,

(I) The photoelectric effect (II) The compton scattering (III) The pair production

Their occurrence probability depends on the incident photon energy for a particular element. Among all these three processes the photoelectric effect is one of the major interest while rest are considered as interference sources.

2.3.1 *Photoelectric Effect*

When photon interact with the atoms of material surface specifically with inner shell atomic electrons (K and L shells), in consequence photon itself vanishes by transferring its energy

to the ejected electron with kinetic energy E_e and behaves as free electron.

$$E_e = \hbar\nu - E_b \quad (2.1)$$

Here binding energy of the electron is shown by E_b , γ is for incident photon frequency while \hbar presenting Planck's constant. The emitted electrons energy must be equal to the difference between the incident photon energy and binding energy of the level from which the electron was emitted. Vacant position generated by the ejection of free electron is filled by other valence shell electron. Due to the difference in energy between two shells Auger electron or X-ray will be ejected. This effect is consider as extensive gamma ray interaction in low energy ($<200 \text{ keV}$) range. It is quite probable that a fraction of X rays will absconded from the detector. An important property of photoelectric effect is related to the monoenergetic photons, which could interact through photo process resulted the generation of the monoenergetic photoelectrons within the detector volume which results through various processes inside the detector in the form of discrete and uniform signal for further processing. Although there is a possibility that the signal might not be generated only by the single event of the photoelectric effect but also occurs if the total energy of the incident photon is absorbed by the detector body.

2.3.2 Compton Scattering

In this type of matter interaction a free electron collides with the gamma photon. The incident photon pass a part of its energy to free electron and scattered in different low energy angles by the partial loss of energy. Energy of gamma incident photon directly depends upon its scattering angle and can be described by the following relation,

$$E'_\gamma = \frac{E_\gamma}{1 + \frac{E_\gamma}{m_0c^2}(1 - \cos\theta)} \quad (2.2)$$

here E'_γ and E_γ stands for energies after and before the knocking respectively, m_0 showing

mass of free electron while c is speed of light in vacuum with scattering angle θ . So, rebounding electron's kinetic energy can be discuss by this relation [30,31].

$$E_e = E_\gamma - E'_\gamma \quad (2.3)$$

The lowest and highest energies for scattered photon can be obtained with angle of scattering as $\theta = \pi$ and 0 respectively. As photon energy grows high the cross section of compton scattering will decreases. With the increase in the available scattering electrons the compton scattering cross section is also increased.

The incident photon energy is distributed between the scattered photon and target electron. Such distribution have not a fix value but relatively ranges in large energy intervals. Hence, because of the broad energy distribution this process happens, which is the main reason that detector signals originating by compton scattering could not utilizes for the photon spectra evaluation.

2.3.3 *Pair Production*

The production of electron positron pair becomes possible when incoming incident photon energy exceeds the rest mass of this pair i.e 1022 keV . Such process occurs close to the nucleus neighborhood in the coulomb field. The incoming ray of photons vanishes after the production of the pair. The total energy equals the primary photon energy. Also the kinetic energy of the pair equals to the difference of total minus rest mass energy of the amount 1022 keV . Since the positron is not stable and an annihilation with the emission of two photons occur between two particles as enters the rest field of the electron. Thus in a detector interaction through pair process will, thus results in the form of loss of energy equals to the energy difference between incident photon energy and 1022 keV , in the case of escape of both annihilation quanta. In the case of single quanta escape the energy difference between incident photon and 511 keV appears. Signals other than sample measured activity are also occurs; which developed by external penetration into the shielding of the detector or from

impurities present within the shielding material. Such signals are known as background radiations. To maintain the accuracy and avoid the misinterpretations about the pulse height spectra these background radiations must be known very well.

Initially gamma rays with energies greater than 1022 keV can go for pair production [30]. As a result of such interaction incident photon vanishes and production of electron and positron pair takes place. This pair of particles share the energy of incident photon by following this relation.

$$E_e^- + E_e^+ = E_\gamma - 2m_0c^2 \quad (2.4)$$

in consequence of annihilation of positron with electron two photons with energy of 511 keV are created. Cross section or attenuation coefficient provides the knowledge about the emission of gamma ray photon from beam undergoing one interaction phenomenon among the three (photoelectric effect, Compton scattering and pair production) [30]. Linear attenuation coefficient is the sum of such probabilities for interaction per unit path length which is denoted as μ ;

$$\mu = \tau(\textit{Photoelectric}) + \sigma(\textit{Compton}) + \kappa(\textit{PairProduction}) \quad (2.5)$$

In Fig. 2.6 left hand side shows the energy at which chances of occurrence for photoelectric effect and compton scattering (as function of absorber atomic number) are equal. Photoelectric effect is dominant over the probability line and towards down or below of this line for compton scattering. On the other hand right hand side depicts the energy at which chances of occurrence of compton scattering and pair production are equal.

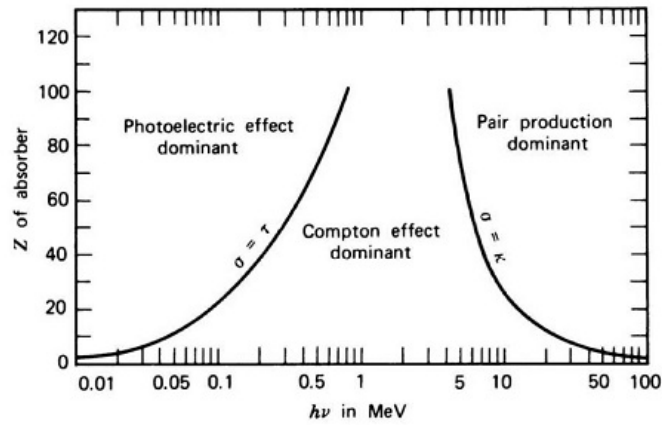


Figure 2.6: The importance for these three major phenomenons at different gamma ray energies for different absorber material has been illustrated [32].

2.4 Principle Devices

2.4.1 *Clinical Linear Accelerator*

Generally clinical linear accelerators are used for the radiation treatment of patients diagnosed with cancer but recent applications uses these cLINACs also for research purposes. Here in present work and experiment this device is one of the main and key instrument that has been used for irradiation purpose. The irradiation is interaction between radiation (energy) and matter as a result of such interaction ionization produced. Thus creation of such radiation utilizing some reliable gadgets like clinical LINAC is fascinating and provides a convenient way for research applications [33]. The generation of electron beam which we can also say as primary beam takes place in a gun known as electron gun with energy of 50 keV . In a cavity of copper these electrons are accelerated after their generation with radiofrequency (RF) of 3 GHz by peak power of 5 MW in pulse with pulse repetition frequency (PRF) of 200 Hz or 400 Hz . Direction and pivoting of electron beam is attained with the help of electrostatic and magnetic devices. Upon a heavy tungsten a target beam is transported using achromatic bending system.

At the target point beam of electrons is stopped with bremsstrahlung endpoint energy to generate primary electrons. The photon beam just after a primary collimator with thickness of 10 cm strike a flattening filter. Presence of collimators and filters made bremsstrahlung energy distribution quite complicated coming from linac. Emission process for bremsstrahlung is focused at forward angles. With the help of a package BEAMnrc simulation for photon energy distribution was performed originating from SLI-25. For flux estimation dose deliver rate 5 Gy/min [34] leading 5×10^5 using $E = 6 \text{ MeV}$ were employed. A delicate ionization chamber placed behind the flattening filter. Different parts of chamber are managed to handle the flatness and position of the beam. Due to high sensitivity of photon angular distribution on electron energy, inner and outer segments of ionization chamber's ratio are utilized to handle or control the primary electron beam energy. To control shape of photons beam a diaphragms system in X and Y direction permits to define rectangular fields having size maximum of $40 \times 40 \text{ cm}^2$ at nominal distance of $\text{SSD} = 100 \text{ cm}$. One of most important and key part of the cLINAC includes ionization chamber which is responsible for beam control system. Which restricts the target samples positioning in case of photoactivation experiments to larger distances more than 20 cm from point-like photon source. Typically primary electron beam has diameter less than 2 mm . Some components of cLINAC need to be removed in order to get such closest position otherwise this close position to the target is not accessible. A classical cLINAC has ability to supply beam of electrons at fixed energies. Via readjusting operational parameters for cLINAC an alteration can be possible in fixed pre-defined energy. The utilized cLINAC due to its digital working mode, by means of software program reloading actual parameters and pre-defined beams can be restored within seconds [35]. Time for irradiation is restricted by means of software from a maximum of 300 GY to 55 minutes. It can be possible to extend and shorten the irradiation time by setting manually restarting the beam.

2.4.2 High Purity Germanium Detector

In nuclear physics experiments gamma ray spectroscopy is being used with the help of high purity semiconductor detectors. Due to high efficiency of energy resolution these are employed to get information where it need to identify the gammas of nearby energy. These are more efficient in some specific range of energy and performance varies for different gamma-rays energy range. High energy resolution means gamma-rays associated peaks in an energy spectrum of interest should be separated or narrow as much as possible. To fulfill the requirement of high efficiency Ge crystal (in case of using germanium detector) in large size are employed. Typical size for large size Ge detector incudes cylinders having diameter of 7cm having 8cm length. Most commonly used high efficiency and high purity semiconductor detector are known as High Purity Germanium (HPGe) detector. Generally such detectors are used to deal with gamma ray spectroscopy. Germanium detectors are semiconductor diodes, consisting P-I-N structure means intrinsic region (which is very much sensitive for ionizing radiation) sandwiched between p and n type regions as shown in Fig. 2.7.

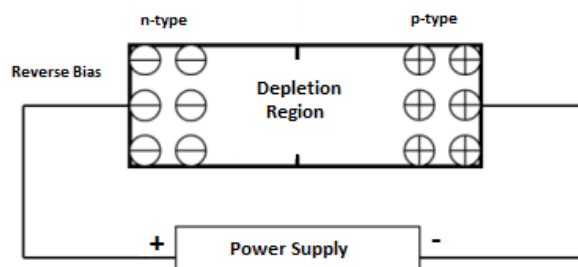


Figure 2.7: Depletion region generates in Ge crystal when applied to reverse biasing. Electron-hole pair are drawn away from junction resulting depletion of charge carriers [36].

When ionizing radiation induce ionization in semiconductor material, detector start to collect charges. As a result of the ionization production of electron-hole pair takes place. For the preparation and fabrication of Ge crystals with high purity, in case of impurities with accepting property, it will be mildly like p type otherwise n type [30, 37]. These

impurities are too low so we call it as intrinsic Germanium therefore mostly known as intrinsic semiconductor. Germanium treated as intrinsic semiconductor in HPGe, there is a huge vicinity for intrinsic Ge in the center surrounded through n-type and p-type semiconductor contacts.

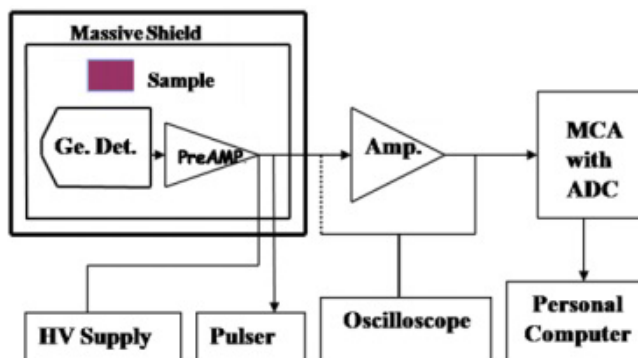


Figure 2.8: Electronic block diagram of high resolution γ -ray spectrometry system [36]

The PIN diode is employed to reverse biasing, under such biasing diode on the whole does not conduct. A photon getting into the intrinsic area generates an electron-hole pair. In present work p-type germanium detector is used and generally it can be made with boron implantation over germanium crystal. Due to the less band gap in germanium it is necessary to cool in order to decrease the heat production by charge carriers. Consequently the noise could effect resolution efficiency badly. To coup up this problem liquid nitrogen as cooling agent having 770 K temperature is employed. The overall performance of a detector relies upon on depth of its depletion region, which have inverse relation with concentration of impurity in detector material [36]. HPGe detector with its experimental setup and associated set up can be seen in Fig. 2.8

Chapter 3

The pn-QRPA Theory and Formalism

3.1 Introduction

Present project is based on both approaches theory and experiment for the measurement and calculations of half life. For the experimental part important instruments and principle devices has been discussed in the previous chapter. Theoretical work has been performed within the framework of proton neutron quasiparticle random phase approximation (pn-QRPA) model which will be described in present chapter. Different microscopic theories had been presented to grip the real idea about nuclear shape, structure, properties and core collapse in stellar environment. Two distinctive microscopic theoretical predictions, i.e, the (pn-QRPA) and nuclear shell-model are being used considerably for the β -decay half-lives, stellar weak rates and strength distribution calculations. Many from these theories have been evolved from independent particle model (IPM). In which nucleons are considered as non-interacting particles shifting in mean field generated by mean of all particles. Nucleons motion is supposed to occur in proper orbits having shell spaced with quantized energy with magnitude of $\hbar\omega=41A^{1/3}MeV$ confirming Pauli's Exclusion Principle. Nuclei having same proton and neutron number ($Z=N$) called doubly magic nuclei having fully complete levels, forming symmetric spherical core without angular momentum. Which means over this core

all levels are fully empty acting as no residual interaction, resulting no smearing in fermi surface. Therefore independent particle model (IPM) is so rigid in this respect to ensure the presence of minimum of one unpaired nucleon in one shell and one hole in the other shell. Thus shifting of nucleons to unoccupied level from occupied level set up correlations by the residual interaction, high energy is required for many particle and many hole excitations. That's why these excitations belong to very high temperature environment ($kT \sim 1MeV$).

Halbleib and Sorensen first introduced and developed the microscopic theory named as pn-QRPA which can deal with $1p - - 1h$, $2p - - 2h, \dots$, $np - - nh$ configurations. pn-QRPA proves it self a smart approach for the representation of charge changing transitions. It believes that due to Gamow-Teller (GT) separable force of spherical basis, allowed beta transitions take place. For GT strength function calculation, particle-hole (ph) interaction from GT force were introduced by the Halbleib and Sorensen, while particle-particle (pp) term has been taken into account by D. Cha [38]. As we know about two types of β decay, particle-particle (pp) interaction plays crucial role in case of β^+ decay [39, 40] and have minute impact in case of β^- decay [41].

Hamiltonian employed in QRPA formalism includes (pp) interaction through addition of schematic GT interaction. This hamiltonian when introduced for terrestrial conditions and input parameters yield good terrestrial half-lives. So, calculation in stellar environment for weak interaction rates and energy losses using this theory has been extended using QRPA approach and hence one can rely on terrestrial decay rates. This model proves itself more effective for calculation of those nuclei which lie far from stability at stellar conditions [42]. Study of such nuclei's is of crucial importance for astrophysical and cosmological research applications [43].

3.2 Assumptions and Model Formalism

Theoretical work needs some hypothesis taken from previous work or various theoretical approaches. For present work following are some assumptions to be considered.

1. In stellar environment very high temperature is considered and matter is in the form of plasma at this high temperature. Plasma matter consists on ionic particles and as a result positron and electron pairs produced following the Fermi Dirac (FD) statistics.
2. Only Gamow-Teller transitions are taken into account for present calculations, while forbidden contributions are assumed to be negligible.
3. For capture and decay rate calculation emission of neutron or proton from excited state taken under observation.
4. At stellar conditions with density of finite value absorption of neutrinos and anti-neutrinos is very small so will be considered to be negligible. Therefore these particles can escape freely with emission of energy.

3.3 Model Description and Parameters

The theory of mean field performs very well for doubly closed shell nuclei. The pairing correlation concept was considered in HartreeFock-Bogoliubov (HBF) theory for open shell nuclei. The production of long range field as well as short range pairing forces are dealt and the estimation of ground level wave function for a nuclei is also done. Short range pairing forces act as a vacuum for Bogoliubov quasi-particle (q-p) and are of deterministic structures. Basically these q.p are generalized as fermions. The linear combination of particle states and holes completely specifies these fermions therefore one can build the QRPA wave-function. To learn the collective states of a nuclei with open shell the QRPA provides a very convenient procedure. The Hamiltonian for pn-QRPA model is defined:

$$H^{QRPA} = H^{s.p} + V^{pair} + V_{GT}^{p.p} + V_{GT}^{p.h} \quad (3.1)$$

where $H^{s.p}$ are single particle Hamiltonian, V^{pair} pairing force, $V^{p.p}_{GT}$ particle-particle (p.p) GT force and $V^{p.h}_{GT}$ particle-hole (p.h) GT force respectively. The (p.p) force in quasi-particle transitions produce the phonon-correlation terms.

The wave function and associated single particle energy has been calculated by Nilsson model as well as nuclear deformation [44]. Transformation to deformed axial-symmetric basis from spherical nucleon basis is performed by following transformation relation

$$d_{m\alpha}^\dagger = \sum_j D_j^{m\alpha} c_{mj}^\dagger \quad (3.2)$$

as d^\dagger is the deformed operator of particle creation, c^\dagger is for creation operator, and $D_j^{m\alpha}$ is the transformation matrices with j as angular momentum and its specified z-component m . Nilsson eigen functions (obtained while Nilsson Hamiltonian diagonalization) could be described by such transformation matrices. Nilsson eigen states are located by m and additional quantum number as α [45]. Within the Nilsson basis BCS calculation is done by considering for proton and neutron systems separately.

The BCS approach has been employed for pairing process, In BCS approximation the pairing is described with strength. Here 'G' stands for strength interaction,

$$V^{pair} = -G \sum_{jmj'm'} (-1)^{L+j-m} c_{jm}^\dagger c_{j-m}^\dagger (-1)^{L'+j'-m'} c_{j'-m'} c_{j'm'} \quad (3.3)$$

the limitations are $m, m' > 0$, and orbital angular momentum (L). The energies ($\epsilon_{m\alpha}$) of quasi-particles (q-p) are calculated by the BCS theory.

The basis of (q-p) is described by

$$\alpha_{m\alpha}^\dagger = u_{m\alpha} d_{m\alpha}^\dagger - v_{m\alpha} d_{\bar{m}\alpha}, \quad (3.4)$$

$$\alpha_{\bar{m}\alpha}^\dagger = u_{m\alpha} d_{\bar{m}\alpha}^\dagger - v_{m\alpha} d_{m\alpha}, \quad (3.5)$$

where reverse state of time, for m is highlighted by \bar{m} , in Nilsson basis $d_{m\alpha}^\dagger$ and $d_{m\alpha}$ are

the creation or annihilation operators. The creation and annihilation operator for quasi-particles are α^\dagger and α which is used in the Random Phase Approximation equation. While u and v stand for amplitudes of occupation.

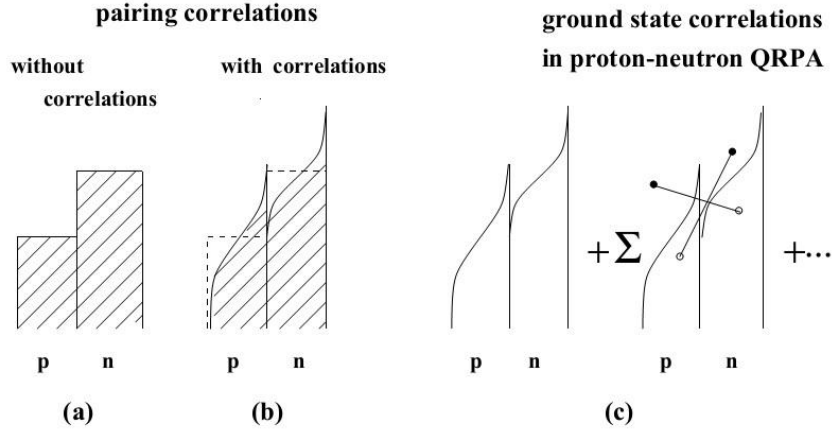


Figure 3.1: In a nucleus the nucleons distributions among single-particle orbits ; (a) with no pairing correlations (the simplest shell model), (b) with pairing correlations. (c) Ground-state wave function in pn-QRPA. The line connecting circles, which denotes q-p denotes angular momentum coupling of the proton-neutron pair. Both pairs have similar J^π spin-parity [45].

In orbits, the comparison of nucleon distributions is shown in the Fig. 3.1 without and with correlation. Orbits without correlations have three categories (Fig.3.1a), first the completely filled low occupied, other is near the Fermi energy which is technically half filled and third empty is the upper-laying orbit. On the other side in the (Fig.3.1b). Nucleons paired in according to $J^+ = 0^+$ while vacuum state is for quasi-particle (Fig.3.1c) shows wave function for ground state (Fig.3.1b) shows the wave function have no quasi particles in ground state is four-quasi particle mixture.

For description of charge-changing transitions, phonon creation plays key role in pn-QRPA model can be define in term of phonon creation, the phonon creation operator is defined by,

$$A_{\omega}^{\dagger}(\mu) = \sum_{pn} (X_{\omega}^{pn}(\mu) \alpha_p^{\dagger} \alpha_n^{\dagger} - Y_{\omega}^{pn}(\mu) \alpha_n^{\dagger} \alpha_p^{\dagger}) \quad (3.6)$$

Where subscripts n and p are used to specify $m_n \alpha_n$ and $m_p \alpha_p$ respectively. The phonon excitation energy (ω) is acquired as eigen-value in RPA equation. We take sum for the total pairs of proton and the neutron, with projection $\mu = m_p - m_n = -1, 0, 1$ and $m_{p(n)}$ represents component of the angular momentum. For q-p state of proton and neutron the creation operator is denoted by $\alpha_{p(n)}^{\dagger}$. The ground state level in pn-QRPA model is considered as vacuum for QRPA phonon, $A_{\omega}(\mu) |QRPA\rangle$. The well known random phase approximation equation in the form of matrix representation is given as

$$\begin{pmatrix} N & O \\ -O^* & -N^* \end{pmatrix} \begin{pmatrix} R \\ S \end{pmatrix} = \omega \begin{pmatrix} R \\ S \end{pmatrix} \quad (3.7)$$

here ω (the excitation energy), plays role of eigen value for QRPA state, R , and S are the forward and backward going amplitudes respectively. The terms N and O are for matrix elements of the QRPA given by,

$$\begin{aligned} N_{pn,p'n'} = & \delta(pn, p'n')(\epsilon_p + \epsilon_n) + V_{pn,p'n'}^{pp}(u_p u_n u_{p'} u_{n'} + v_p v_n v_{p'} v_{n'}) \\ & + V_{pn',p'n'}^{ph}(u_p v_n u_{p'} v_{n'} + v_p u_n v_{p'} u_{n'}) \end{aligned} \quad (3.8)$$

$$O_{pn,p'n'} = V_{pn,p'n'}^{pp}(u_p u_n v_{p'} v_{n'} + v_p v_n u_{p'} u_{n'}) - V_{pn,p'n'}^{ph}(u_p v_n v_{p'} u_{n'} + v_p u_n u_{p'} v_{n'}) \quad (3.9)$$

here the quasi particle energy of states linked with proton and neutron are indicated by ϵ_p (ϵ_n). The occupied and unoccupied amplitudes are v_k and u_k and are calculated by BCS calculation. The Y (back ward going amplitude) stands responsible for ground state correlation(GSC). The QRPA matrix is derived from GSC small correction. Where $|Y| \ll |X|$ not means that the ground state correlation are not under consideration. For

the calculation of matrix element of beta transitions the product of uvY and $u'v'X$ should be considered. If uv is greater than $u'v'$ then decay will be β^+ this doesn't neglect GSC. The eigen value equation for RPA can be solved by considering various projection values of μ for example $\mu = -1, 0$ and $+1$. The spectral eigenvalue of $\mu = -1$ and $\mu = 1$ are same while for the $\mu = 0$ the eigenvalue have two fold degeneracy because of axial symmetry employed in the Nilsson potential. In Random Phase Approximation two channels of interactions for proton and neutron are used such as particle-hole (p.h) and particle-particle (p.p) interaction, symbolized by χ and κ respectively. The χ and κ values may be applied by using optimal method. In β^- decay (p.p) interactions have non significant role [42,46,47] but for β^+ decay (p.p) interactions have significant part [48].

The (p.h) GT force is given by

$$V_{GT}^{p.h} = 2\chi \sum_{\mu} (-1)^{\mu} S_{\mu} S_{-\mu}^+ \quad (3.10)$$

where

$$S_{\mu} = \sum_{j_p m_p j_n m_n} \langle j_p m_p | t - \sigma_{\mu} | j_n m_n \rangle c_{j_p m_p}^+ c_{j_n m_n} \quad (3.11)$$

and the (p.p) GT force is given by

$$V_{GT}^{p.p} = -2\kappa \sum_{\mu} (-1)^{\mu} \mu_{\mu}^+ P_{-\mu} \quad (3.12)$$

where

$$P_{\mu}^+ = \sum_{j_p m_p j_n m_n} \langle j_n m_n | (t - \sigma_{\mu})^+ | j_p m_p \rangle (-1)^{l_n + j_n - m_n} c_{j_p m_p}^+ c_{j_n - m_n}^+ \quad (3.13)$$

The χ and κ represents interaction constant having positive values with units of MeV . The -ve sign of particle-particle force ($V^{p.p}$) shows that particle-particle force is attractive while ($V^{p.h}$) the particle-hole force is repulsive. Then matrix elements given in random phase

approximation separately are described as,

$$V_{pn,p'n'}^{p,h} = +2\chi f_{pn}(\mu) f_{p'n'}(\mu) \quad (3.14)$$

$$V_{pn,p'n'}^{p,p} = -2\kappa f_{pn}(\mu) f_{p'n'}(\mu) \quad (3.15)$$

where

$$f_{pn}(\mu) = \sum_{j_p j_n} D_{j_p}^{m_p \alpha_p} D_{j_n}^{m_n \alpha_n} \langle j_p m_p | t_{-\sigma_\mu} | j_n m_n \rangle \quad (3.16)$$

Which single particle GT transitions of Nilsson basis. For separable force the well RPA matrix Eq. 3.7 can be rewritten as,

$$R_\omega^{pn} = \frac{1}{\omega - \epsilon_{pn}} [2\chi(q_{pn} Z_\omega^- + \tilde{q}_{pn} Z_\omega^+) - 2\kappa(q_{pn}^U Z_\omega^{--} + q_{pn}^V Z_\omega^{++})] \quad (3.17)$$

$$S_\omega^{pn} = \frac{1}{\omega + \epsilon_{pn}} [2\chi(q_{pn} Z_\omega^+ + \tilde{q}_{pn} Z_\omega^-) + 2\kappa(q_{pn}^U Z_\omega^{++} + q_{pn}^V Z_\omega^{--})] \quad (3.18)$$

where $\epsilon_{pn} = \epsilon_p + \epsilon_n$, $q_{pn} = f_{pn} u_p v_n$, $q_{pn}^U = f_{pn} u_p u_n$, $\tilde{q}_{pn} = f_{pn} v_p u_n$, $q_{pn}^V = f_{pn} v_p v_n$

$$Z_\omega^- = \sum_{pn} (R_\omega^{pn} q_{pn} - S_\omega^{pn} \tilde{q}_{pn}) \quad (3.19)$$

$$Z_\omega^+ = \sum_{pn} (R_\omega^{pn} \tilde{q}_{pn} - S_\omega^{pn} q_{pn}) \quad (3.20)$$

$$Z_\omega^{--} = \sum_{pn} (R_\omega^{pn} q_{pn}^U + S_\omega^{pn} q_{pn}^V) \quad (3.21)$$

$$Z_\omega^{++} = \sum_{pn} (R_\omega^{pn} q_{pn}^V + S_\omega^{pn} q_{pn}^U) \quad (3.22)$$

with insertion of Eq. 3.17 and Eq. 3.18 in Eq. 3.19 and Eq. 3.22 directs the exclusion of terms R_ω^{pn} and S_ω^{pn} which depends explicitly on single proton and neutron quasi-particle pairs separately. Hence, a bunch of equations is obtained for each Z^+ , Z^- , Z^{--} and Z^{++} ,

that are similar to Eq. 3.7,

$$Mz = 0 \quad (3.23)$$

here

$$M = \begin{bmatrix} \chi M_1 - 1 & \chi M_0 & -\kappa M_5 & -\kappa M_7 \\ \chi M_0 & \chi M_2 - 1 & -\kappa M_8 & -\kappa M_6 \\ \chi M_5 & \chi M_8 & -\kappa M_3 - 1 & -\kappa M_0 \\ \chi M_7 & \chi M_6 & -\kappa M_0 & -\kappa M_4 - 1 \end{bmatrix} \quad (3.24)$$

$$Z = \begin{bmatrix} Z_{\omega}^{-} \\ Z_{\omega}^{+} \\ Z_{\omega}^{--} \\ Z_{\omega}^{++} \end{bmatrix} \quad (3.25)$$

and

$$\begin{aligned}
M_0 &= 2 \sum_{pn} \left(\frac{q_{pn} \tilde{q}_{pn}}{\omega - \epsilon_{pn}} - \frac{q_{pn} \tilde{q}_{pn}}{\omega + \epsilon_{pn}} \right) \\
&= 2 \sum_{pn} \left(\frac{q_{pn}^U q_{pn}^V}{\omega - \epsilon_{pn}} - \frac{q_{pn}^U q_{pn}^V}{\omega + \epsilon_{pn}} \right) \\
M_1 &= 2 \sum_{pn} \left(\frac{q_{pn}^2}{\omega - \epsilon_{pn}} - \frac{\tilde{q}_{pn}^2}{\omega + \epsilon_{pn}} \right) \\
M_2 &= 2 \sum_{pn} \left(\frac{\tilde{q}_{pn}^2}{\omega - \epsilon_{pn}} - \frac{q_{pn}^2}{\omega + \epsilon_{pn}} \right) \\
M_3 &= 2 \sum_{pn} \left(\frac{q_{pn}^{U^2}}{\omega - \epsilon_{pn}} - \frac{q_{pn}^{V^2}}{\omega + \epsilon_{pn}} \right) \\
M_4 &= 2 \sum_{pn} \left(\frac{q_{pn}^{V^2}}{\omega - \epsilon_{pn}} - \frac{q_{pn}^{U^2}}{\omega + \epsilon_{pn}} \right) \\
M_5 &= 2 \sum_{pn} \left(\frac{q_{pn} q_{pn}^U}{\omega - \epsilon_{pn}} - \frac{\tilde{q}_{pn} q_{pn}^V}{\omega + \epsilon_{pn}} \right) \\
M_6 &= 2 \sum_{pn} \left(\frac{\tilde{q}_{pn} q_{pn}^V}{\omega - \epsilon_{pn}} - \frac{q_{pn} q_{pn}^U}{\omega + \epsilon_{pn}} \right) \\
M_7 &= 2 \sum_{pn} \left(\frac{q_{pn} q_{pn}^V}{\omega - \epsilon_{pn}} - \frac{\tilde{q}_{pn} q_{pn}^U}{\omega + \epsilon_{pn}} \right) \\
M_8 &= 2 \sum_{pn} \left(\frac{\tilde{q}_{pn} q_{pn}^U}{\omega - \epsilon_{pn}} - \frac{q_{pn} q_{pn}^V}{\omega + \epsilon_{pn}} \right)
\end{aligned} \tag{3.26}$$

Taking determinant of M matrix=0 we get the solution of the Eq. 3.23

$$|M| = 0 \tag{3.27}$$

about the M_k ($k = 0$ to 8) is energy dependant function (ω). Now applying the Eq. 3.7 for finding the roots of Eq. 3.27. For (p.p) and no (p.p) force ($k \neq 0$) the Eq. 3.27 can be simplified to obtain the 2nd and 4th order equations in terms of M_k respectively. The detail

of such relations could be find in [49].

For every value of ω , GT transition amplitudes to Random Phase Approximation eigenfunctions are as follows. N_ω^- , N_ω^+ , N_ω^{--} , and N_ω^{++} are co-determinants of M respectively at energy ω . With the solution of determinant M w.r.t first row expansion these co-determinants values could be obtained as,

$$\det M = (\chi M_1 - 1)N^- + \chi M_0 N^+ - \kappa M_5 N^{--} - \kappa M_7 N^{++} \quad (3.28)$$

hence Z_ω 's ratios are calculated by

$$\frac{Z_\omega^-}{N_\omega^-} = \frac{Z_\omega^+}{N_\omega^+} = \frac{Z_\omega^{--}}{N_\omega^{--}} = \frac{Z_\omega^{++}}{N_\omega^{++}} \quad (3.29)$$

The normalization condition for amplitudes of phonon are used to find the absolute values,

$$\sum_{pn} [(R_\omega^{pn})^2 - (S_\omega^{pn})^2] = 1 \quad (3.30)$$

by inserting the Z_ω 's in Eq. 3.17 and Eq. 3.18. The amplitudes for the GT strength transitions from the QRPA g.s is $|-\rangle$ (for vacuum $N_\omega(\mu) |-\rangle = 0$). Similarly for single phonon orbits $|\omega, \mu\rangle = N_\omega^+(\mu) |-\rangle$ can be calculated easily.

$$\langle \omega, \mu | t_\pm \sigma(\mu) |-\rangle = \mp Z_\omega^\pm \quad (3.31)$$

For single phonon states, the excitation energies are $\omega - (\epsilon_p + \epsilon_n)$, ϵ_p and ϵ_n are the energies for proton and neutron orbits respectively in a (q-p) system.

3.4 Quasi-Particle Transitions

From Random Phase Approximation we can calculate the excitation of even-even nuclei at ground-state $J^\pi = 0^+$ for even-even nuclei. The ground-state may be termed as one quasi-particle state if nucleons are odd in number of parent nuclei. So two types of transitions are

considered, phonon transition and quasi-particle transition. Such transitions are described by the equations,

$$\begin{aligned} |p_{corr}\rangle &= \alpha_p^\dagger |-\rangle + \sum_{n,\omega} \alpha_n^\dagger N_\omega^\dagger(\mu) |-\rangle \langle - | [\alpha_n^\dagger N_\omega^\dagger(\mu)]^\dagger H_{31} \alpha_p^\dagger |-\rangle E_p(n, \omega) \\ |n_{corr}\rangle &= \alpha_n^\dagger |-\rangle + \sum_{p,\omega} \alpha_p^\dagger N_\omega^\dagger(-\mu) |-\rangle \langle - | [\alpha_p^\dagger N_\omega^\dagger(-\mu)]^\dagger H_{31} \alpha_n^\dagger |-\rangle E_n(p, \omega) \end{aligned} \quad (3.32)$$

also with

$$E_\alpha(b, \omega) = \frac{1}{\epsilon_a - \epsilon_b - \omega} \quad (3.33)$$

The Eq. 3.32 has two parts, first part outline the nucleons quasi particle state while second part depicts the hamiltonian H_{31} of phonon coupling which is the mixture of random phase approximation correlation of quasi-particles [50]. The final relation for amplitudes of GT transition is given in terms of separable forces and can be represented as

$$\begin{aligned} \langle p_{corr} | t_- \sigma_\mu | n_{corr} \rangle &= q_{pn}^U + 2\chi [q_{pn}^U \sum_{\omega} ((Z_\omega^{-2}) E_p(n, \omega) + Z_\omega^{+2} E_n(p, \omega)) \\ &- q_{pn}^V \sum_{\omega} Z_\omega^- Z_\omega^+ (E_p(n, \omega) + E_n(p, \omega))] + 2\kappa [q_{pn} \sum_{\omega} (Z_\omega^- Z_\omega^{--} E_p(n, \omega) - Z_\omega^+ Z_\omega^{++} E_n(p, \omega)) \\ &- \tilde{q}_{pn} \sum_{\omega} Z_\omega^- Z_\omega^{++} (E_p(n, \omega) - Z_\omega^+ Z_\omega^{++} E_n(p, \omega))] \end{aligned} \quad (3.34)$$

$$\begin{aligned} \langle p_{corr} | t_+ \sigma_\mu | n_{corr} \rangle &= q_{pn}^V + 2\chi [q_{pn}^V \sum_{\omega} (Z_\omega^{+2} E_p(n, \omega) + Z_\omega^{-2} E_n(p, \omega)) \\ &- q_{pn}^U \sum_{\omega} Z_\omega^- Z_\omega^+ (E_p(n, \omega) + E_n(p, \omega))] + 2\kappa [\tilde{q}_{pn} \sum_{\omega} (Z_\omega^+ Z_\omega^{++} E_p(n, \omega) \\ &- Z_\omega^- Z_\omega^{--} E_n(p, \omega)) - q_{pn} \sum_{\omega} Z_\omega^+ Z_\omega^{--} E_p(n, \omega) - Z_\omega^- Z_\omega^{++} E_n(p, \omega)] \end{aligned} \quad (3.35)$$

and

$$\langle n_{corr} | t_\pm \sigma_{-\mu} | p_{corr} \rangle = (-1)^\mu \langle p_{corr} | t_\mp \sigma_\mu | n_{corr} \rangle \quad (3.36)$$

The phonon and (q-p) odd-neutron parent nuclear transitions are given in Fig. 3.2.

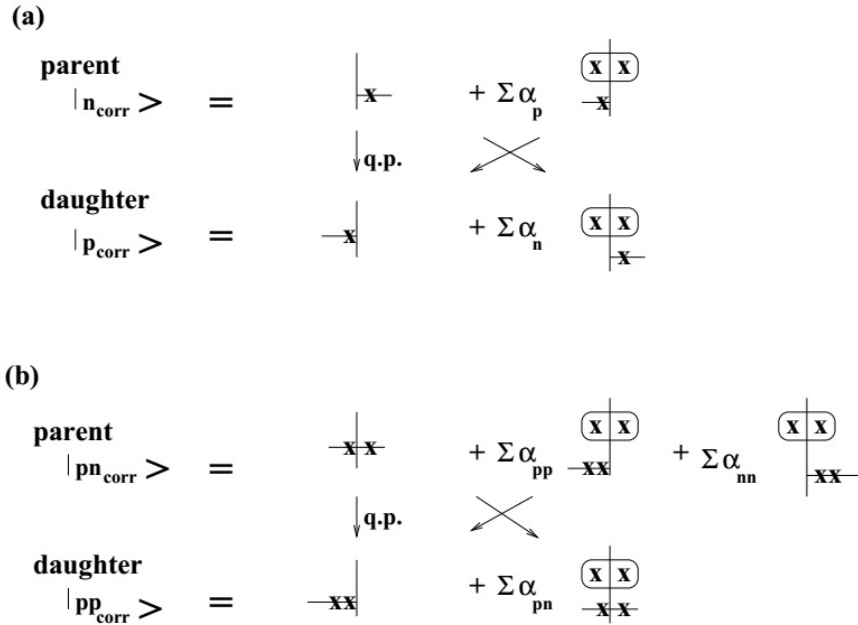


Figure 3.2: For parent nucleus containing odd nucleon, an example of (q-p) and QRPA phonon transitions. The (q-p) are represented by cross and phonons by an oval symbol with two crosses in it. (a) Transitions from the even-proton odd-neutron parent nucleus to the odd-proton even-neutron daughter nucleus. (b) Transitions from the ground-state of an odd-odd nucleus, which is described by a proton-neutron (q-p) pair state, to a two-proton (q-p) state in the even-even daughter nucleus [45].

The (q-p) transition scheme considering the 1st order correlation could be extended for the parent nuclei having odd number of proton and neutron [42, 50]. Schematically it has been shown in the Fig. 3.2. The ground-state is to be consider as proton-neutron quasi-particle pair state having small energy. The GT transitions of quasi-particle in the even-even daughter nucleus leads to quasi-particle state of two protons or two neutrons. The two

quasi-particle states are generated via phonon correlations in the 1st order perturbation.

$$\begin{aligned}
|pn_{corr}\rangle &= \alpha_p^+ \alpha_n^+ |-\rangle + \frac{1}{2} \sum_{p_1 p_2'} \alpha_{p_1}^+ \alpha_{p_2'}^+ N_\omega^+(-\mu) |-\rangle \langle - | [\alpha_{p_1}^+ \alpha_{p_2'}^+ N_\omega^+(-\mu)]^+ \\
H_{31} \alpha_p^+ \alpha_n^+ |-\rangle E_{pn}(p_1 p_2', \omega) &+ \frac{1}{2} \sum_{n_1 n_2'} \alpha_{n_1}^+ \alpha_{n_2'}^+ N_\omega^+(\mu) |-\rangle \langle - | [\alpha_{n_1}^+ \alpha_{n_2'}^+ N_\omega^+(\mu)]^+ \\
&H_{31} \alpha_p^+ \alpha_n^+ |-\rangle E_{pn}(n_1 n_2', \omega)
\end{aligned} \tag{3.37}$$

$$\begin{aligned}
|p_1 p_2 corr\rangle &= \alpha_{p_1}^+ \alpha_{p_2}^+ |-\rangle + \sum_{p' n'} \alpha_{p'}^+ \alpha_{n'}^+ N_\omega^+(\mu) |-\rangle \langle - | [\alpha_{p'}^+ \alpha_{n'}^+ N_\omega^+(\mu)]^+ \\
&H_{31} \alpha_{p_1}^+ \alpha_{p_2}^+ |-\rangle E_{p_1 p_2}(p' n', \omega)
\end{aligned} \tag{3.38}$$

$$\begin{aligned}
|n_1 n_2 corr\rangle &= \alpha_{n_1}^+ \alpha_{n_2}^+ |-\rangle + \sum_{p' n'} \alpha_{p'}^+ \alpha_{n'}^+ N_\omega^+(-\mu) |-\rangle \langle - | [\alpha_{p'}^+ \alpha_{n'}^+ N_\omega^+(-\mu)]^+ \\
&H_{31} \alpha_{n_1}^+ \alpha_{n_2}^+ |-\rangle E_{n_1 n_2}(p' n', \omega)
\end{aligned} \tag{3.39}$$

where

$$E_{ab}(cd, \omega) = \frac{1}{(\epsilon_a + \epsilon_b) - (\epsilon_c + \epsilon_d + \omega)} \tag{3.40}$$

The amplitude of GT transition can be rewritten for single (q-p) level as,

$$\begin{aligned}
\langle p_1 p_2 corr | t_\pm \sigma_\mu | pn_{corr} \rangle &= \delta(p_1, p) \langle p_2 corr | t_\pm \sigma_\mu | n_{corr} \rangle - \delta(p_2, p) \\
&\langle p_1 corr | t_\pm \sigma_\mu | n_{corr} \rangle
\end{aligned} \tag{3.41}$$

$$\begin{aligned}
\langle n_1 n_2 corr | t_\pm \sigma_{-\mu} | pn_{corr} \rangle &= \delta(n_2, n) \langle n_1 corr | t_\pm \sigma_{-\mu} | p_{corr} \rangle - \delta(n_1, n) \\
&\langle n_2 corr | t_\pm \sigma_{-\mu} | p_{corr} \rangle
\end{aligned} \tag{3.42}$$

The (q-p) amplitude from Eqs. 3.34, 3.35, and 3.36 is obtained by neglecting second order

in the phonon correlation terms. It is possible for parent nuclei having odd nucleons in phonon excitation of Quasi-particle Random Phase Approximation. The quasi pair remains in same orbit of the single quasi acts as spectator.

$$E_a(b, \omega) = \frac{1}{(\epsilon_a - \epsilon_b - \omega)} \quad (3.43)$$

this switches the pole from the real axis of energy variable ω .

3.5 Extension of the pn-QRPA model

It is part of common knowledge about scattering of GT strength over large range between initial and final states, hence complete picture understanding about initial and final structure about nuclear level is crucial. The extension in pn-QRPA model is necessary for detail study of nuclear structural properties in stellar environment. The parent excited levels can be constructed same as the (q-p) levels of phonon correlation.

With single nucleon the low level excited states are attainable. The characterization of the occupation of two similar nucleons in ground state is same as that in quasi-particle description [49]. The configuration of initial and final states must be known for distribution of GT strength of final nuclear levels. After that for computation of weak rates the extension for pn-QRPA is required. This enhancement is worth for the calculation and simulations in astrophysical problems in stellar reinforcement and elaborating the inside mystery of stellar entities. In the inner core structure nuclei are not necessary to be reside in ground state, due to the high temperature, high pressure and high density conditions, nucleons reside in highly excited states, where the transitions take place. Under following sections the transition amplitude is described between the collective to single quasi-particle states.

3.5.1 Even Even Nuclei

If a nuclei consist of even even number of nucleons it means excited states will be populated by two protons and two neutrons quasi particle levels given in Eqs. 3.38 and 3.39. The even even parent nuclear states have transition only into odd-odd daughter nuclei. The transitional amplitude and correlated conversion of quasi-particle state is given as

$$\langle p^f n_c^f | t_{\pm} \sigma_{-\mu} | p_1^i p_{2c}^i \rangle = -\delta(p^f, p_2^i) \langle n_c^f | t_{\pm} \sigma_{-\mu} | p_{1c}^i \rangle + \delta(p^f, p_1^i) \langle n_c^f | t_{\pm} \sigma_{-\mu} | p_{2c}^i \rangle \quad (3.44)$$

$$\langle p^f n_c^f | t_{\pm} \sigma_{\mu} | n_1^i n_{2c}^i \rangle = +\delta(n^f, n_2^i) \langle p_c^f | t_{\pm} \sigma_{\mu} | n_{1c}^i \rangle - \delta(n^f, n_1^i) \langle p_c^f | t_{\pm} \sigma_{\mu} | n_{2c}^i \rangle \quad (3.45)$$

where, the spherical component of spin operators are $\mu = -1, 0, 1$.

3.5.2 Odd A Nuclei

In nuclei consisting odd number of nucleons low lying states are attainable. Where quasi-particles transit from lower to higher energy levels. For 3-protons and 2-neutrons, the odd-proton and even-neutron state is attainable, when the quasi-particles are lifted from lowest energy state to higher state. These levels are expressed by 1p-2n levels or 3p levels, related to a proton or neutron excitation..

$$\begin{aligned} |p_1 p_2 p_{3corr} \rangle &= \alpha_{p_1}^+ \alpha_{p_2}^+ \alpha_{p_3}^+ |-\rangle + \frac{1}{2} \sum_{p'_1 p'_2 n' \omega} \alpha_{p'_1}^+ \alpha_{p'_2}^+ \alpha_{n'}^+ N_{\omega}^+(\mu) |-\rangle \\ \langle - | [\alpha_{p'_1}^+ \alpha_{p'_2}^+ \alpha_{n'}^+ N_{\omega}^+(\mu)]^+ H_{31} \alpha_{p_1}^+ \alpha_{p_2}^+ \alpha_{p_3}^+ |-\rangle & E_{p_1 p_2 p_3}(p'_1 p'_2 n', \omega) \end{aligned} \quad (3.46)$$

$$\begin{aligned}
|p_1 n_1 n_{2corr}\rangle &= \alpha_{p_1}^+ \alpha_{n_1}^+ \alpha_{n_2}^+ |-\rangle + \frac{1}{2} \sum_{p'_1 p'_2 n'_\omega} \alpha_{p'_1}^+ \alpha_{p'_2}^+ \alpha_{n'_\omega}^+ N_\omega^+(-\mu) |-\rangle \\
\langle - | [\alpha_{p'_1}^+ \alpha_{p'_2}^+ \alpha_{n'_\omega}^+ N_\omega^+(-\mu)]^+ H_{31} \alpha_{p_1}^+ \alpha_{n_1}^+ \alpha_{n_2}^+ |-\rangle E_{p_1 n_1 n_1}(p'_1 p'_2 n'_\omega, \omega) &+ \frac{1}{6} \\
\sum_{n'_1 n'_2 n'_3 \omega} \alpha_{n'_1}^+ \alpha_{n'_2}^+ \alpha_{n'_3}^+ N_\omega^+(\mu) |-\rangle \langle - | [\alpha_{n'_1}^+ \alpha_{n'_2}^+ \alpha_{n'_3}^+ N_\omega^+(\mu)]^+ & \\
H_{31} \alpha_{p_1}^+ \alpha_{n_1}^+ \alpha_{n_2}^+ |-\rangle E_{p_1 n_1 n_2}(n'_1 n'_2 n'_3, \omega) &
\end{aligned} \tag{3.47}$$

having energy in denominators for first order perturbation,

$$E_{abc}(def, \omega) = \frac{1}{(\epsilon_a + \epsilon_b + \epsilon_c) - (\epsilon_d + \epsilon_e + \epsilon_f + \omega)} \tag{3.48}$$

The excited levels in a nucleus containing even number of protons and odd number of neutrons are established as following

- (i) With the excitation of odd number of neutron from the ground state to higher (excited state) energy levels.
- (ii) By 3n levels, linked with excitation of neutron,
- (iii) In 2n levels, linked to the excitation of proton.

The relation for multi quasi particle transitions and their reduction to correlated (c) one quasi particle state as:

$$\begin{aligned}
\langle p_1^f n_1^f n_{2c}^f | t_\pm \sigma_\mu | n_1^i n_2^i n_{3c}^i \rangle &= \delta(n_1^f, n_2^i) \delta(n_2^f, n_3^i) \langle p_{1c}^f | t_\pm \sigma_\mu | n_{1c}^i \rangle \\
&- \delta(n_1^f, n_1^i) \delta(n_2^f, n_3^i) \langle p_{1c}^f | t_\pm \sigma_\mu | n_{2c}^i \rangle \\
&+ \delta(n_1^f, n_1^i) \delta(n_2^f, n_2^i) \langle p_{1c}^f | t_\pm \sigma_\mu | n_{3c}^i \rangle
\end{aligned} \tag{3.49}$$

$$\begin{aligned}
\langle p_1^f n_1^f n_{2c}^f | t_{\pm} \sigma_{-\mu} | p_1^i p_2^i n_{1c}^i \rangle &= \delta(p_1^f, p_2^i) [\delta(n_1^f, n_1^i) \langle n_{2c}^f | t_{\pm} \sigma_{-\mu} | p_{1c}^i \rangle \\
&\quad - \delta(n_2^f, n_1^i) \langle n_{c1}^f | t_{\pm} \sigma_{-\mu} | p_{1c}^i \rangle] \\
&\quad - \delta(p_1^f, p_1^i) [\delta(n_1^f, n_1^i) \langle n_{2c}^f | t_{\pm} \sigma_{-\mu} | p_{2c}^i \rangle \\
&\quad - \delta(n_2^f, n_1^i) \langle n_{1c}^f | t_{\pm} \sigma_{-\mu} | p_{2c}^i \rangle]
\end{aligned} \tag{3.50}$$

$$\begin{aligned}
\langle p_1^f p_2^f p_{3c}^f | t_{\pm} \sigma_{\mu} | p_1^i p_1^i n_{1c}^i \rangle &= \delta(p_2^f, p_1^i) \delta(p_3^f, p_2^i) \langle p_{1c}^f | t_{\pm} \sigma_{\mu} | n_{1c}^i \rangle \\
&\quad - \delta(p_1^f, p_1^i) \delta(p_3^f, p_2^i) \langle p_{2c}^f | t_{\pm} \sigma_{\mu} | n_{1c}^i \rangle \\
&\quad + \delta(p_1^f, p_1^i) \delta(p_2^f, p_2^i) \langle p_{3c}^f | t_{\pm} \sigma_{\mu} | n_{1c}^i \rangle
\end{aligned} \tag{3.51}$$

3.5.3 Odd-Odd Nuclei

The nucleus containing odd number of the neutrons and also odd number of the protons are represented in quasi particle transformation with the help of using two (q-p) states of neutron and proton pair states and four quasi-particle states of two nucleons. The two quasi-particle states reduction into correlated (c) one quasi-particle state are illustrated as

$$\langle p_1^f p_{2c}^f | t_{\pm} \sigma_{\mu} | p^i n_c^i \rangle = \delta(p_1^f, p^i) \langle p_{2c}^f | t_{\pm} \sigma_{\mu} | n_c^i \rangle - \delta(p_2^f, p^i) \langle p_{1c}^f | t_{\pm} \sigma_{\mu} | n_c^i \rangle \tag{3.52}$$

$$\langle n_1^f n_{2c}^f | t_{\pm} \sigma_{-\mu} | p^i n_c^i \rangle = \delta(n_2^f, n^i) \langle n_{1c}^f | t_{\pm} \sigma_{-\mu} | p_c^i \rangle - \delta(n_1^f, n^i) \langle n_{2c}^f | t_{\pm} \sigma_{-\mu} | p_c^i \rangle \tag{3.53}$$

the four quasi-particle states can be simplified as following

$$\begin{aligned}
\langle p_1^f p_2^f n_1^f n_{2c}^f | t_{\pm} \sigma_{-\mu} | p_1^i p_2^i p_3^i n_{1c}^i \rangle &= \delta(n_2^f, n_1^i) [\delta(p_1^f, p_2^i) \delta(p_2^f, p_3^i) \langle n_{1c}^f | t_{\pm} \sigma_{-\mu} | p_{1c}^i \rangle \\
&\quad - \delta(p_1^f, p_1^i) \delta(p_2^f, p_3^i) \langle n_{1c}^f | t_{\pm} \sigma_{-\mu} | p_{2c}^i \rangle + \delta(p_1^f, p_1^i) \delta(p_2^f, p_2^i) \langle n_{1c}^f | t_{\pm} \sigma_{-\mu} | p_{3c}^i \rangle] \\
-\delta(n_1^f, n_1^i) [\delta(p_1^f, p_2^i) \delta(p_2^f, p_3^i) \langle n_{2c}^f | t_{\pm} \sigma_{-\mu} | p_{1c}^i \rangle &- \delta(p_1^f, p_1^i) \delta(p_2^f, p_3^i) \langle n_{2c}^f | t_{\pm} \sigma_{-\mu} | p_{2c}^i \rangle \\
&\quad + \delta(p_1^f, p_1^i) \delta(p_2^f, p_2^i) \langle n_{2c}^f | t_{\pm} \sigma_{-\mu} | p_{3c}^i \rangle]
\end{aligned} \tag{3.54}$$

$$\begin{aligned}
\langle p_1^f p_2^f p_3^f p_{4c}^f | t_{\pm} \sigma_{\mu} | p_1^i p_2^i p_3^i n_{1c}^i \rangle &= -\delta(p_2^f, p_1^i) \delta(p_3^f, p_2^i) \delta(p_4^f, p_3^i) \langle p_{1c}^f | t_{\pm} \sigma_{\mu} | n_{1c}^i \rangle \\
+\delta(p_1^f, p_1^i) \delta(p_3^f, p_2^i) \delta(p_4^f, p_3^i) \langle p_{2c}^f | t_{\pm} \sigma_{\mu} | n_{1c}^i \rangle &- \delta(p_1^f, p_1^i) \delta(p_2^f, p_2^i) \delta(p_4^f, p_3^i) \langle p_{3c}^f | t_{\pm} \sigma_{\mu} | n_{1c}^i \rangle \\
&\quad + \delta(p_1^f, p_1^i) \delta(p_2^f, p_2^i) \delta(p_3^f, p_3^i) \langle p_{4c}^f | t_{\pm} \sigma_{\mu} | n_{1c}^i \rangle
\end{aligned} \tag{3.55}$$

$$\begin{aligned}
\langle p_1^f p_2^f n_1^f n_{2c}^f | t_{\pm} \sigma_{\mu} | p_1^i n_1^i n_2^i n_{3c}^i \rangle &= \delta(p_1^f, p_1^i) [\delta(n_1^f, n_2^i) \delta(n_2^f, n_3^i) \langle p_{2c}^f | t_{\pm} \sigma_{\mu} | n_{1c}^i \rangle \\
&\quad - \delta(n_1^f, n_1^i) \delta(n_2^f, n_3^i) \langle p_{2c}^f | t_{\pm} \sigma_{\mu} | n_{2c}^i \rangle + \delta(n_1^f, n_1^i) \delta(n_2^f, n_2^i) \langle p_{2c}^f | t_{\pm} \sigma_{\mu} | n_{3c}^i \rangle] \\
-\delta(p_2^f, p_1^i) [\delta(n_1^f, n_2^i) \delta(n_2^f, n_3^i) \langle p_{1c}^f | t_{\pm} \sigma_{\mu} | n_{1c}^i \rangle &- \delta(n_1^f, n_1^i) \delta(n_2^f, n_2^i) \langle p_{1c}^f | t_{\pm} \sigma_{\mu} | n_{2c}^i \rangle \\
&\quad + \delta(n_1^f, n_1^i) \delta(n_2^f, n_2^i) \langle p_{1c}^f | t_{\pm} \sigma_{\mu} | n_{3c}^i \rangle]
\end{aligned} \tag{3.56}$$

$$\begin{aligned}
\langle n_1^f n_2^f n_3^f n_{4c}^f | t_{\pm} \sigma_{-\mu} | p_1^i n_1^i n_2^i n_{3c}^i \rangle &= +\delta(n_2^f, n_1^i) \delta(n_3^f, n_2^i) \delta(n_4^f, n_3^i) \langle n_{1c}^f | t_{\pm} \sigma_{-\mu} | p_{1c}^i \rangle \\
&\quad - \delta(n_1^f, n_1^i) \delta(n_3^f, n_2^i) \delta(n_4^f, n_3^i) \langle n_{2c}^f | t_{\pm} \sigma_{-\mu} | p_{1c}^i \rangle \\
&\quad + \delta(n_1^f, n_1^i) \delta(n_2^f, n_2^i) \delta(n_4^f, n_3^i) \langle n_{3c}^f | t_{\pm} \sigma_{-\mu} | p_{1c}^i \rangle \\
&\quad - \delta(n_1^f, n_1^i) \delta(n_2^f, n_2^i) \delta(n_3^f, n_3^i) \langle n_{4c}^f | t_{\pm} \sigma_{-\mu} | p_{1c}^i \rangle
\end{aligned} \tag{3.57}$$

for all the available amplitudes of (q-p) transition anti symmetrization of single (q-p) levels are:

$$p_4^f > p_3^f > p_2^f > p_1^f,$$

$$\begin{aligned}
n_4^f &> n_3^f > n_2^f > n_1^f, \\
p_4^i &> p_3^i > p_2^i > p_1^i, \\
n_4^i &> n_3^i > n_2^i > n_1^i.
\end{aligned}$$

phonon excitation for GT strength for each excited state are also determined. Where it is assumed that quasi-particle's in parent nucleus remain in the same quasi-particle states.

This extended model of pn-QRPA provides a proper way to calculate the allowed GT strength distribution for any nuclide. These GT strength are considered to have a decisive role in weak interaction reactions, which are then employed as key parameters in the stellar simulations codes.

3.6 Calculation of Stellar β -Decay and Positron Capture Rates

Present model provides us a smart choice to calculate the stellar β -decay and positron capture rates comparable with experimental data at stellar temperature and densities [44].

The stellar weak interaction rates from i th orbit of parent nuclide to daughter nuclide j th orbit is specified by

$$\lambda^{bd/pc} = \ln 2 \frac{f_{ij}(T, \rho, E_f)}{(ft)_{ij}} \quad (3.58)$$

where $\lambda^{bd/pc}$ specifies the stellar β -decay and positron capture rates in stellar environment, $(ft)_{ij}$ is connected to the reduced transition probability $(B)_{ij}$ by

$$(ft)_{ij} = \frac{C}{B_{ij}} \quad (3.59)$$

where C is a compound constant given as

$$C = \frac{2 \ln 2 \hbar^7 \pi^3}{g_v^2 m_e^5 c^4} \quad (3.60)$$

and $(B)_{ij}$ can be defined as

$$B_{ij} = B(F)_{ij} + (g_A/g_V)^2 B(GT)_{ij} \quad (3.61)$$

$B(GT)$ and $B(F)$ are denoting the reduced transition probabilities for Gamow-Teller and Fermi transitions, respectively. The $B(F)$ and $B(GT)$ are explained by

$$B(F)_{ij} = \frac{1}{2J_i + 1} |\langle f \parallel \Sigma_k t_{\pm}^k \parallel i \rangle|^2 \quad (3.62)$$

$$B(GT)_{ij} = \frac{1}{2J_i + 1} |\langle f \parallel \Sigma_k t_{\pm}^k \vec{\sigma}^k \parallel i \rangle|^2 \quad (3.63)$$

here $\vec{\sigma}^k$ stands for the spin operator and t_{\pm}^k illustrates isospin raising and lowering operator. The phase space (f) integral was taken over total energy. Adopting natural units ($\hbar = c = m_e = 1$), for positron capture (PC) it is specified by

$$f_{ij} = \int_1^{\omega_m} \omega \sqrt{\omega^2 - 1} (\omega_m - \omega)^2 F(-Z, \omega) (1 - G_+) d\omega \quad (3.64)$$

for the positron emission,

$$f_{ij} = \int_{\omega_1}^{\infty} \omega \sqrt{\omega^2 - 1} (\omega_m - \omega)^2 (\omega_m - \omega)^2 F_1(-Z, \omega) + (\omega^2 - 1) F_2(-Z, \omega) (1 - G_+) d\omega \quad (3.65)$$

In above equations the total kinetic energy of electron is represented by ω while ω_l stands for the energy of rest mass of electron and represents the threshold energy of positron capture.

The total beta decay energy is ω_m , it is noted that if ω_m exceeds -1 then $\omega_l = 1$, but if $\omega_m = 1$ or less than 1 then $\omega_l = |\omega_m|$.

$$\omega_m = m_p - m_d + E_i - E_j \quad (3.66)$$

Here m_p and E_i are mass of parent nucleus and excitation energies of parent nuclei and m_d is mass of daughter nucleus and E_j is their excitation energies. In Eq. 3.64 the G_{\pm} is distribution function for positron and electron, respectively

$$G_+ = \frac{1}{\exp\left(\frac{E + 2 + E_f}{kT}\right) + 1} \quad (3.67)$$

$$G_- = \frac{1}{\exp\left(\frac{E - E_f}{kT}\right) + 1} \quad (3.68)$$

Here E_f , T and k are the Fermi energy, temperature and Boltzman constant respectively and also consider the term $E = (\omega - 1)$.

Now calculating the number density of \bar{e} correlated with proton and nuclei is given by

$$\rho Y_e = \frac{m_e^3 c^3}{\pi^2 N_A \hbar^3} \int_0^\infty (G_- - G_+) p^2 dp \quad (3.69)$$

where ρ is baryon density, Y_e electron to baryon ratio, and N_A is Avogadro number, $p = \sqrt{\omega^2 - 1}$ is the electron or positron momentum. Eqs. 3.69 was employed for an iterative computation of Fermi energies at given temperature and Y_e values. At thermal equilibrium in the stellar environment the occupation probability for i^{th} state is given by

$$P_i = \frac{\exp(-E_i/kT)}{\sum_{i=1} \exp(-E_i/kT)} \quad (3.70)$$

where E_i is the excitation energy of the i^{th} state. Finally, for β decay and positron capture rates per unit time are,

$$\lambda^{bd/pc} = \sum_{ij} P_i \lambda_{ij} \quad (3.71)$$

For initial and final states sum is taken over all levels to achieve the desired convergence of computed total weak rates in stellar environment.

Chapter 4

Analysis of β -Decay Half-life of ^{44}Sc

4.1 Introduction

Accurate measurements and reliable calculations of beta decay half-lives are prerequisites for a better understanding of the nucleosynthesis processes.

In the field of nuclear physics being basic, prime and salient tool of nucleosynthesis half-life has been focused and studied since last century to achieve better results with less uncertainty. The concept of half-life was first introduced by Ernest Rutherford [53]. The history of half-life includes investigation with the help of theoretical models [54–56] as well as various experiments [57–59]. The motivation of present study is to investigate, analyze and test the accuracy of half-life results by using both techniques (theoretical model and experiment). We employed the proton-neutron quasiparticle random phase approximation (pn-QRPA) model for theoretical approach. The theory of pn-QRPA is used for microscopic calculation in the field of nuclear astrophysics. By employing the framework of pn-QRPA one becomes able to analyze energy transitions state by state, nuclear matrix elements (NME), branching ratio and partial half-life about a particular nuclei. Similarly, for measurements of half-life various activation processes like charged particle activation (CPA), neutron activation etc were employed. One advantageous approach among these techniques

is photon activation approach (PAA). Photon activation process is used for experimental part of present work, and done at FEN Faculty Physics department Akdeniz University, Antalya, Turkey. The idea was to compare the measured half life using PAA with the calculated half life using pn-QRPA model.

In order to perform the needful we selected the $Z=21$ element scandium (^{44}Sc). The ^{44}Sc was chosen because of its distinctive role and applications in medical field [60,61]. Previous study reveals one of its key role about pre-clinical positron emission tomography (PET) for large variety of radiotracers with comparatively low clearance like fragments or monoclonal antibodies and nanobodies of interest for molecular imaging [62]. ^{44}Sc is one of the few positron emitters that can be obtained with the help of radionuclide generator system, thus avoiding the need of employing a cyclotron [63]. In the disease diagnosis, therapeutic assessment responses, therapy and dosimetry evaluation ^{44}Sc in combination with its isotopic element ^{47}Sc generates matchless employment in the field of medicine [64,65].

The detailed description of results by PAA and theoretical model (pn-QRPA) will be discussed in the succeeding sections. In this work the successful demonstration of clinical linear accelerator (cLINAC) about practical application other than medical field has also been depicted.

4.2 Measurement of β -Decay Half-life

There are three kinds of half-lives under consideration in the field of research and everyday life. These three types include physical, biological and effective half-life. Among these three categories physical is the most important among all others. The time period required to lose one half level by radioactivity from its original value because of radioactive decay is referred to as physical half-life. It is denoted by T_{phys} or generally $T_{1/2}$. By default, the term $T_{1/2}$ refers to physical half-life in this work. Only β -decay half-lives will be discussed in this thesis. Knowledge about β decay is very important for element creation in stellar

environment. Investigation about β -decay makes situation complex because in this decay an large number of levels could populate in the daughter nucleus. Investigations based on theoretical and experimental field is being done in this dissertation. There are many methods for the extraction of half-lives from measured raw data but efficient one is chosen in this work which I discussed below.

4.2.1 *Experiment*

A photon source needs to activate or excite nuclei of target element in our experiment. In this work clinical linear accelerator SLI-25 fabricated by Philips Medical Systems has been utilized for the activation of photons. A stable and decent performance of cLINAC with clinical conditions was used basic research in physics. Details about technical documentation of accelerator can be seen in [35]. Fig. 4.1 shows cLINAC used in present experiment.



Figure 4.1: Philips SLI-25 clinical linear electron accelerator of Elekta TM Synergy.

Irradiation of target sample was performed with the help of cLINAC. It can also be known as origin of photons production. These photons have been generated with the help of an electron gun using energy of 50 keV . These produced photons accelerated just after their injection into the linac's copper cavity. This acceleration has been performed by wave of

radio-frequency with 3 GHz , S-band. Copper cavity in SLI-25 was designed for traveling of wave. Power supply was introduced by magnetron with the nominal power of 2.5 MW at 4 MeV (low energy) and 5 MW at 25 MeV (high energy).

For experiment, the sample target was placed 58 cm distant from a target high-Z element (in present case tungsten). This tungsten works as an electron stopper. Generated bremsstrahlung photons were flattened and collimated with the help of several filters, yielding a uniform focused beam of photons without position dependence. Whole scheme is displayed in Fig. 4.2. All cLINAC follows a standard feature of collimation and focusing. Irradiation time for target sample in present experiment was 35 minutes.

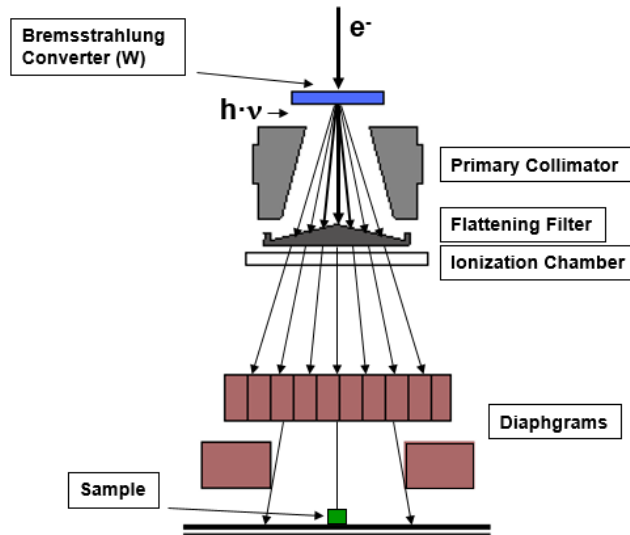


Figure 4.2: The diagrammatic view for creation of photon beam for the cLINAC employed in present experiment.

After sample irradiation using cLINAC it was shifted to Nuclear Physics laboratory, Physics Department of Akdeniz University, which was equipped with high purity Germanium detector (HPGe). It was an electrically cooled, p-type, coaxial detector. This detector was covered by a lead layer of 10 cm thick with inner surface shielded with 0.2 cm copper foil for reduction of Pb X-rays. The HPGe detector used in present study had 40% rela-

tive efficiency and resolution of 768 eV FWHM at 122 keV and 1.85 keV FWHM at 1332 keV (MAESTRO 2012). Standard point sources consists on the following isotopes ^{22}Na , ^{54}Mn , ^{57}Co , ^{60}Co , ^{109}Cd , ^{133}Ba , ^{137}Cs and were employed for energy calibrations. These point source were provided by Nuclear Research and Training Center (IAEA 1364-43-2). A soil sample in addition with these point sources (supplied by Turkish Atomic Energy Authority (TAEK) containing the naturally radioactive isotopes ^{40}K , ^{226}Ra and ^{232}Th) was also utilized for calibration. During spectrum analysis only strong peaks of γ -rays has been analyzed. The HPGe detector was attached to standard Nuclear Instrumentation Module (NIM) equipment, containing an analog-to-digital converter (ADC), ORTEC pre-amplifier, spectroscopy amplifier, bias supply and computer, respectively. Data acquisition was performed using MAESTRO32 software (MAESTRO, 2012). At uniform intervals of time the same spectra were recorded automatically. Initially time intervals were set short for $\sim 3\text{s}$. These short intervals were selected to analyze the short lived isotopes, while the later ones became longer ~ 20 min when focusing on longer lived isotopes. Once the γ -ray computation for the sample was finished, spectrum for natural background was also recorded. Data evaluation procedure and experimental approach performed in present study was similar to that described in [57].

4.3 Calculation of Half-life

To achieve the target regarding theoretical prediction of beta decay half life we employed a deformed basis within the framework of pn-QRPA model involving the Nilsson+BCS formalism. Additionally we consolidate multi-shell single-particle states incorporating a schematic interaction [41, 49, 54]. To investigate ^{44}Sc having important applications in medical field, pn-QRPA has been employed. With the help of this microscopic theory we calculated half-life for ^{44}Sc odd-odd nuclei.

We originated with spherical basis (a_{jk}^\dagger, a_{jk}) , including j as its total angular momentum



Figure 4.3: HPGe detector setup used in this work.

and the associated z-component as k . The spherical basis follows the interconversion to the deformed (axial-symmetric) basis $(d_{k\alpha}^\dagger, d_{k\alpha})$ employing the equation of transformation

$$d_{k\alpha}^\dagger = \sum_j K_j^{k\alpha} a_{jk}^\dagger. \quad (4.1)$$

The prevailed transformation matrix from set of Nilsson eigenfunctions in Eq. 4.1 is shown by symbol K , and α (removing k , which shows the Nilsson eigenstates) depicts the additional quantum numbers. We utilized BCS calculation for the neutron (n) & proton (p) systems independently. We took constant pairing force possessing strength of $V(V_n, V_p$ for the neutrons and the protons, respectively),

$$F^{pair} = -V \sum_{jkj'k'} (-1)^{l+j-k} a_{jk}^\dagger a_{j-k}^\dagger (-1)^{l'+j'-k'} a_{j'-k} a_{j'k'}, \quad (4.2)$$

where the sum over k and k' was restricted to $k, k' > 0$ and orbital angular momentum is denoted by l . The BCS calculation provides occupation amplitudes $u_{k\alpha}, v_{k\alpha}$ (which attains

the following relation, $u_{k\alpha}^2 + v_{k\alpha}^2 = 1$) and (q-p) energies $\varepsilon_{k\alpha}$. Later we added a quasiparticle basis $(c_{k\alpha}^\dagger, c_{k\alpha})$ by introducing a Bogoliubov transformation

$$c_{k\alpha}^\dagger = u_{k\alpha} d_{k\alpha}^\dagger - v_{k\alpha} d_{\bar{k}\alpha} c_{\bar{k}\alpha}^\dagger = u_{k\alpha} d_{k\alpha}^\dagger + v_{k\alpha} d_{k\alpha}. \quad (4.3)$$

Here \bar{k} is the time reversed state of k and c/c^\dagger stands for the (q-p) annihilation/creation operators which is eventually included our RPA equation. Creation operators of QRPA phonons was instigated applying the following relation

$$C_\omega^\dagger(\mu) = \sum_{pn} [R_\omega^{pn}(\mu) c_p^\dagger c_n^\dagger - S_\omega^{pn}(\mu) c_n c_p]. \quad (4.4)$$

Indices n and p in Eq. 4.4 stands for $m_n \alpha_n$ and $m_p \alpha_p$, respectively, and discriminate between neutron and proton single-(quasi)-particle states. R_ω^{pn} and S_ω^{pn} are amplitudes for forward and backward going, respectively, and are in fact the eigenfunctions for the RPA matrix equation. ω represents the corresponding energy eigenvalues of the eigenstates.

For RPA calculation we examine the (p.h) GT force with the help of following relation

$$F^{p,h} = +2\chi \sum_{\mu=-1}^1 (-1)^\mu S_\mu S_{-\mu}^\dagger \quad (4.5)$$

$$S_\mu = \sum_{j_p m_p j_n m_n} \langle j_p m_p | \tau_- \sigma_\mu | j_n m_n \rangle c_{j_p m_p}^\dagger c_{j_n m_n}. \quad (4.6)$$

The corresponding (p.p) GT force was calculated employing

$$F^{p,p} = -2\kappa \sum_{\mu=-1}^1 (-1)^\mu Z_\mu^\dagger Z_{-\mu}. \quad (4.7)$$

with

$$Z_{\mu}^{+} = \sum_{j_p m_p j_n m_n} \langle j_n m_n | (\tau_{-} \sigma_{\mu})^{+} | j_p m_p \rangle \quad (4.8)$$

$$(-1)^{l_n + j_n - m_n} c_{j_p m_p}^{+} c_{j_n - m_n}^{+},$$

In Eqs. 4.6 and 4.8, τ_{\pm} denotes isospin raising (lowering) operator. The τ_{+} (τ_{-}) operator added for conversion of proton (neutron) to neutron (proton), σ is for pauli matrix and all remaining symbols have ordinary meanings.

Initially Nilsson model [66] was introduced for calculation of single particle energies and wave functions. Nuclear deformation was taken considered within the framework of Nilsson model. Pairing correlations were tackled employing the BCS approach. We considered proton-neutron residual interaction in two routes namely particle particle (attractive) and particle hole (repulsive) interactions. A reasonable choice for GT force parameters (χ and κ) may lead to smart and decent comparison of measured half-lives with the calculated ones (e.g. Refs. [41, 54]). In present section we used same range values for the strength parameters as reported in Ref. [67]. The value of $\chi = 61.20/A$ (MeV) and $\kappa = 4.85/A$ (MeV) [67] is used in the present work. The chosen values of χ and κ presents the $1/A$ dependence as suggested in previous references [68–71].

The partial half-lives to daughter excited states (E_f) can be calculated using the formula

$$t_{1/2}^{par} = \frac{K}{(g_A/g_V)^2 f_A(Z, A, E) B_{GT}(E_f) + f_V(Z, A, E) B_F(E_f)} \quad (4.9)$$

In Eq. (4.9) K is a compound constant taken 6143s from [51], $E = Q - E_f$ (where Q is the amount of energy released by the nuclear reaction), g_A and g_V stands for axial and vector coupling constants, f_A (f_V) is the Fermi integral function for axial vector (vector) transitions and B_F and B_{GT} are the reduced transition probabilities for the Fermi and Gamow-Teller (GT) transitions, respectively. In the form of matrix elements the reduced

transition probabilities can be expressed as

$$B_{GT} = \frac{1}{2I_i + 1} |\langle f \| M_{GT} \| i \rangle|^2 \quad (4.10)$$

and

$$B_F = \frac{1}{2I_i + 1} |\langle f \| M_F \| i \rangle|^2, \quad (4.11)$$

M_{GT} stands for GT transition operator in Eq. (4.10) given by

$$M_{GT} = \sum_k \tau_{\pm}(k) \sigma(k). \quad (4.12)$$

The sum is carried for all nucleons present in the nucleus. For this work we only carried calculations for τ_+ σ transitions. M_F is the corresponding operator for Fermi transitions in Eq. (4.11). Spin for parent state is denoted by I_i in these expressions.

The deformation parameter β_2 is another significant parameter in nuclear model (pn-QRPA) containing deformed basis states. For the calculation of β_2 we employ the following formula, instead of using values reported by different theoretical models

$$\beta_2 = \frac{125(Q_2)}{1.44(A)^{2/3}(Z)}. \quad (4.13)$$

The electric quadrupole moment, Q_2 , is taken from Ref. [72]. Q -values are taken from the NUBASE2016 data [73]. Pairing gaps computation has been calculated by employing two different empirical formulae rather than former trivial formulation. So, for the calculation of pairing gaps, in units of MeV , first formula as a function of neutron separation energies (S_n) and other as function of proton separation energies (S_p) has been shown in Eqs. (4.14 - 4.15) respectively,

$$\Delta_{pp} = \frac{1}{4}(-1)^{Z+1}[S_p(A+1, Z+1) - 2S_p(A, Z) + S_p(A-1, Z-1)] \quad (4.14)$$

$$\Delta_{nn} = \frac{1}{4}(-1)^{A-Z+1}[S_n(A+1, Z) - 2S_n(A, Z) + S_n(A-1, Z)] \quad (4.15)$$

The β -decay half-life of a nucleus could be obtained by summing up all transition probabilities to states in the daughter nucleus with excitation energies lying within the Q_β window

$$T_{1/2} = \left(\sum_{0 \leq E_f \leq Q_\beta} \frac{1}{t_{1/2}^{par}} \right)^{-1}. \quad (4.16)$$

E_f in Eq. (4.16) represents daughter energy states and $t_{1/2}^{par}$ are the partial half-lives introduced in Eq. (4.9).

4.4 Comparison between Measured and Calculated Results

We focused significantly on half-life (experiment and calculation) and measuring gamma ray energy transitions for ^{44}Sc . These transitions were produced at bremsstrahlung energy of 18 MeV measured with the help of HPGe detector. In this section the comparison between the results for γ -ray energy calibrations from measured and those from NUDAT [74] data sheets will be presented. Simultaneously the measured and calculated data results for half-life comparison will be discussed.

For data analysis the best option was chosen to unify two dissimilar programs. First is the use of standard gf3 RadWare code written by David Radford [75] of the Physics Division at Oak Ridge National Laboratory. Second is the ROOT [76] package having comprehensive library structure, developed by CERN. These programs were employed to check the gamma ray energy peak value for ^{44}Sc and its half-lives during its decay activity. The used functions for fitting procedure is shown in Fig. 4.4 on the strongest peak 1157 keV. The corresponding gamma spectrum for ^{44}Sc has been shown in Fig. 4.5.

Instantly before counting the selected sample, set of calibration sources was counted. After completing the sample counting, an equivalently long natural background spectrum was

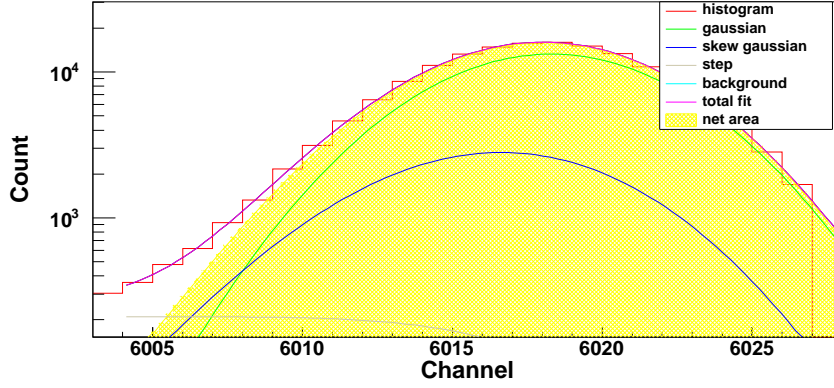


Figure 4.4: The functions used for fitting procedure during the analysis.

recorded. Once the background spectrum recording was finished, the experiment followed a second measurement about the calibration source. A linear series fit function was used before and after calibrations. The error propagation from calibration were counted using following relation:

$$\sigma_E^2 = \sum_i^n \left(\frac{\partial E}{\partial c_i}\right)^2 \sigma_{c_i}^2 + 2 \sum_i^n \sum_{j>i}^n \text{cor}_{ij} \sigma_i \sigma_j \left(\frac{\partial E}{\partial c_i}\right) \left(\frac{\partial E}{\partial c_j}\right) + \left(\frac{\partial E}{\partial ch}\right)^2 \sigma_{ch}^2 \quad (4.17)$$

In Eq. (4.17) E was calibration polynomial, as $E = \sum_i^n c_i ch^i$, calibration parameter is shown by 'c' while fitting parameters error presented with σ_{c_i} , σ_{ch} for centroid errors and cor_{ij} for correlation matrix element.

Two combinations of calibration for before and after counting performed to obtain final results were [77],

$$\sigma_E^2 = \frac{\sigma_{E_{bef}}^2 + \sigma_{E_{aft}}^2 + (\bar{E}_{bef} - \bar{E})^2 + (\bar{E}_{aft} - \bar{E})^2}{2} \quad (4.18)$$

$$\bar{E} = \frac{\bar{E}_{bef} + \bar{E}_{aft}}{2} \quad (4.19)$$

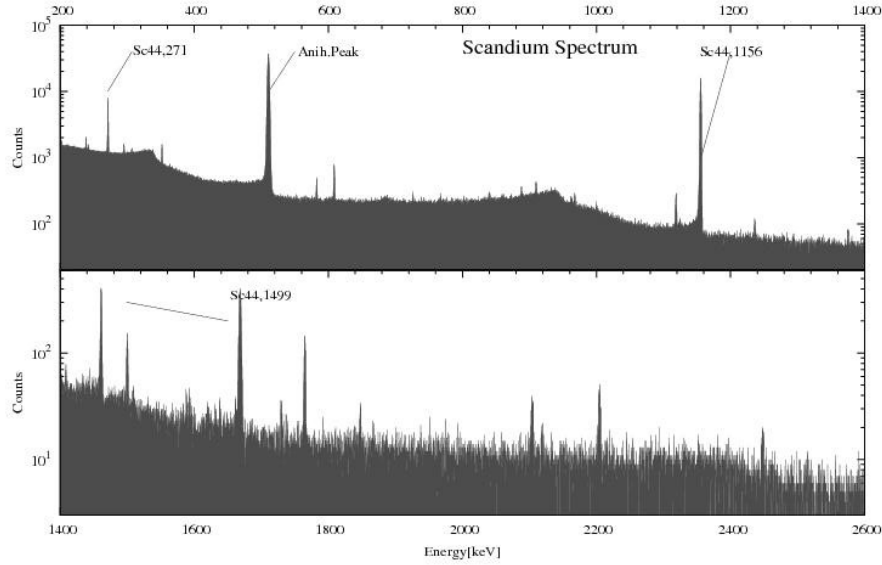


Figure 4.5: ^{44}Sc spectrum without any subtraction which was irradiated for three days of counting. Labeled peaks were based on energy calibration.

Energies for before and after calibration and associated errors were denoted by \bar{E}_{bef} , \bar{E}_{aft} , $\sigma_{E_{bef}}$ and $\sigma_{E_{aft}}$, respectively.

Table 4.1: Comparison of γ -ray energies obtained in the present measurement by average the results of before and after calibration with values found in the literature (NUDAT)

Element	E_{NU} (keV)	σ_{NU}	E (keV)	σ_E
^{44}Sc	1157.02	0.015	1157.114	0.05782
^{44}Sc	271.24	0.01	271.263	0.01105

In Table. 4.1, comparison between average energy and combined variance with literature values is shown. Cited results were taken from nuclear data sheets publications and NUDAT [74]. A comparison between present results and literature demonstrates that particular peaks in the spectrum (shown in Fig. 4.5) depicts the presence of ^{44}Sc . In this spectrum only prominent peaks for ^{44}Sc were labeled while rest were either sum of escape or background

peaks. Analysis for only significant peaks of ^{44}Sc spectrum specially at 1157 keV and 271 keV was done. Results of this work were in agreement with the NUDAT error bars. Precision regarding gamma-ray energies and errors were quite satisfactory and accuracy concerning the half-life results are in good precision with the literature value. One major cause for the differences of measured energy values concerns with the energy resolution of HPGe detector. The energy resolution of the HPGe detector employed in present study was 1.85 keV at 1.33 MeV . These factors can cause unfavorable effects on the measured data of the peak of interest, and plays significant role for the creation of ambiguity. To calculate the half-life value, we integrated the activity concentration within the time-intervals of same length:

$$C(T) = \int_{T-\Delta T}^{T+\Delta T} A(t)dt = C_0 e^{-\lambda T} (e^{\lambda\Delta T} - e^{-\lambda\Delta T}) \quad (4.20)$$

where $C_0 = A_0/\lambda$ and T is counting time. Because ΔT and λ are constants, this function only depends on T .

Through this way, one can solve the correlation problem between two successive spectra. The independent spectra has been measured using same ΔT time intervals. A new counting restarted automatically on the completion of previous one. Fig. 4.6 shows the evolution of the spectra between ΔT time interval for the peak at 271 keV energy of isomeric transition decay set (from 271 keV level) of ^{44}Sc and Fig. 4.7 show the evolution of the spectra between ΔT time interval for the peak at 1157 keV energy of positron decay set (from ground state) of ^{44}Sc .

Using the logarithmic form of the Eq. (4.20), a linear function was obtained:

$$\ln(C(T)) = A - \lambda T \quad (4.21)$$

After the fitting procedure, calculation of the measured half-life value applying the equation $T_{1/2} = \ln 2/\lambda$ was performed.

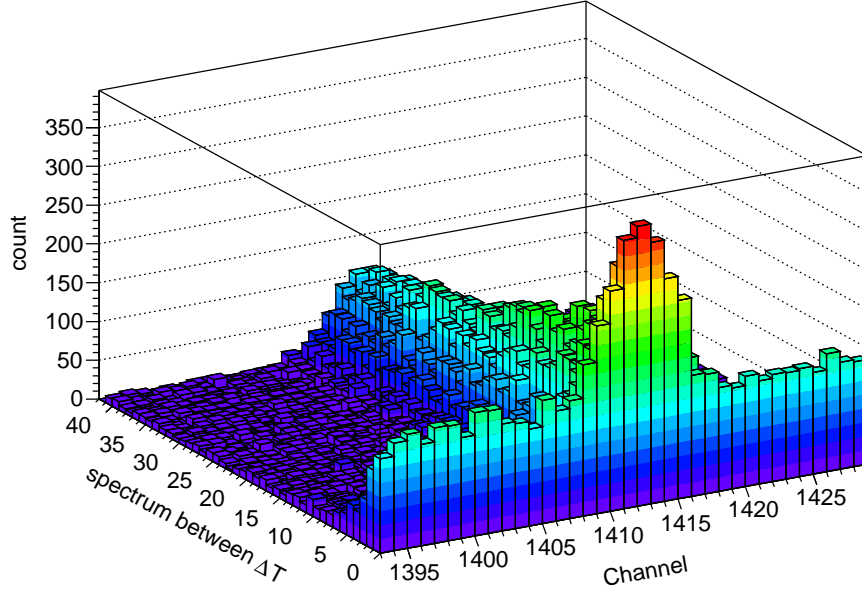


Figure 4.6: Evolution of the spectra between ΔT time interval for the peak 271 *keV* of isomeric transition decay set (from 271 *keV* level) of ^{44}Sc .

Present results for half-life and associated error of ^{44}Sc in comparison with literature statistics is shown in Table. 4.2 It can be seen that results for small half-life and errors are in decent comparison with the literature values [74, 78].

Table 4.2: Measured half-life for this work (TW) with associated error in comparison with literature (NUDAT) half-life, error and calculated half-life using half-life

Decay Set	$T_{1/2}$ NU[hour]	$T_{1/2}$ TW[hour]	σ_{NU}	σ_{TW}
$^{44}\text{Sc}(\text{IT})$	58.61	59.81	0.1	2.2
$^{44}\text{Sc}(\varepsilon)$	3.97	3.95	0.04	0.04

Table 4.3: Measured half-life for this work (TW) in comparison with literature (NUDAT) and calculated half-life using pn-QRPA

Decay Set	$T_{1/2}$ NU[hour]	$T_{1/2}$ PAA[hour]	$T_{1/2}$ pn-QRPA[hour]
^{44}Sc	3.97	3.95	3.91

We fitted transitions for ^{44}Sc positron decay from the ground state and value of $3.95 \pm$

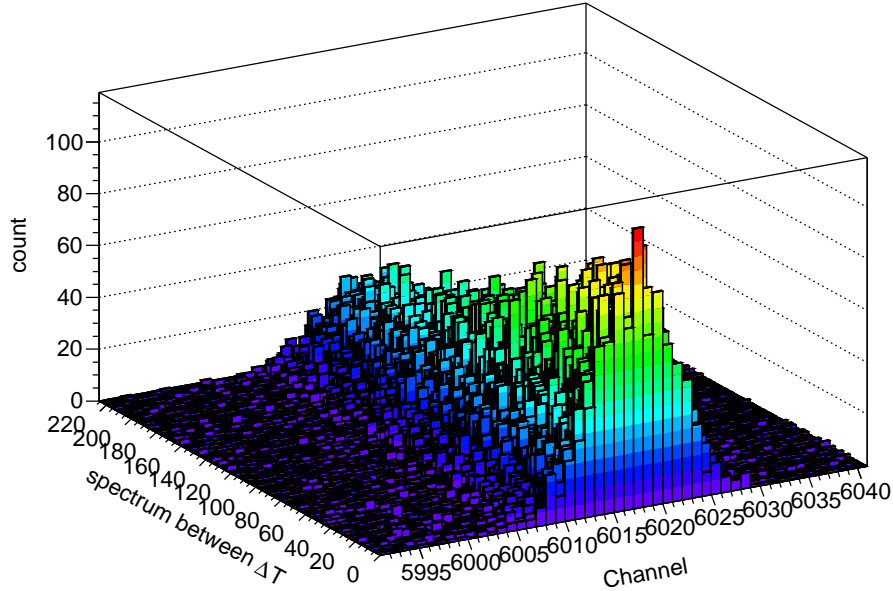


Figure 4.7: Evolution of the spectra between ΔT time interval for the peak 1157 keV of positron decay set (from ground state) of ^{44}Sc .

0.04 hours as measured value of half-life has been obtained while its literature value is 3.97 ± 0.04 hours. On the other hand, half-life value of ^{44}Sc isomeric transition from 271 keV level was not in good precision with the literature value. Reason for this might be due to long half-life and as a result of this reason, weak statistic. Because of the same reason, we could not determine properly the half-life value using 1157 keV peak for ^{44}Sc positron decay from the level 271 keV . Nevertheless, if one takes into account that our sample was not isotopically pure leading to the pollution of the counts by all decays, this might be reasonable basis.

As seen from present results given in Table 4.1 and Table 4.2, although the photon activation method was used, the values were satisfactory and comparable. In Table. 4.3 measured and calculated half-life results in comparison with literature value for ^{44}Sc are shown. Both approaches (PAA and pn-QRPA) present decent comparison with the value

from literature (NUDAT).

4.5 Summary

In present work the spectra for half-life of ^{44}Sc obtained by photon activation approach (PAA) was analyzed by MAESTRO and ROOT packages. The photonuclear reaction was produced using a cLINAC which generated bremsstrahlung photon beam to activate the desired sample. One novelty of this work was the comparison of measured results by (PAA) with those calculated from pn-QRPA model. The other uniqueness was the successful implementation of medical cLINAC for research purpose in the field of nuclear physics. In the measurement part for ^{44}Sc , 18 *MeV* as end point energy was implemented which is bigger than neutron and proton separation energies. Crucial part of the experiment was the measurement of sample spectrum, its calibration and analysis. Present results were calibrated carefully to achieve reliable results. These results demonstrate quite satisfactory comparison with the literature as well as calculated data.

Chapter 5

Implications of pn-QRPA Model Parameters on β -Decay Half-lives

5.1 Implications of Pairing Correlations on Terrestrial Half-lives

The β -decay properties are useful tools to better understand the overall picture of nuclear structure [6]. Research on unstable nuclei reveals that β -decay plays a pivotal role among decay channels [79]. In the field of nuclear astrophysics β -decay properties of neutron deficient nuclei are involved in astrophysical rp -process and are required as input parameters for associated numerical simulations [80].

The β^+ -decay, at times also referred to as positron decay (in which a proton inside a nucleus is converted into a neutron), is a very important decay mode for neutron deficient nuclei. Various nuclear models have been used in the past to study the properties of β -decay. Special mention are those calculations based on gross theory [81], quasiparticle random phase approximation (QRPA) approaches [41, 44, 54, 79, 82–87] and shell model [88]. The gross theory adopts a statistical approach to provide an estimation about the β -decay properties. On the other hand, the shell model and QRPA approaches are microscopic in nature. Implementation of shell model has the obvious constraint of number of basis states

which creeps in as soon as one started to study heavy nuclei. Shell model results might be accurate only for light cases [79]. The QRPA approach leads to precise and schematic information about β -decay properties [82]. Using this method one can reproduce experimental available data for β -decay half-lives in a reliable and efficient manner. Previously the finite-range droplet model (FRDM) and folded-Yukawa single-particle potential was used to study nuclear properties of around 9000 nuclei ranging from ^{16}O to $^{339}\text{136}$ using the QRPA approach [89]. In past research it was reported that β -decay half-lives were significantly affected by the proton-neutron pairing interaction [79, 82, 90].

The calculation and analysis of the half-lives of β^+ -decay for even-even medium mass neutron deficient nuclei with atomic number in the range $Z = 24 - 34$ far from β stability line has been performed in present investigation. Execution of calculation using the proton-neutron QRPA (pn-QRPA) base model in a multi-shell single-particle deformed space with schematic and separable Gamow-Teller (GT) potential was done. In current calculation, the proton-neutron pairing interaction was neglected and considered only the neutron-neutron and proton-proton pairing interactions. It can be notice from results that a reasonable choice of the particle-particle (p.p) and particle-hole (p.h) GT strength parameters may lead to accurate and reliable calculations of β^+ -decay half-lives without going into the need of invoking proton-neutron pairing interaction in the Hartree-Fock-Bogoliubov equation. The calculated half-lives were later compared with measured data [73], FRDM calculation [89] and the recent extended QRPA (EQRPA) calculation [79].

For present study the pn-QRPA model was employed in a deformed basis using the Nilsson+BCS formalism. Further incorporated multi-shell single-particle states and included a schematic interaction [41, 49, 54]. Using this base model half-lives were calculated for neutron deficient even-even nuclei of nuclear β -decay possessing neutron number N in the range of 18 to 36. The formalism and parameters were same as discussed in previous section.

Further investigations about pairing gaps effect the calculated β -decay half-lives. For the calculation of pairing gap, in units of MeV , two different empirical formulae were used. The

first formula was a function of neutron (S_n) and proton (S_p) separation energies (referred to as $Emp - 1$ throughout this manuscript) and shown in Eqs. (5.1 - 5.2)

$$\Delta_{pp} = \frac{1}{4}(-1)^{Z+1}[S_p(A+1, Z+1) - 2S_p(A, Z) + S_p(A-1, Z-1)] \quad (5.1)$$

$$\Delta_{nn} = \frac{1}{4}(-1)^{A-Z+1}[S_n(A+1, Z) - 2S_n(A, Z) + S_n(A-1, Z)] \quad (5.2)$$

The second formula for calculation of pairing gaps was the traditionally used mass dependent recipe and same for protons and neutrons (this formula was referred as $Emp - 2$ throughout this section) and given as

$$\Delta_{pp} = \Delta_{nn} = 12/\sqrt{A} \quad (5.3)$$

5.1.1 Terrestrial Half-lives Calculation for *fp*-Shell Nuclei

The extended QRPA (EQRPA) model, with and without proton-neutron (p-n) pairing, using two body interaction with charge-dependent Bonn forces, was employed for calculation of β^+ /EC-decay half-lives of some medium mass neutron deficient even-even isotopes of Cr, Fe, Ni, Zn, Ge and Se [79]. The pn-QRPA model was used for calculations of β -decay half-lives for selected Cr, Fe, Ni, Zn, Ge and Se isotopes as chosen in Ref. [79]. These nuclei were important constituents of stellar core of massive stars. All selected nuclei were even-even, medium mass, *fp*-shell nuclei which plays key role in *rp*-process. This model could be employed for β -decay half-lives calculation for any arbitrary nucleus and not necessarily for even-even nuclei.

Fig. 5.1 illustrates how the calculated half-life values vary with the pairing gaps using the $Emp - 1$ scheme in present model. Calculated half-lives for the three test nuclei were shown on y-axis.

The values of Δ_{pp} and Δ_{nn} were also shown. The Δ_{pp} values shown on x-axis whereas

Δ_{nn} values, calculated using Eq. (5.1) and (5.2) has been shown on top right corner.

Similarly, half-life dependence on pairing gap values using $Emp - 2$ approach has shown in Fig. 5.2. The values of pairing interactions $\Delta_{pp} = \Delta_{nn}$ were presented along x-axis while calculated half-lives along y-axis. In order to provide a direct comparison with data shown in Ref. [41] and Fig. 5.2 of present work on the y-axis (in the bottom panel) the ratio of calculated to experimental half-life was presented. It may be noted from Fig. 5.1 and Fig. 5.2 that calculated half-life changes with pairing gap values significantly, specially if differ from each other. It can also seen that the variation of calculated half-lives on pairing gaps was rather smooth using the $Emp - 2$ scheme. Further in Fig. 5.2 (below) and its comparison with Fig. 2 of Ref. [92] and Fig. 3 of Ref. [41]. One can notice different values of calculated half-lives for the same values of pairing gaps using the same nuclear model. This difference was attributed to significantly different values of model parameters. It could to be noted that in previous calculations deformation parameter β_2 was calculated using [72] and Q -values from [93]. For cases with no experimental Q -values the corresponding parameters were calculated from [94]. Ref. [41] used the above mentioned references as well as an additional reference [95], for the calculation of these parameters. The latest values for these parameters were used for this work. Our code allows one to vary the model space for calculation of β -decay half-lives from $1\hbar\omega$ to $7\hbar\omega$. In current calculation the model space was chosen as $6\hbar\omega$. It was suspected that previous calculations used a model space of $5\hbar\omega$ for the calcium isotopes. Two additional key model parameters were the (p.p) and (p.h) strength parameters (κ and χ , respectively). The selection choice of these GT force parameters can be seen from [41,92] for previous calculations. The model parameters significantly effect the calculated half-life values. The change in model parameters resulted in different calculated values of β -decay half-lives as compared with previous calculations.

Both increasing and decreasing trend can noted for calculated pn-QRPA half-lives with increasing values of Δ_{nn} and Δ_{pp} in previous calculations. This trend was also witnessed in Fig. 5.1 and Fig. 5.2.

Table 5.1: Measured [73] and pn-QRPA calculated half-lives using the $Emp - 1$ and $Emp - 2$ schemes. Half-lives are stated in units of s and pairing gaps in units of MeV .

Nucleus	$T_{1/2}^{[EXP]}$	$T_{1/2}^{[pn-QRPA(Emp-1)]}$	$T_{1/2}^{[pn-QRPA(Emp-2)]}$	$\Delta_{pp}^{(Emp-1)}$	$\Delta_{nn}^{(Emp-1)}$	$\Delta_{nn,pp}^{(Emp-2)}$
^{38}Ca	0.4437	0.3071	0.3080	1.95824	1.48363	1.94665
^{52}Ca	4.6000	4.4830	4.8265	2.41773	1.00030	1.66410
^{123}Ag	0.3000	0.1712	0.1933	1.32743	0.85250	1.08200

Table 5.1 depicts the comparison of the measured and calculated half-lives for the three nuclei $^{38,52}\text{Ca}$ and ^{123}Ag employing $Emp - 1$ and $Emp - 2$ approaches. The values of pairing gaps were also given.

5.1.2 Pairing Gaps Effect on GT Strength, Terrestrial Half-lives

Next, the impact of changing pairing strength parameters on calculated GT strength distributions was investigated. Fig. 5.3 depicts calculated Gamow-Teller strength distributions for ^{46}Cr , ^{50}Fe and ^{54}Ni using the two schemes.

It was noted that calculated GT strength distribution changes appreciably for ^{46}Cr and remains more or less, same for ^{50}Fe and ^{54}Ni using the two different values of pairing gaps. Similarly Fig. 5.4 displays the corresponding result for ^{62}Zn , ^{66}Ge and ^{70}Se . The calculated strength distributions do change appreciably with change in values of $\Delta_{pp}(\Delta_{nn})$ (albeit less for the case of ^{70}Se).

Table 5.2 shows the value of calculated total strength (in arbitrary units) and centroid values (in units of MeV) of the calculated GT strength distributions using different values of pairing gaps $\Delta_{nn}^{(Emp-1)}$, $\Delta_{pp}^{(Emp-1)}$ and $\Delta_{nn,pp}^{(Emp-2)}$ using $Emp - 1$ and $Emp - 2$ formulae for all the nuclei considered in present investigation. It was clear from Table 5.2 that the pn-QRPA calculated Gamow-Teller strength distribution was a sensitive function of pairing strength parameter. The S_p (S_n) dependent value of pairing strength ($Emp - 1$) results for calculated half-lives were in good comparison with the measured data.

Table 5.3 presents the performance of pn-QRPA model calculation. Shown were this work

Table 5.2: Comparison between pn-QRPA calculated Gamow-Teller strength distributions using different values of pairing gaps: $\Delta_{nn}^{(Emp-1)}$, $\Delta_{pp}^{(Emp-1)}$ and $\Delta_{nn,pp}^{(Emp-2)}$. Shown were the calculated pairing gaps (in MeV), total Gamow-Teller strength, centroid values and cut off energy (in MeV) using the pn-QRPA($Emp-1$) and pn-QRPA($Emp-2$) scheme for selected nuclei.

Nucleus	$\Delta_{nn}^{(Emp-1)}$	$\Delta_{pp}^{(Emp-1)}$	$\Delta_{nn,pp}^{(Emp-2)}$	$\sum GT^{Emp-1}$	$\sum GT^{Emp-2}$	\bar{E}^{Emp-1}	\bar{E}^{Emp-2}	E_{cutoff}
⁴² Cr	1.78	1.97	1.85	11.6	4.58	7.40	5.69	13.8
⁴⁴ Cr	2.07	1.78	1.81	1.66	1.69	0.45	0.45	13.9
⁴⁶ Cr	2.24	1.94	1.77	1.63	1.72	0.43	0.43	8.0
⁴⁶ Fe	3.04	1.79	1.77	10.7	10.9	6.43	7.03	13.5
⁴⁸ Fe	1.79	1.67	1.73	2.42	0.78	1.51	4.59	13.5
⁵⁰ Fe	1.86	1.51	1.70	26.6	26.6	4.37	4.22	8.1
⁴⁸ Ni	1.87	0.66	1.73	40.3	14.0	8.18	9.93	15.6
⁵⁰ Ni	2.09	1.86	1.70	10.4	2.89	6.98	5.39	12.7
⁵² Ni	2.02	1.69	1.66	7.97	5.23	3.92	2.92	11.0
⁵⁴ Ni	1.48	1.64	1.62	1.71	1.71	0.002	0.002	11.0
⁵⁶ Zn	1.71	1.35	1.60	14.4	3.56	9.94	7.03	12.3
⁵⁸ Zn	1.90	1.23	1.58	11.3	25.1	5.30	4.68	9.2
⁶⁰ Zn	1.71	1.64	1.55	1.83	2.78	2.83	2.17	4.5
⁶² Zn	1.60	1.37	1.52	0.98	0.51	1.10	0.06	1.6
⁶⁰ Ge	1.97	1.41	1.55	14.4	4.00	9.30	8.19	12.2
⁶² Ge	1.30	1.21	1.52	13.7	10.7	6.90	7.25	10.0
⁶⁴ Ge	1.90	1.88	1.50	0.58	0.50	1.55	1.58	4.5
⁶⁶ Ge	1.76	3.47	1.48	0.58	0.66	1.05	1.26	2.0
⁶⁴ Se	1.60	1.42	1.50	15.9	14.3	6.87	7.20	12.7
⁶⁶ Se	1.55	1.44	1.48	14.7	6.57	4.36	3.15	10.6
⁶⁸ Se	1.94	2.08	1.46	3.85	8.99	3.18	0.57	4.7
⁷⁰ Se	1.88	1.73	1.43	0.99	1.05	1.24	1.19	2.4

pn-QRPA calculated half-lives along with previous half-life calculations and measured half-lives for selected even-even nuclei. The Q values and experimental half-lives were taken from Ref. [73]. Column IV and Column V presents calculated half-lives using the $Emp-1$ and $Emp-2$ formulae for pairing strength. The last three columns display previous theoretical results. Column VI shows the calculated half-lives using the FRDM model [89] whereas the last two columns show the recent results by using the EQRPA model [79]. Here both EQRPA results with and without the inclusion of proton-neutron pairing correlations were shown. All entries were given in units of s . Comparison between measured data and pn-QRPA($Emp-1$) shows decent agreement.

Table 5.3: Comparison between experimental [73], pn-QRPA^(Emp-1), pn-QRPA^(Emp-2), FRDM model [89] and EQRPA model (with and without pn pairing) [79] calculated half-lives. Q_β values were taken from Ref. [73] and given in units of MeV . All half-lives were given in units of s .

Nucleus	Q_β	$T_{1/2}^{[EXP]}$	$T_{1/2}^{[pn-QRPA(Emp-1)]}$	$T_{1/2}^{[pn-QRPA(Emp-2)]}$	$T_{1/2}^{[FRDM]}$	$T_{1/2}^{[EQRPA(no-pn)]}$	$T_{1/2}^{[EQRPA(with-pn)]}$
⁴² Cr	13.7	0.013	0.013	0.013	0.045	0.013	0.012
⁴⁴ Cr	10.5	0.042	0.038	0.037	0.118	0.056	0.038
⁴⁶ Cr	7.60	0.224	0.218	0.209	0.671	0.404	0.375
⁴⁶ Fe	13.5	0.013	0.012	0.012	0.018	0.014	0.011
⁴⁸ Fe	10.9	0.045	0.042	1.123	0.059	0.037	0.034
⁵⁰ Fe	8.14	0.152	0.135	0.119	0.542	0.301	0.301
⁴⁸ Ni	15.6	0.003	0.003	0.003	0.005	0.005	0.002
⁵⁰ Ni	12.9	0.018	0.018	0.018	0.017	0.018	0.016
⁵² Ni	10.5	0.041	0.039	0.039	0.077	0.056	0.052
⁵⁴ Ni	8.79	0.114	0.102	0.102	0.646	0.329	0.299
⁵⁶ Zn	12.7	0.032	0.029	0.285	0.083	0.025	0.021
⁵⁸ Zn	9.37	0.086	0.048	0.043	0.597	0.192	0.162
⁶⁰ Zn	4.17	142.8	142.5	37.33	>100	268.3	60.29
⁶² Zn	1.62	33094	32101	7399	>100	39372	31372
⁶⁰ Ge	12.2	0.030	0.025	0.245	0.082	0.494	0.424
⁶² Ge	10.1	0.129	0.117	0.081	0.868	0.125	0.102
⁶⁴ Ge	4.52	63.70	48.62	50.16	80.88	752.2	665.6
⁶⁶ Ge	2.12	8136	7452	9557	>100	25125	23144
⁶⁴ Se	12.7	0.030	0.028	0.030	0.097	0.022	0.020
⁶⁶ Se	10.7	0.030	0.031	0.033	0.648	0.073	0.065
⁶⁸ Se	4.71	35.50	35.06	0.759	42.32	17.69	17.68
⁷⁰ Se	2.41	2466	2041	1865	>100	3388	3387

Noticeable differences in calculated pn-QRPA half-lives (using the $Emp - 1$ and $Emp - 2$ formulae) were seen for four cases. For the cases of ^{48}Fe , ^{56}Zn , ^{60}Ge and ^{68}Se the $Emp - 2$ calculated half-lives found considerably bigger than those calculated using the $Emp - 1$ formula. The reason may be traced back to Table 5.2 where it was noted that total calculated GT strength using the $Emp - 1$ formula was appreciably bigger than the corresponding strength using the $Emp - 2$ formula. Bigger total strength translates to bigger decay rates and correspondingly smaller half-lives. For the nucleus ^{68}Se the $Emp - 2$ calculated half-lives were appreciably smaller than those calculated using the $Emp - 1$ formula. It could be noted, from Table 5.2, that for ^{68}Se the $Emp - 2$ formula places the centroid of the GT distribution at considerably lower daughter excitation energies than those using the $Emp - 1$ formula. This in turn translates to smaller corresponding half-lives. In addition the $Emp - 1$ formula calculated total GT strength was also much smaller than those calculated using the $Emp - 2$ formula. The possible reasons for significant effects of pairing gaps on calculated GT strength distributions and consequently on calculated half-lives for ^{48}Fe , ^{56}Zn , ^{60}Ge and ^{68}Se was explored. It can be noticed that for all four cases the first 1^+ states in daughter nuclei were calculated at relatively higher values. For the case of $^{46,48,50}\text{Fe}$ the first 1^+ states were calculated at 0.36, 0.90 and 0.65 MeV , respectively, in daughter. For $^{56,58,60,62}\text{Zn}$ the GT transitions occurred at 1.72, 0.00, 0.07 and 0.00 MeV , respectively. The lowest 1^+ states in daughter $^{60,62,64,66}\text{Ga}$ were calculated at 1.32, 0.58, 0.70 and 0.04 MeV , respectively. For the selenium nuclei $^{64,66,68,70}\text{Se}$ present model calculated lowest lying 1^+ transitions at 0.65, 0.36, 0.92 and 0.08 MeV , respectively. It may be concluded that in cases where present model calculates high-lying 1^+ states in daughter nuclei the pairing gaps had noticeable effects on calculated GT strength distributions and hence on calculated half-lives. The ground state of daughter (odd-odd) nucleus was assumed to be a proton-neutron q-p, pair state of smallest energy. In the current pn-QRPA model, the low-lying states in an odd-odd nucleus were expressed in the q-p picture by proton-neutron pair states (two q-p states) or by states which were obtained by adding two-proton or two-neutron q-p's

(four q-p states) [49]. The two q-p states and four q-p states can be reduced into phonon-correlated one q-p states by the recipe prescribed in Ref. [49]. The phonon-correlated one q-p states were proton/neutron q-p state including contribution from terms representing correlations of RPA phonons admixed by the phonon q-p coupling Hamiltonian (obtained from the separable (p.h) and (p.p) forces by the Bogoliubov transformation). GT transitions of phonon excitations of each excited state were also taken into account. Here it was assumed that the q-p in the parent nucleus remained in the same q-p orbits. It was possible that for these four cases the pairing interaction forces, the phonon-correlated one q-p states/phonon excitations to relatively high-lying excited states. It was evident that β -decay half-lives obtained as a result of present $Emp - 1$ scheme were in excellent agreement with measured half-lives. Better agreement with measured data than the previous calculations of Ref. [79] (using the EQRPA model) and Ref. [89] (using the FRDM model) was achieved.

5.2 Summary

In this portion the calculated β^+ -decay terrestrial half-lives using the pn-QRPA model for neutron deficient fp -shell nuclei was investigated. The β -decay properties of chosen nuclei had a key role to play in the nucleosynthesis problem. It was concluded that the pn-QRPA model, in a multi-shell single-particle deformed space with schematic interaction and smart choice of interaction constants κ for particle-particle and χ for particle-hole parameters, results in accurate prediction of β -decay half-lives. It was shown that pairing gaps strength alter the calculated GT strength distributions and effect the calculated half-life values. It was further demonstrated that $Emp - 1$ formula for calculation of pairing gaps resulted in better prediction of calculated half-life values than by using $Emp - 2$ scheme. Present calculated β^+ -decay half-lives were in excellent agreement with the measured one and showed marked improvement over the former calculations. Because of the available large model space (up to $7\hbar\omega$) present model can calculate the half-lives for any arbitrary

heavy nucleus. It was expected that the current investigation would lead to a better and reliable calculation of β -decay properties of unstable nuclei.

5.3 Newly Calculated Phase Space Factor

The phase space factors (PSF) for β -decay were calculated since long time ago [96, 97] and were considered to be evaluated with sufficient accuracy. However, in those works the distortion of the electron wave functions (w.f.) by the Coulomb field of the nucleus was taken into account through Fermi functions which were expressed in terms of approximate radial solutions of the Dirac equation at the nuclear surface. Also, other corrections were introduced in the calculations in approximate ways. Thus, the screening effect on the β spectrum included by various recipes, for example by replacing the $V(Z)$ potential with a momentum dependent screening (for low energy positrons) [97] and by modifying the electron radial w.f. [98, 99]. Also, the finite size of the nucleus (FNS) was taken into account by adding to the Fermi functions obtained in the "point-nucleus" approximation, corrections that depend on the β particle energy and nuclear charge Z [100, 101]. Also, for the nuclear radius, older formula was used [97, 102]. For the EC process the electron bound-state radial w.f. were also obtained as approximate solution of the Dirac equation evaluated at the nuclear surface. They could improved by including exchange and overlap corrections, which were obtained within a relativistic HF approach.

In this work recalculation of the computation of the PSF involved in the positron decay and electron capture (EC) processes for light and heavy nuclei of experimental interest will be performed. The Dirac equation was solved numerically with a Coulomb potential derived from a realistic proton distribution in the nucleus which includes the FNS correction. The numerical procedure follows the power series method described in Ref. [103] and was similar to that described in Refs. [104, 105]. The screening effect was introduced by using a screened Coulomb potential, obtained by multiplying the Coulomb potential by a function

$\phi(x)$, solution of the Thomas-Fermi equation obtained by the Majorana method [106]. The accuracy imposed in present numerical algorithms used to solve the Dirac equation which always exceeds the convergence criteria given in previous references. Also, a more efficient procedure to identify without ambiguity the electron bound states were developed.

5.3.1 For β^+ /*Electron Capture-Decay*

In order to make comparison between the actual PSF values found in literature and this study, the same PSF were computed with the approach described in Ref. [97] and using the same Q -values. For positron decays present work results were in close agreement with the previous results, while for the EC process relevant differences were noticed. For these processes it was found that the screening effect shows notable influence on the computed PSF values for light nuclei. Further, re-computation of the same PSF values using up-dated Q -values, reported recently in literature [107], which for several light nuclei differ significantly from the older ones. As an example, the maximum β -particle energy (referred to as W_0 throughout this section) stated in Table 2 of [108]. These W_0 values differ considerably from those given in [107, 109]. One reason for this big difference could be that Wilkinson and Macefield, in order to compare their calculation with those performed earlier by Towner and Hardy [110], restricted their phase space to only pure Fermi transitions. In other words, the Gamow-Teller window was not accessed in phase space calculation of [108]. Thus, in this paper, new PSF values were computed with a more accurate method and using updated Q -values, for a large number of nuclei of experimental interest. Present calculations can be useful for more reliable computation of the beta-decay rates of nuclei far from the stability line, as well as for better understanding of the stellar evolution.

A nucleus with atomic mass A and charge Z decays for an allowed β -branch was given by:

$$\lambda_0 = g^2/2\pi^3 \int_1^{W_0} pW(W_0 - W)^2 S_0(Z, W) dW, \quad (5.4)$$

where g stands for the weak interaction coupling constant, p for the momentum of β -particle, $W = \sqrt{p^2 + 1}$ shows the total energy of β -particle and W_0 shows the maximum β particle energy. $W_0 = Q - 1$, in β^+ -decay (Q was the mass difference between initial and final states of neutral atoms). Eq. (5.4) was written in natural units ($\hbar = m = c = 1$) so that the unit of momentum is mc , the unit of energy was mc^2 , and the unit of time was \hbar/mc^2 . The shape factors $S_0(Z, W)$ for allowed transitions which appear in Eq. (5.4) could defined as:

$$S_0(Z, W) = \lambda_1(Z, W) |M_{0,1}|^2, \quad (5.5)$$

where $M_{0,1}$ shows the nuclear matrix elements and the Fermi functions $\lambda_1(Z, W)$. Thus, for calculating the β^+ -decay rates one needs to calculate the nuclear matrix elements and the PSF, that can be defined as:

$$F_{BP} = \int_1^{W_0} pW(W_0 - W)^2 \lambda_1(W) dW. \quad (5.6)$$

For the allowed β -decays the Fermi functions are expressed as:

$$\lambda_1(Z, W) = \frac{g_{-1}^2 + f_1^2}{2p^2}, \quad (5.7)$$

where $g_{-1}(Z, W)$ and $f_1(Z, W)$ are the large and the small radial components of the positron radial wave functions evaluated at the nuclear radius R which can be obtained by solving the Dirac equation:

$$\begin{aligned} \left(\frac{d}{dr} + \frac{\kappa}{r}\right) g_{\kappa}(W, r) &= (W + V + 1)f_{\kappa}(W, r) \\ \left(\frac{d}{dr} + \frac{\kappa}{r}\right) f_{\kappa}(W, r) &= -(W + V - 1)g_{\kappa}(W, r) \end{aligned} \quad (5.8)$$

where V denotes the central potential for the positron and $\kappa = (l - j)(2j + 1)$ for the relativistic quantum number. It can be noted that Eq. (5.8) was written in natural units.

An important step in the PSF calculation for β^+ decay was the method of obtaining the positron continuum radial functions. For this, a new method (code) of solving the Dirac equation was developed, which was adapted from the method used previously for the computation of PSF for double beta decay (DBD) process [111, 112].

By solving Eq. (5.8) in a nuclear potential $V(r)$, derived from a realistic proton density distribution in the nucleus. This was done by solving the Schrodinger equation for a Woods-Saxon potential. In this case,

$$V(Z, r) = \alpha \hbar c \int \frac{\rho_e(\vec{r}')}{|\vec{r} - \vec{r}'|} d\vec{r}', \quad (5.9)$$

In the case of the β^+ process, the potential used to obtain the electron w.f. was,

$$rV_{\beta^+}(Z, r) = (rV(Z, r) + 1) \times \phi(r) - 1 \quad (5.10)$$

to taken into account the fact that β -decay releases a final negative ion with charge -1, $V(Z, r)$ was positive. In present approach, the solution of the Thomas-Fermi equation as an universal function, giving an effective screening was considered. Here the product $\alpha \hbar c = 1$, for atomic units. The asymptotic potential between a positron and an ionized atom was $rV_{\beta^+} = -1$. In this case, the charge number $Z = Z_0 - 1$ corresponds to the daughter nucleus, Z_0 being the charge number of the parent nucleus. Asymptotically $\phi(r)$ tends to 0.

For β^+ -decays, it can be noticed that previous PSF results computed with approximate

methods [108, 110] for sixteen nuclei of astrophysical interest. Table 5.4 displays the PSF values for these nuclei calculated with present new method (TW) and for comparison, the values taken from [108, 110]. Also the PSF values computed by us using the recipe described in [97].

Table 5.4: Calculated phase space of β^+ -decay (BP) compared with previous calculations. The value of maximum β -decay energy was taken from [108] for pure Fermi transitions. The last two columns show present calculated results.

Nucleus	W_0 [108] (MeV)	F_{BP} [110]	F_{BP} [108]	F_{BP} [TW]	F_{BP} [97]
^{10}C	0.8884	2.361	2.361	2.325	2.326
^{14}O	1.8098	43.398	43.378	42.822	42.814
^{18}Ne	2.383	136.83	136.83	135.19	135.08
^{22}Mg	3.109	427.02	426.88	422.19	421.51
^{26}Al	3.211	483.84	483.68	478.3	477.43
^{26}Si	3.817	1036.8	1035.9	1025.51	1023.059
^{30}S	4.439	1990.2	1987.8	1969.24	1963.9
^{34}Cl	4.468	2014.7	2013.4	1993.13	1987.4
^{34}Ar	5.021	3388.3	3383.8	3351.58	3339.85
^{38}K	5.028	3346.9	3344.9	3312.82	3300.54
^{38}Ca	5.620	5515.9	5510.3	5457.95	5449
^{42}Sc	5.409	4533.5	4531.7	4490.19	4462.21
^{42}Ti	5.964	7025.4	7024.1	6934.9	6853.74
^{46}V	6.032	7285.9	7284.2	7186.04	7091.9
^{50}Mn	6.609	10818	10810	10492.76	10262
^{54}Co	7.227	15956	15951	14988.470	14412.5

One can see that the agreement between TW results and the other results was in general under 1%, except the last two (heavy) nuclei where the differences reach $\sim 3\%$. Table 5.5 displays this work computed PSF with the new method for few heavy nuclei for which previous calculation results were not found. For comparison, the computed PSF values were same as in the recipe adopted from [97]. W_0 -values were taken from [113], for both sets of calculations. One can notice a rather good agreement between the two sets of results, with differences generally, a few percent. There was one exception, ^{105}Ag where the difference was large (\sim a factor 10). This was a case where W_0 -value was very small (0.325 MeV), and this might make present numerical routine inaccurate at such small values. However,

this discrepancy may not be so significant, as long as the calculated PSF value was small enough to have little contribution to the corresponding beta-decay rates.

Table 5.5: Calculated phase space of β^+ -decay (BP) for heavy nuclei compared with the ones calculated by using recipe of [97].

Nucleus	W_0 [113] (Mev)	$F_{BP}[TW]$	F_{BP} [97]
^{52}Fe	1.3525	8.3403	8.4132
^{56}Ni	1.1109	3.4439	3.5250
^{62}Zn	0.5974	0.2344	0.2438
^{66}Ga	4.153	1125.6442	1132.5483
^{76}Br	3.9409	835.1982	843.3343
^{81}Rb	1.2161	4.3222	6.8878
^{88}Y	2.6006	120.2644	121.8624
^{90}Nb	5.0893	2503.0555	2533.7049
^{102}Cd	1.565	11.2214	11.5267
^{103}In	5.0005	2100.3727	2136.0153
^{105}Ag	0.325	0.0102	0.1127
^{107}Sb	6.837	8528.5047	8931.8197
^{113}Sb	2.8891	168.1487	172.0209
^{113}Te	5.048	2124.1816	2165.2927
^{115}I	4.7029	1517.2376	1549.2409
^{116}I	6.7547	7913.1790	8272.0244
^{116}Xe	3.235	352.3565	361.4082
^{120}Ba	3.98	678.0918	705.0294
^{120}Xe	0.5587	0.1047	0.1108
^{126}Cs	3.7731	542.4653	563.8184
^{182}Re	0.1836	0.0002	0.0003
^{205}Bi	1.6835	12.3984	13.4576

Table 5.6 shows state-by-state transitions for the two cases. Shown were also the adopted NMEs using the pn-QRPA model, the calculated PSFs (separately for both EC and β^+ -decay reactions), partial half-lives (PHL), Q -values and branching ratios $I_{(\beta^+/EC)}$. The branching ratio ' I ' for each transition was calculated using the formula

$$I = \frac{T_{1/2}}{t_f} \times 100(\%), \quad (5.11)$$

where $T_{1/2}$ for the total β -decay half-life and t_f for the calculated partial half-life of the corresponding transition.

The entries in the first two columns of Table 5.6 were model dependent. The excited states in daughter nuclei (shown in the first column) and NMEs (presented in the second column) were calculated using the pn-QRPA model. The computed excited states satisfied the selection criteria for allowed transitions within the chosen model. A different nuclear model can change the entries in the first two columns and as stated earlier, was not the focus of current study. Q -values were presented in column III and column VI of Table 5.6 using following relation

$$Q_{EC} = m_p - m_d - E_x, \quad (5.12)$$

and

$$Q_{BP} = m_p - m_d - E_x - 2m_e c^2. \quad (5.13)$$

Here m_p and m_d denotes masses of parent and daughter nuclei, respectively whereas E_x for the calculated energy levels in the daughter nucleus. It can be noted that present recipe results in a systematic smaller values of calculated PSF for the EC reaction which in turn lead to systematically bigger values of calculated PHL. For the nucleus ^{56}Ni we noted calculation of much smaller PSF for EC decay to daughter energies using our recipe. The PSFs calculated from (GM) recipe was on average within 3 % smaller. This in turn led to a 4 % larger calculated half-life value for ^{56}Ni using our recipe.

Electron capture was always an alternate decay mode for radioactive isotopes that do not have sufficient energy to decay by positron emission. This was a process which competes with positron decay. In order for EC leading to a vacancy in say, the K-shell to occur, the atomic mass difference between initial and final states, Q , must be greater than the binding energy of a K-shell electron in the daughter atom, ϵ_K . The energy carried off by the neutrino given by

Table 5.6: State-by-state comparison of calculated PSF (for β^+ /EC-decay) using recipe of [97] and current prescription (TW). Shown also were the daughter energy levels, nuclear matrix elements NME, Q values, partial half-lives (PHL) for β^+ /EC-decay and branching ratio $I_{(\beta^+/EC)}$ of the selected nuclei.

⁵² Fe											
E_x (MeV)	NME	Q_{EC} (MeV)	$F_{EC}^{(GM)}$ [97]	$F_{EC}^{(TW)}$	Q_{β^+} (MeV)	$F_{\beta^+}^{(GM)}$ [97]	$F_{\beta^+}^{(TW)}$	PHL ^(GM) [97]	PHL ^(TW)	$I_{(\beta^+/EC)}^{(GM)}$ [97]	$I_{(\beta^+/EC)}^{(TW)}$
0.000	0.02768	2.3733	1.22206	1.20150	1.3512	8.41032	8.31627	1.501E+04	1.519E+04	85.701	85.713
0.004	0.00170	2.3693	1.21794	1.19744	1.3472	8.30402	8.21074	2.466E+05	2.496E+05	5.2160	5.2160
0.196	0.00325	2.1773	1.02771	1.01077	1.1552	4.29193	4.24688	2.313E+05	2.340E+05	5.5620	5.5640
0.291	0.00134	2.0823	0.94007	0.92425	1.0602	2.98166	2.94390	7.605E+05	7.710E+05	1.6920	1.6890
0.720	0.00253	1.6533	0.59198	0.58175	0.6312	0.33565	0.32942	1.707E+06	1.738E+06	0.7540	0.7490
0.939	0.00087	1.4343	0.44543	0.43734	0.4122	5.69E-02	5.53E-02	9.208E+06	9.390E+06	0.1400	0.1390
1.011	0.00350	1.3623	0.40124	0.39435	0.3402	2.53E-02	2.47E-02	2.679E+06	2.727E+06	0.4800	0.4780
1.362	0.00255	1.0113	0.22076	0.21663	-0.0107	-	-	7.108E+06	7.244E+06	0.1810	0.1800
1.467	0.00052	0.9063	0.17691	0.17374	-0.1157	-	-	4.367E+07	4.447E+07	0.0290	0.0290
1.685	0.00017	0.6883	1.01706E-01	9.97773E-02	-0.3371	-	-	2.352E+08	2.397E+08	0.0050	0.0050
1.754	0.00009	0.6193	8.22094E-02	8.06130E-02	-0.4027	-	-	5.318E+08	5.424E+08	0.0020	0.0020
1.821	0.00972	0.5523	6.54251E-02	6.39581E-02	-0.4697	-	-	6.293E+06	6.437E+06	0.2040	0.2020
2.119	0.00282	0.2543	1.35835E-02	1.32041E-02	-0.7677	-	-	1.045E+08	1.075E+08	0.0120	0.0120
2.143	0.00572	0.2303	1.10469E-02	1.07735E-02	-0.7917	-	-	6.338E+07	6.499E+07	0.0200	0.0200

Table 5.7: Same as Table 5.6 but for ⁵⁶Ni depicting highest PD among all selected cases

E_x (MeV)	NME	Q_{EC} (MeV)	$F_{EC}^{(GM)}$ [97]	$F_{EC}^{(TW)}$	Q_{β^+} (MeV)	$F_{\beta^+}^{(GM)}$ [97]	$F_{\beta^+}^{(TW)}$	PHL ^(GM) [97]	PHL ^(TW)	$I_{(\beta^+/EC)}^{(GM)}$ [97]	$I_{(\beta^+/EC)}^{(TW)}$
⁵⁶ Ni											
1.196	0.00038	0.9357	0.24313	0.23335	-0.0862	-	-	4.315E+07	4.496E+07	0.986	0.988
1.247	0.00019	0.8847	0.21729	0.20842	-0.1372	-	-	9.852E+07	1.027E+08	0.432	0.432
1.252	0.00034	0.8797	0.21476	0.20605	-0.1422	-	-	5.550E+07	5.785E+07	0.767	0.768
1.288	0.00009	0.8437	0.19721	0.18939	-0.1782	-	-	2.137E+08	2.225E+08	0.199	0.200
1.289	0.00009	0.8427	0.19676	0.18894	-0.1792	-	-	2.315E+08	2.411E+08	0.184	0.184
1.299	0.00008	0.8327	0.19227	0.18444	-0.1892	-	-	2.690E+08	2.804E+08	0.158	0.158
1.309	0.00001	0.8227	0.18754	0.18000	-0.1992	-	-	1.739E+09	1.812E+09	0.024	0.024
1.313	0.00002	0.8187	0.18593	0.17824	-0.2032	-	-	1.226E+09	1.278E+09	0.035	0.035
1.318	0.00001	0.8137	0.18344	0.17605	-0.2082	-	-	1.764E+09	1.838E+09	0.024	0.024
1.363	0.00000	0.7687	0.16374	0.15695	-0.2532	-	-	4.349E+10	4.537E+10	0.001	0.001
1.363	0.00000	0.7687	0.16372	0.15695	-0.2532	-	-	2.361E+10	2.463E+10	0.002	0.002
1.373	0.00000	0.7587	0.15927	0.15285	-0.2632	-	-	7.543E+10	7.860E+10	0.001	0.001
1.471	0.00000	0.6607	0.12034	0.11558	-0.3612	-	-	1.514E+10	1.577E+10	0.003	0.003
1.482	0.00001	0.6497	0.11645	0.11172	-0.3722	-	-	3.315E+09	3.455E+09	0.013	0.013
1.503	0.00001	0.6287	0.10904	0.10454	-0.3932	-	-	3.722E+09	3.883E+09	0.011	0.011
1.711	0.07180	0.4207	4.82788E-02	4.62700E-02	-0.6012	-	-	1.154E+06	1.204E+06	36.85	36.85
1.742	0.13730	0.3897	4.13076E-02	3.95910E-02	-0.6322	-	-	7.058E+05	7.364E+05	60.30	60.30

$$q_K = Q - \epsilon_K \quad (5.14)$$

If the energy requirement $Q > \epsilon_K$ was satisfied EC from the K-shell was more probable than that from any other shell because of the greater density at the nucleus of the K-shell electrons. The total K-shell capture rate can be expressed as

$$\lambda_{EC,K}^0 = \lambda_K^0 B_K, \quad (5.15)$$

where

$$\lambda_K^0 = \frac{g^2 |M_{0,1}|^2}{4\pi^2} q_K^2 g_K^2, \quad (5.16)$$

where g^2 stands for a constant (with dimension of $time^{-1}$), the M's for specific combinations of nuclear matrix elements, g_K for the large component of the bound-state radial w.f. of the captured K-shell electron (evaluated at the nuclear surface R_A), q_K was the neutrino energy in units of mc^2 and B_K was the "exchange" correction factor for the K-shell. In analogy with Eq. (5.15), the L-shell total capture rate will be

$$\lambda_{EC,L_i}^0 = \lambda_{L_i}^0 B_{L_i}, \quad (5.17)$$

where L_i denotes a particular L -subshell. The contribution of L_1 pertaining to the $2s_{1/2}$ orbital was the most important, so for present calculations only the contribution of this subshell has been taken into account. The expressions for $\lambda_{L_1}^0$ can be obtained from Eq. (5.16) by the replacement of q_K, g_K by q_{L_1}, g_{L_1} . EC from the M, N and higher shells may be defined in a similar fashion, but they have negligible contributions in comparison with the K and L shells. Hence for an allowed transition, the PSF expression of EC can be written in this approximation as follows

$$F_{EC}^{K,L_1} = \frac{\pi}{2} (q_K^2 g_K^2 B_K + q_{L_1}^2 g_{L_1}^2 B_{L_1}). \quad (5.18)$$

For the q_{K/L_1} quantities the following expressions were used:

$$q_{K/L_1} = W_{EC} - \epsilon_{K/L_1} \quad (5.19)$$

Where, W_{EC} was the Q -value of the β^+ -decay in $m_e c^2$ units, ϵ_i were the binding energies of the $1s_{1/2}$ and $2s_{1/2}$ electron orbitals of the parent nucleus, g_i stands for the radial densities on the nuclear surface. $B_i \approx 1$ represent the values of the exchange correction. These were due to an imperfect overlap of the initial and final atomic states caused by the one unit charge difference [114]. In current method these exchange corrections were considered to be unity, for the investigated nuclei, the estimated error in doing that was under 1%. The relation $W_0 = W_{EC} - 1$ holds.

The wave function were normalized such that

$$\int_0^\infty [g_{n,\kappa}^2(r) + f_{n,\kappa}^2(r)] dr = 1. \quad (5.20)$$

For simplicity, solutions of the Dirac equations $g_{n,\kappa}$ and $f_{n,\kappa}$ that were divided by the radial distance r were considered. An asymptotic solution was obtained by means of the WKB approximation and by considering that the potential V was negligibly small:

$$\frac{f_{n,\kappa}}{g_{n,\kappa}} = \frac{c\hbar}{\epsilon + m_e c^2} \left(\frac{g'_{n,\kappa}}{g_{n,\kappa}} + \frac{\kappa}{r} \right) \quad (5.21)$$

where

$$\frac{g'_{n,\kappa}}{g_{n,\kappa}} = -\frac{1}{2}\mu' \mu^{-1} - \mu \quad (5.22)$$

with

$$\mu = \left[\frac{\epsilon + m_e c^2}{\hbar^2 c^2} (V - \epsilon + m_e c^2) + \frac{\kappa^2}{r^2} \right]^{1/2}. \quad (5.23)$$

In this calculation the number node $n=0$ and $n=1$ were used for the orbital $1s_{1/2}$ and $2s_{1/2}$

respectively, κ being -1. Numerically the eigenvalues of the discrete spectrum were obtained by matching two numerical solutions of the Dirac equation: the inverse solution that starts from the asymptotic conditions and the direct one that starts at $r=0$.

For the *EC* processes, the potential used to obtain the electron w.f. reads

$$rV_{EC}(Z, r) = rV(Z, r)\phi(r) \quad (5.24)$$

and the charge number $Z = Z_0$ corresponds to the parent nucleus $V(Z, r)$ was negative.

The numerical solutions of the Dirac equation were obtained within the power series method of Ref. [103], by using similar numerical algorithm as that of Refs. [104, 105]. The method provide numerical solutions of the Dirac equation for central fields. The radial w.f. was expanded as in an infinite power series that depends on the radial increment and the potential values. The w.f. was calculated step by step in the mesh points. The increment and the number of terms in the series expansion determine the accuracy of the solutions. In present calculations, the increment interval was 10^{-4} *fm* and at least 100 terms were taken into account in the series expansion.

These values exceed the convergence criteria of Ref. [104]. To renormalize the numerical solutions this work made use of the fact that at very large distances the behavior of the wave function must resemble to that of the Coulomb function. Therefore, the amplitudes and the phase shifts can be extracted by comparing the numerical solution with the analytical one. For discrete states, the asymptotic behavior of the w.f. gives a guess for the inverse solutions. The eigenvalue was obtained when the direct solutions and the inverse ones match together. Present work constructed an adequate procedure to find the bound states of the electron up to an accuracy of 0.3 *keV*, or lower by searching solutions up to 130 *keV* binding energies.

In this range of energies, all the possible bound state energies were considered. This study calculates the solutions starting outward from $r = 0$ and inward from a very large value of the radius r . The bound states should be obtained when both solutions were equal

in an intermediate point, for the two components of the wave function. The radial wave functions $f_{n,\kappa}$ and $g_{n,\kappa}$ that had same number of nodes $n=0$ or 1 were selected.

For the PSF computation, all integrals in Eq. (5.8) were performed accurately with Gauss-Legendre quadrature in 32 points. Present investigation also calculated the PSF for EC process using Eq. (5.18) but employing essentially the formalism adopted by Ref. [96]. Here, the electron radial density (and density ratios) as given in Table 2 of [96] was used. Further present calculation used values of exchange corrections for the various shells which were slightly different than unity and given in Table 1 of [96]. Binding energies were also taken from same reference.

Table 5.8 present this work results for EC for the same set of nuclei. The Q -values for positron decay were taken from Ref. [108] for nuclei marked with \star . For the rest of nuclei the Q -values were taken from Ref. [113]. Together with the PSF values for EC, the electron densities, g_{K,L_1} , their ratios and the binding energies ϵ for the orbitals $1s_{1/2}$ and $2s_{1/2}$ were also given in Table 5.8. Comparison of the results was performed between the new method (TW) and those calculated using the recipe of Ref. [96]. For these transitions the differences between the two sets of results were significantly larger than for the positron decays, ranging from a few percent to about a mammoth 35%. Which attribute these differences in the calculated PSF values mainly due to electron densities g_K , whose values calculated with the "old" and "new" methods differ significantly from each other. The influence of the screening effect on the PSF values was also checked. It was found that while for the positron decays this effect was very small for the EC transitions there were some differences between the "screened" and "un-screened" PSF values. For small values of Z the results without screening give PSF values that were 10-15% larger than those listed in Table 5.8. For heavier nuclei, these differences are only up to 2-3%. The screening effect in PSF calculation was more important for light nuclei and lead to a decrease in the PSF values up to 15%. Finally, Table 5.9 displays PSF values for EC transitions, re-computed with up-dated Q -values taken from Ref. [107].

Table 5.8: Calculated phase space factors F_{EC} for electron capture (assuming exchange corrections to be equal to 1). The value of maximum β -decay energy was taken from [108] for pure Fermi transitions. The electron densities, their ratios, and the binding energies ϵ were also provided for the orbitals $1s_{1/2}$ and $2s_{1/2}$, including those given in [96]. Binding energies were given in units of keV .

Nucleus	Q_{β^+} (MeV)	g_K^2 [96]	g_K^2 [TW]	$g_{L_1}^2/g_K^2$ [96]	$g_{L_1}^2/g_K^2$ [TW]	ϵ_K [96]	ϵ_K [TW]	ϵ_{L_1} [96]	ϵ_{L_1} [TW]	F_{EC}^{K,L_1} [TW]	F_{EC}^{K,L_1} [96]
$^{10}\text{C}^*$	1.9104	0.00031	0.00031	0.04930	0.02867	0.18790	0.62660	0.12600	0.01176	0.00703	0.00640
$^{14}\text{O}^*$	2.83186	0.00075	0.00065	0.05640	0.04420	0.40160	1.03733	0.02440	0.03251	0.03297	0.03786
$^{18}\text{Ne}^*$	3.405	0.00151	0.00118	0.05840	0.05794	0.68540	1.48302	0.03400	0.06659	0.08713	0.11005
$^{22}\text{Mg}^*$	4.131	0.00268	0.00199	0.06660	0.06811	1.07210	2.11143	0.06330	0.15721	0.218	0.29060
$^{26}\text{Al}^*$	4.2331	0.00344	0.00251	0.06990	0.07265	1.30500	2.40715	0.08940	0.14631	0.27558	0.39270
$^{26}\text{Si}^*$	4.839	0.00435	0.00312	0.07290	0.07661	1.55960	2.74689	0.11770	0.18077	0.47240	0.65060
$^{30}\text{S}^*$	5.461	0.00664	0.00467	0.07810	0.08342	2.14550	3.49498	0.18930	0.25934	0.90680	1.27140
$^{34}\text{Cl}^*$	5.4908	0.00807	0.00563	0.08040	0.08628	2.47200	3.91749	0.22920	0.30899	1.10727	1.56600
$^{34}\text{Ar}^*$	6.043	0.00970	0.00675	0.08240	0.08862	2.82240	4.33190	0.27020	0.36199	1.61130	2.28490
$^{38}\text{K}^*$	6.05	0.01156	0.00802	0.08440	0.09079	3.20600	4.77984	0.32630	0.41921	1.92311	2.73480
$^{38}\text{Ca}^*$	6.642	0.01367	0.00947	0.08620	0.09259	3.60740	5.25087	0.37710	0.48351	2.74237	3.90650
$^{42}\text{Sc}^*$	6.4311	0.01600	0.01113	0.08790	0.09430	4.03810	5.73657	0.43780	0.54865	3.02434	4.28930
$^{42}\text{Ti}^*$	6.986	0.01870	0.01300	0.08960	0.09579	4.49280	6.25222	0.50040	0.62068	4.17496	5.92320
$^{46}\text{V}^*$	7.0543	0.02170	0.01512	0.09100	0.09699	4.96640	6.78377	0.56370	0.69826	4.95575	7.02120
$^{50}\text{Mn}^*$	7.6311	0.02870	0.02016	0.09380	0.09920	5.98920	7.92722	0.69460	0.86703	7.74617	10.9103
^{52}Fe	2.374	0.0328	0.0232	0.0950	0.0987	7.1120	8.5130	0.8461	0.958	0.859	1.2033
$^{54}\text{Co}^*$	8.2498	0.03730	0.02651	0.09620	0.10077	7.11200	9.14731	0.84610	1.05584	11.91799	16.6144
^{56}Ni	2.136	0.0423	0.0303	0.0974	0.1013	8.3328	9.7882	1.0081	1.158	0.907	1.2580
^{62}Zn	1.626	0.0538	0.0390	0.0995	0.1025	9.6586	11.157	1.1936	1.380	0.675	0.9261
^{66}Ga	5.175	0.0604	0.0410	0.1006	0.1029	10.3671	11.875	1.2977	1.498	7.80	10.613
^{76}Br	4.963	0.0935	0.0704	0.1035	0.1048	13.4737	15.000	1.7820	2.021	11.45	15.162
^{81}Rb	2.23815	0.1149	0.0883	0.1063	0.1080	15.1997	16.690	2.0651	2.263	9.069	11.744
^{88}Y	3.6226	0.1402	0.1091	0.1080	0.1174	17.0384	18.450	2.3725	2.438	9.528	12.114
^{90}Nb	6.111	0.170	0.1344	0.1098	0.1059	18.9856	20.421	2.6977	2.994	33.17	41.975
^{102}Cd	2.587	0.319	0.2663	0.1159	0.1102	26.7112	28.044	4.0180	4.351	11.66	14.019
^{103}In	6.050	0.348	0.2930	0.1168	0.1116	27.9399	29.232	4.2375	4.548	71.05	84.541
^{105}Ag	1.345	0.293	0.2423	0.1150	0.1086	25.5140	26.864	3.8058	4.161	2.816	3.4256
^{107}Sb	7.920	0.413	0.3526	0.1187	0.1096	30.4912	31.726	4.6983	5.095	146.5	172.43
^{113}Sb	3.913	0.413	0.3516	0.1187	0.1096	30.4912	31.726	4.6983	5.095	35.38	41.804
^{113}Te	6.070	0.449	0.3844	0.1196	0.1113	31.8138	33.041	4.9392	5.314	93.70	109.93
^{115}I	5.729	0.488	0.4121	0.1205	0.1124	33.1694	34.345	5.1881	5.542	91.54	106.40
^{116}I	7.780	0.488	0.4215	0.1205	0.1124	33.1694	34.345	5.1881	5.542	169.3	196.75
^{116}Xe	4.450	0.529	0.4609	0.1215	0.1123	34.5644	35.705	5.4528	5.822	60.15	69.410
^{120}Ba	5.00	0.623	0.5496	0.1234	0.1130	37.4406	38.514	5.9888	6.375	90.65	103.51
^{120}Xe	1.617	0.529	0.4599	0.1215	0.1123	34.5644	35.705	5.4528	5.821	7.72	8.9482
^{126}Cs	4.824	0.574	0.501	0.1224	0.112	35.9846	37.111	5.7143	6.128	76.88	88.697
^{182}Re	2.800	2.69	2.593	0.1448	0.128	71.6764	72.491	12.5267	13.26	22.86	24.152
^{205}Bi	2.708	4.88	4.837	0.1561	0.138	90.5259	91.373	16.2370	17.25	228.17	233.83

Table 5.9: Calculated phase space factors F_{EC} for electron capture, with Q -values from [107].

Nucleus	Q_{EC} [107] (MeV)	F_{EC} [TW]	F_{EC} [96]	F_{BP} [TW]	F_{BP} [97]
¹⁰ C	3.64613	0.07318	2.33265	226.780	226.834
¹⁴ O	5.14131	0.21794	0.12483	1644.76	1643.41
¹⁸ Ne	4.44215	0.27831	0.18733	677.970	677.912
²² Mg	4.77904	0.61616	0.39020	995.887	995.685
²⁶ Al	4.00231	0.62642	0.35240	343.398	343.658
²⁶ Si	5.06645	0.51788	0.71694	1339.344	1339.30
³⁰ S	6.13834	1.14585	1.61931	3805.276	3803.16
³⁴ Cl	5.48869	1.10642	1.57889	1994.797	1995.09
³⁴ Ar	6.05858	1.61963	2.31915	3410.133	3409.96
³⁸ K	5.91093	1.83565	2.64042	2917.839	2918.62
³⁸ Ca	6.73867	2.82284	4.07367	5924.355	5929.26
⁴² Sc	6.42269	3.01643	4.33609	4470.946	4471.87
⁴² Ti	7.01275	4.20702	6.05196	7100.190	7130.06
⁴⁶ V	7.04865	4.94781	7.11022	7175.692	7209.06
⁵⁰ Mn	7.63042	7.74479	11.0705	10516.941	10744.5
⁵² Fe	2.37330	0.8584	1.22082	14942.286	15765.2
⁵⁴ Co	8.24017	11.89015	16.8306	8.354	8.43206
⁵⁶ Ni	2.13175	0.9029	1.27259	3.444	3.49486
⁶² Zn	1.61859	0.6687	0.93259	0.234	0.24131
⁶⁶ Ga	5.17225	7.7902	10.7797	1125.644	1131.60
⁷⁶ Br	4.96024	11.439	15.4388	835.295	841.531
⁸¹ Rb	2.23696	2.9044	3.84415	4.321	4.41092
⁸⁸ Y	3.62067	9.5180	12.3759	120.264	121.864
⁹⁰ Nb	6.10809	33.141	42.9337	2502.372	2526.00
¹⁰² Cd	2.58562	11.652	14.4027	11.221	11.5468
¹⁰³ In	6.01928	70.333	15.7203	2099.402	2133.61
¹⁰⁵ Ag	1.34679	2.8233	3.53114	0.01027	1.12362
¹⁰⁷ Sb	7.85483	144.059	174.745	8528.505	8918.59
¹¹³ Sb	3.90909	35.311	42.9919	168.122	172.036
¹¹³ Te	6.06682	93.601	113.234	2124.182	2162.53
¹¹⁵ I	5.72192	91.3148	109.531	1509.977	1547.75
¹¹⁶ I	7.77260	168.959	202.635	7930.046	8250.78
¹¹⁶ Xe	4.44315	59.963	71.4659	354.467	361.241
¹²⁰ Ba	4.99761	90.562	106.993	685.518	703.098
¹²⁰ Xe	1.57992	7.3638	8.82085	0.105	0.11187
¹²⁶ Cs	4.79256	75.871	90.4835	542.400	555.411
¹⁸² Re	2.79851	131.273	145.184	16.123	17.2282
²⁰⁵ Bi	2.70412	227.499	247.263	12.415	13.4798

5.3.2 For β^- -Decay

Table 5.10 shows the state by-state calculation of PHL for ¹⁰⁰Sr (largest PD=3.82 %) and ¹⁵²Nd (PD=2.04 %). The values of Q_{β^-} (calculated PSF, NME and branching ratios I_{β^-})

were also given in this Table. An overall agreement between our calculated PSF values and those using the (GM) recipe in the case of both analyzed nuclei was observed.

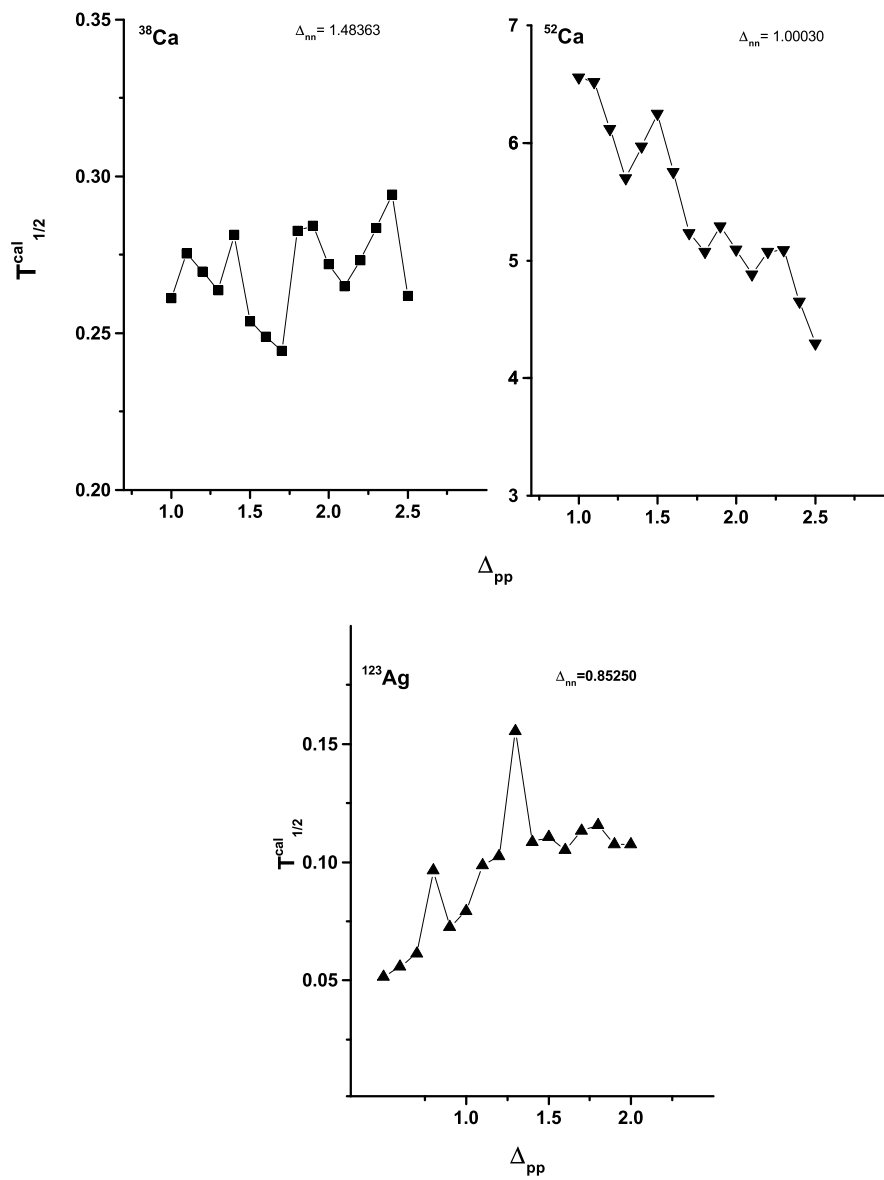


Figure 5.1: Dependence of pn-QRPA calculated half-lives on pairing gaps using the $Emp - 1$ scheme for the three cases analyzed in previous works [41, 92]. The pairing gaps are given in units of MeV .

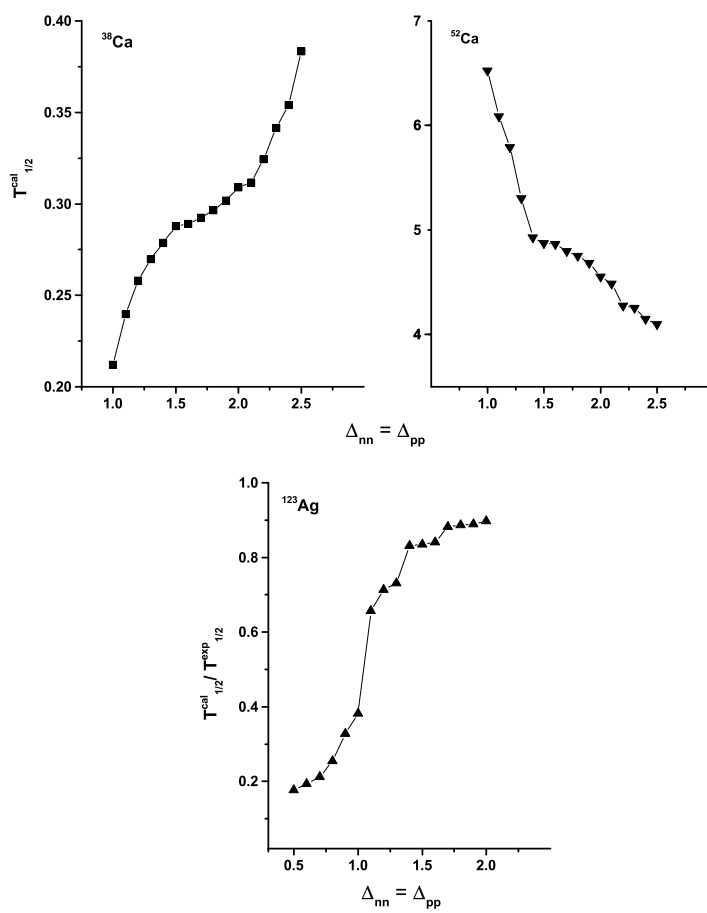


Figure 5.2: Same as Fig. 5.1 but employing $Emp - 2$ scheme.

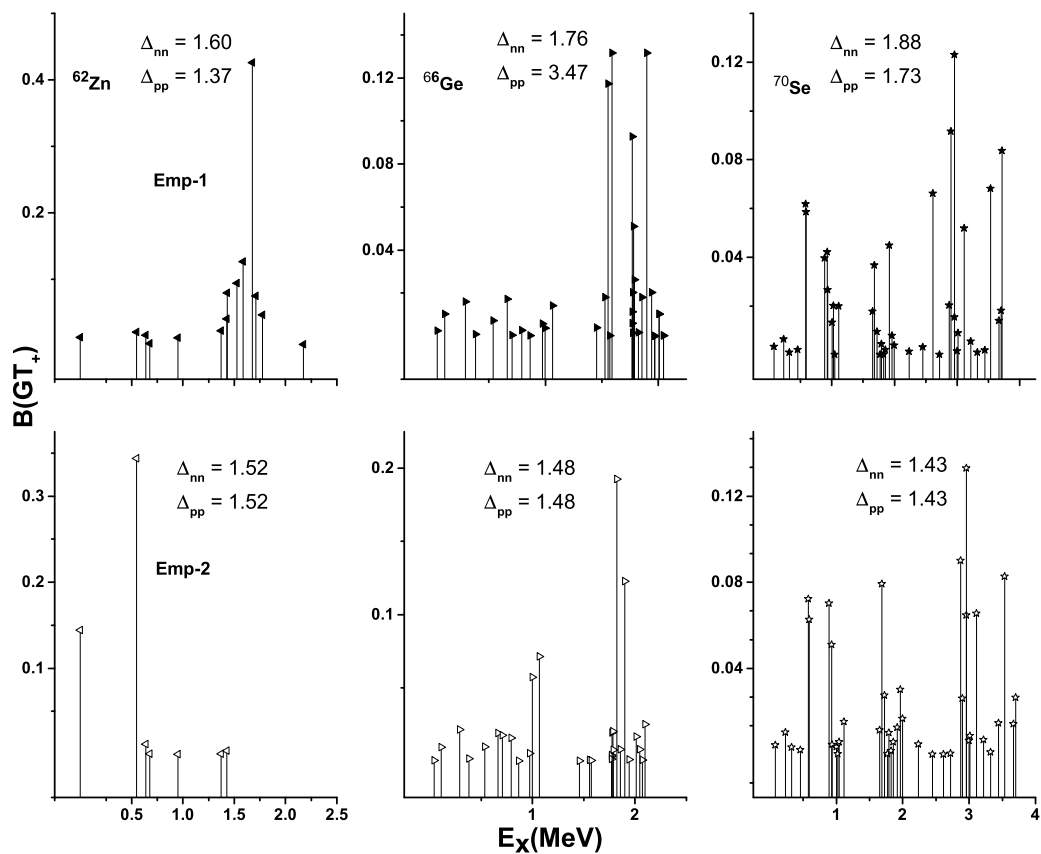


Figure 5.4: Calculated Gamow-Teller strength distributions for ^{62}Zn , ^{66}Ge and ^{70}Se using pn-QRPA $^{(Emp-1)}$ and pn-QRPA $^{(Emp-2)}$ schemes.

Table 5.10: State-by-state comparison of calculated PSF (for β -decay) using recipe of [97] and current prescription (TW). Shown also were the daughter energy levels, nuclear matrix elements NME, Q values, partial half-lives (PHL) and branching ratio $I_{(\beta^-)}$ for β^- -decay of the selected nuclei.

^{100}Sr								
E_x (MeV)	NME	Q_{β^-} (MeV)	$F_{\beta^-}^{(GM)}$ [97]	$F_{\beta^-}^{(TW)}$	PHL $^{(GM)}$ [97]	PHL $^{(TW)}$	$I_{(\beta^-)}^{(GM)}$ [97]	$I_{(\beta^-)}^{(TW)}$
0.13300	0.01473	7.50300	86906.3	72966.7	3.12798E+00	3.72554E+00	7.2730	6.3720
0.35700	0.00115	7.14579	69557.1	64334.6	4.99967E+01	5.40553E+01	0.4550	0.4390
0.86400	0.00510	6.63935	49775.9	47317.7	1.57827E+01	1.66026E+01	1.4410	1.4300
1.00300	0.00322	6.50023	45212.0	43184.3	2.75281E+01	2.88207E+01	0.8260	0.8240
1.06300	0.00429	6.44024	43349.3	41485.6	2.15140E+01	2.24805E+01	1.0570	1.0560
1.10400	0.00278	6.39893	42102.4	40346.8	3.42401E+01	3.57299E+01	0.6640	0.6640
1.35000	0.26502	6.15278	35247.6	33999.4	4.28548E-01	4.44280E-01	53.084	53.434
1.41900	0.01521	6.08400	33499.6	32359.0	7.85740E+00	8.13437E+00	2.8950	2.9180
1.62000	0.00002	5.88283	28778.0	27883.9	7.89102E+03	8.14407E+03	0.0030	0.0030
1.64200	0.00000	5.86112	28301.8	27429.7	2.05672E+05	2.12210E+05	0.0000	0.0000
1.66900	0.00080	5.83372	27709.5	26864.9	1.81631E+02	1.87341E+02	0.1250	0.1270
2.03600	0.03084	5.46720	20688.6	20109.3	6.27339E+00	6.45412E+00	3.6260	3.6780
2.19100	0.00096	5.31207	18180.4	17678.5	2.30158E+02	2.36693E+02	0.0990	0.1000
2.21100	0.00002	5.29152	17867.1	17374.4	1.26201E+04	1.29779E+04	0.0020	0.0020
2.21700	0.00126	5.28623	17787.1	17296.8	1.79065E+02	1.84140E+02	0.1270	0.1290
2.33500	0.01496	5.16812	16074.2	15633.6	1.66481E+01	1.71173E+01	1.3660	1.3870
2.40500	0.00704	5.09834	15125.2	14712.6	3.75885E+01	3.86428E+01	0.6050	0.6140
2.48600	0.05959	5.01712	14077.3	13695.1	4.77186E+00	4.90505E+00	4.7670	4.8400
2.55600	0.00015	4.94728	13222.8	12865.6	2.04511E+03	2.10190E+03	0.0110	0.0110
2.59700	0.00001	4.90586	12735.9	12392.7	3.58668E+04	3.68600E+04	0.0010	0.0010
2.71000	0.00051	4.79275	11477.9	11170.8	6.88307E+02	7.07229E+02	0.0330	0.0340
2.73300	0.04131	4.76967	11233.8	10933.7	8.62714E+00	8.86390E+00	2.6370	2.6780
2.92100	0.00092	4.58202	9397.47	9150.19	4.64906E+02	4.77470E+02	0.0490	0.0500
3.04900	0.00007	4.45378	8285.68	8069.38	7.37202E+03	7.56963E+03	0.0030	0.0030
3.19200	0.00721	4.31146	7176.38	6990.87	7.73167E+01	7.93683E+01	0.2940	0.2990
3.29000	0.00845	4.21307	6480.88	6314.67	7.30755E+01	7.49989E+01	0.3110	0.3170
3.29600	0.01583	4.20677	6438.24	6273.21	3.92753E+01	4.03085E+01	0.5790	0.5890
3.36400	0.00058	4.13861	5990.84	5838.16	1.15661E+03	1.18685E+03	0.0200	0.0200
3.43900	0.00029	4.06433	5531.71	5391.47	2.52582E+03	2.59152E+03	0.0090	0.0090
3.45000	0.01045	4.05281	5463.09	5324.69	7.01033E+01	7.19255E+01	0.3250	0.3300
3.47100	0.00612	4.03206	5341.13	5205.96	1.22440E+02	1.25619E+02	0.1860	0.1890
3.49600	0.00482	4.00734	5198.67	5067.29	1.59594E+02	1.63732E+02	0.1430	0.1450
3.56900	0.00134	3.93407	4794.07	4673.52	6.24537E+02	6.40647E+02	0.0360	0.0370
3.68200	0.11627	3.82086	4218.21	4112.92	8.16217E+00	8.37111E+00	2.7870	2.8360
3.88800	0.00006	3.61534	3313.42	3232.01	2.10528E+04	2.15831E+04	0.0010	0.0010
4.05100	0.01897	3.45234	2711.28	2645.88	7.78203E+01	7.97437E+01	0.2920	0.2980
4.08800	0.37148	3.41515	2586.91	2524.78	4.16561E+00	4.26810E+00	5.4610	5.5620
4.12800	0.20740	3.37510	2458.04	2399.32	7.85229E+00	8.04448E+00	2.8970	2.9510
4.16900	0.00354	3.33446	2332.50	2277.04	4.84389E+02	4.96188E+02	0.0470	0.0480
4.22200	0.00034	3.28135	2176.15	2124.70	5.47159E+03	5.60410E+03	0.0040	0.0040
4.30800	0.00556	3.19476	1939.11	1893.63	3.71131E+02	3.80044E+02	0.0610	0.0620
4.31100	0.00722	3.19210	1932.17	1886.87	2.87049E+02	2.93941E+02	0.0790	0.0810

^{100}Sr								
$E_x(\text{MeV})$	NME	Q_{β^-} (MeV)	$F_{\beta^-}^{(GM)}$ [97]	$F_{\beta^-}^{(TW)}$	$\text{PHL}^{(GM)}$ [97]	$\text{PHL}^{(TW)}$	$I_{(\beta^-)}^{(GM)}$ [97]	$I_{(\beta^-)}^{(TW)}$
4.40800	0.00101	3.09502	1691.86	1652.46	2.33941E+03	2.39520E+03	0.010	0.010
4.43400	0.00003	3.06860	1630.72	1592.78	8.24004E+04	8.43631E+04	0.000	0.000
4.53600	0.00007	2.96655	1410.81	1378.03	4.15176E+04	4.25053E+04	0.001	0.001
4.56000	0.00318	2.94261	1362.77	1331.13	9.23619E+02	9.45568E+02	0.025	0.025
4.62800	0.00284	2.87494	1233.96	1205.44	1.14035E+03	1.16733E+03	0.020	0.020
4.63100	0.03599	2.87213	1228.83	1200.43	9.05090E+01	9.26499E+01	0.251	0.256
4.68800	0.00938	2.81463	1127.45	1101.55	3.78490E+02	3.87390E+02	0.060	0.061
4.70300	0.01517	2.79959	1102.05	1076.78	2.39492E+02	2.45112E+02	0.095	0.097
4.78400	0.00317	2.71946	974.255	952.119	1.29597E+03	1.32610E+03	0.018	0.018
4.86000	0.33212	2.64278	863.180	843.718	1.39636E+01	1.42857E+01	1.629	1.662
4.87900	0.15890	2.62366	837.107	818.264	3.00956E+01	3.07887E+01	0.756	0.771
4.98800	0.04141	2.51538	700.916	685.342	1.37918E+02	1.41052E+02	0.165	0.168
4.99400	0.00028	2.50876	693.199	677.809	2.02785E+04	2.07390E+04	0.001	0.001
5.02400	0.00000	2.47918	659.521	644.946	2.18678E+06	2.23620E+06	0.000	0.000
5.02400	0.00000	2.47907	659.398	644.827	3.04674E+06	3.11559E+06	0.000	0.000
5.07300	0.00072	2.42998	606.361	593.032	9.17207E+03	9.37823E+03	0.002	0.003
5.07800	0.06105	2.41548	601.620	588.399	1.08997E+02	1.11446E+02	0.209	0.213
5.08800	0.00814	2.41543	591.359	578.371	8.31303E+02	8.49970E+02	0.027	0.028
5.14500	0.00755	2.35801	534.741	523.045	9.90972E+02	1.01313E+03	0.023	0.023
5.18900	0.00337	2.31408	494.418	483.653	2.40044E+03	2.45387E+03	0.009	0.010
5.22000	0.02056	2.28304	467.396	457.267	4.16606E+02	4.25834E+02	0.055	0.056
5.24100	0.01309	2.26217	449.896	440.172	6.79596E+02	6.94608E+02	0.033	0.034
5.31000	0.00883	2.19284	395.410	386.919	1.14639E+03	1.17155E+03	0.020	0.020
5.32100	0.00091	2.18167	387.143	378.840	1.14066E+04	1.16566E+04	0.002	0.002
5.33200	0.00363	2.17111	379.456	371.325	2.90418E+03	2.96777E+03	0.008	0.008
5.38200	0.19989	2.12061	344.315	336.988	5.81626E+01	5.94271E+01	0.391	0.399
5.42200	0.29697	2.08095	318.556	311.801	4.23152E+01	4.32320E+01	0.538	0.549
5.43600	0.00100	2.06672	309.690	303.131	1.28840E+04	1.31628E+04	0.002	0.002
5.44100	0.01497	2.06191	306.737	300.243	8.71971E+02	8.90832E+02	0.026	0.027
5.47800	0.02798	2.02462	284.592	278.578	5.02652E+02	5.13504E+02	0.045	0.046
5.51600	0.00603	1.98731	263.713	258.144	2.51817E+03	2.57250E+03	0.009	0.009
5.58100	0.00030	1.92248	230.309	225.470	5.86286E+04	5.98869E+04	0.000	0.000
5.58200	0.00028	1.92101	229.593	224.770	6.27505E+04	6.40971E+04	0.000	0.000
5.68100	0.00107	1.82168	185.048	181.209	2.02077E+04	2.06358E+04	0.001	0.001
5.68800	0.00137	1.81513	182.369	178.592	1.60203E+04	1.63591E+04	0.001	0.001
5.77800	0.00050	1.72493	148.469	145.430	5.40763E+04	5.52065E+04	0.000	0.000
5.83100	0.34429	1.67201	131.012	128.381	8.87476E+01	9.05664E+01	0.256	0.262
6.01400	0.87770	1.48870	82.5496	80.9479	5.52508E+01	5.63440E+01	0.412	0.421
6.03600	0.00558	1.46719	77.9438	76.4297	9.19758E+03	9.37979E+03	0.002	0.003
6.08500	0.00058	1.41812	68.1847	66.8508	1.01248E+05	1.03268E+05	0.000	0.000
6.21900	0.65507	1.28368	46.2444	45.3545	1.32146E+02	1.34739E+02	0.172	0.176
6.31900	0.15270	1.18405	33.8740	33.2233	7.73910E+02	6.90755E+06	0.029	0.030
6.33400	0.00002	1.16928	32.2838	31.6656	6.77527E+06	6.90755E+06	0.000	0.000
6.42900	0.01233	1.07429	23.3854	22.9594	1.38889E+04	1.41466E+04	0.002	0.002
6.51300	0.01217	0.98992	17.1872	16.8828	1.91431E+04	1.94883E+04	0.001	0.001
6.51600	0.00006	0.98675	16.9821	16.6819	3.95940E+06	4.03065E+06	0.000	0.000

¹⁰⁰ Sr								
E _x (MeV)	NME	Q _{β⁻} (MeV)	F _{β⁻} ^(GM) [97]	F _{β⁻} ^(TW)	PHL ^(GM) [97]	PHL ^(TW)	I _(β⁻) ^(GM) [97]	I _(β⁻) ^(TW)
6.57300	0.00003	0.93005	13.6192	13.3789	9.25172E+06	9.41784E+06	0.000	0.000
6.58400	0.00331	0.91930	13.0440	12.8128	9.25986E+04	9.42691E+04	0.000	0.000
6.70900	0.00618	0.79391	7.61027	7.47817	8.50784E+04	8.65813E+04	0.000	0.000
6.72200	0.11568	0.78109	7.17285	7.04917	4.82458E+03	4.90923E+03	0.005	0.005
6.77000	0.01393	0.73306	5.70097	5.60592	5.04157E+04	5.12705E+04	0.000	0.000
6.89500	0.03451	0.60845	2.93440	2.88738	3.95262E+04	4.01699E+04	0.001	0.001
7.08500	0.00065	0.41782	0.80160	0.78904	7.62566E+06	7.74711E+06	0.000	0.000
7.10800	0.28661	0.39513	0.66388	0.65345	2.10383E+04	2.13742E+04	0.000	0.001
7.25000	0.05443	0.25270	0.15179	0.14949	4.84551E+05	4.92007E+05	0.000	0.000
7.30300	0.00180	0.19970	7.12037E-02	7.01109E-02	3.12973E+07	3.17851E+07	0.000	0.000
7.34900	0.20453	0.15433	3.14666E-02	3.09831E-03	6.21998E+05	6.31705E+05	0.000	0.000
7.43700	0.00053	6.55474E-02	2.22245E-03	2.19039E-03	3.40802E+09	3.45789E+09	0.000	0.000
7.50100	0.00000	2.44828E-03	1.11208E-07	1.39749E-07	1.78361E+18	1.41935E+18	0.000	0.000
¹⁵² Nd								
0.00700	0.00023	1.10500	64.4753	63.0324	2.69504E+05	2.75673E+05	3.206	3.201
0.04300	0.00018	1.06233	57.1811	55.9198	3.98034E+05	4.07012E+05	2.170	2.168
0.04800	0.00034	1.05678	56.0922	54.8558	2.12257E+05	2.17040E+05	4.070	4.066
0.08500	0.00021	1.01958	49.1965	48.1182	3.85716E+05	3.94359E+05	2.240	2.238
0.16100	0.00075	0.94396	37.1767	36.3803	1.42898E+05	1.46027E+05	6.046	6.043
0.16100	0.00142	0.94376	37.1486	36.3528	7.57971E+04	7.74564E+04	11.39	11.39
0.17200	0.00001	0.93269	35.5966	34.8310	9.15658E+06	9.35783E+06	0.094	0.094
0.17500	0.00053	0.93033	35.2726	34.5135	2.13186E+05	2.17876E+05	4.052	4.050
0.19900	0.00037	0.90628	32.0940	31.3982	3.39245E+05	3.46763E+05	2.547	2.545
0.22900	0.00042	0.87600	28.4051	27.7849	3.34891E+05	3.42366E+05	2.580	2.578
0.27400	0.00278	0.83105	23.5294	23.0191	6.12332E+04	6.25907E+04	14.10	14.09
0.32400	0.00006	0.78073	18.8524	18.4532	3.53330E+06	3.60975E+06	0.245	0.244
0.32500	0.00058	0.77950	18.7474	18.3506	3.70394E+05	3.78405E+05	2.332	2.332
0.33100	0.00025	0.77444	18.3211	17.9336	8.65513E+05	8.84212E+05	0.998	0.998
0.33300	0.00003	0.77208	18.1243	17.7411	7.84943E+06	8.01899E+06	0.110	0.110
0.33400	0.00036	0.77115	18.0476	17.6660	6.17153E+05	6.30484E+05	1.400	1.400
0.33500	0.00000	0.77037	17.9829	17.6027	8.69619E+08	8.88405E+08	0.001	0.001
0.34200	0.00008	0.76308	17.3901	17.0228	2.78870E+06	2.84887E+06	0.310	0.310
0.35000	0.00121	0.75540	16.7806	16.4280	1.97513E+05	2.01752E+05	4.374	4.374
0.36800	0.00002	0.73716	15.3978	15.0799	1.05188E+07	1.07405E+07	0.082	0.082
0.37400	0.00000	0.73059	14.9209	14.6152	1.47159E+08	1.50237E+08	0.006	0.006
0.39700	0.00000	0.70821	13.3799	13.1094	2.66595E+08	2.72097E+08	0.003	0.003
0.40200	0.00000	0.70320	13.0521	12.7882	3.55337E+09	3.62670E+09	0.000	0.000
0.45200	0.00003	0.65259	10.0639	9.85865	1.33142E+07	1.35914E+07	0.065	0.065
0.47600	0.00005	0.62948	8.88352	8.70489	9.68863E+06	9.88744E+06	0.089	0.089
0.48800	0.00349	0.61732	8.30575	8.13928	1.38175E+05	1.41001E+05	6.252	6.259
0.51100	0.00796	0.59432	7.29006	7.14343	6.90199E+04	7.04367E+04	12.51	12.53

^{152}Nd								
E_x (MeV)	NME	Q_{β^-} (MeV)	$F_{\beta^-}^{(GM)}$ [97]	$F_{\beta^-}^{(TW)}$	$\text{PHL}^{(GM)}$ [97]	$\text{PHL}^{(TW)}$	$I_{(\beta^-)}^{(GM)}$ [97]	$I_{(\beta^-)}^{(TW)}$
0.54600	0.00061	0.55945	5.92805	5.80563	1.10052E+06	1.12373E+06	0.785	0.785
0.55500	0.00137	0.54988	5.58944	5.47456	5.23679E+05	5.34669E+05	1.650	1.651
0.60100	0.00004	0.50426	4.16753	4.08228	2.47689E+07	2.52862E+07	0.035	0.035
0.60200	0.00299	0.50322	4.13846	4.05387	3.23348E+05	3.30095E+05	2.672	2.673
0.64600	0.00150	0.45851	3.02789	2.97763	8.84107E+05	9.02058E+05	0.977	0.978
0.65000	0.00629	0.45524	2.95622	2.89755	2.15336E+05	2.19696E+05	4.012	4.017
0.69600	0.00589	0.40853	2.06216	2.02139	3.29366E+05	3.36009E+05	2.623	2.626
0.72000	0.00739	0.38524	1.69907	1.66403	3.18926E+05	3.25589E+05	2.709	2.710
0.74100	0.00000	0.36417	1.41219	1.38322	1.21197E+09	1.23735E+09	0.001	0.001
0.74700	0.00029	0.35817	1.33734	1.31027	1.02657E+07	1.04794E+07	0.084	0.084
0.76400	0.00047	0.34126	1.14121	1.11921	7.42169E+06	7.57038E+06	0.116	0.117
0.78500	0.00071	0.31972	0.92353	0.90484	6.12158E+06	6.24805E+06	0.141	0.141
0.80600	0.00082	0.29870	0.74084	0.72553	6.59923E+06	6.73842E+06	0.131	0.131
0.81200	0.00282	0.29257	0.69283	0.67836	2.04836E+06	2.09207E+06	0.422	0.422
0.82100	0.00469	0.28442	0.63250	0.61922	1.34848E+06	1.37739E+06	0.641	0.641
0.85100	0.01661	0.25449	0.44274	0.43351	5.44359E+05	5.55942E+05	1.587	1.587
0.91700	0.00059	0.18846	0.17078	0.16689	3.99157E+07	4.08462E+07	0.022	0.022
0.92400	0.00261	0.18069	0.14965	0.14621	1.02513E+07	1.04925E+07	0.084	0.084
0.96800	0.00007	0.13735	6.3563E-02	6.1968E-02	9.47034E+08	9.71424E+08	0.001	0.001
0.96800	0.00093	0.13673	6.2679E-02	6.1101E-02	6.89166E+07	7.06975E+07	0.013	0.012
1.00300	0.00039	1.0210E-01	2.5429E-02	2.4708E-02	4.00310E+08	4.11999E+08	0.002	0.002

5.4 β -Decay Half-life Calculation

Results for β -decay half-lives based on a new recipe for calculation of phase space factors recently introduced in previous section and [115] will be presented in this section. This section includes half-life results for fp -shell and heavier nuclei of experimental and astrophysical interests. The investigation of the kinematics of some β -decay half-lives was presented, and new phase space factor values were compared with those obtained with previous theoretical approximations.

The β -decay half-lives in agreement with experimental results was a challenging problem for nuclear theorists [41, 54, 85, 87, 116]. Theoretically, the half-life formulas for β -decay can be expressed as a product of nuclear matrix elements (NMEs), involving the nuclear structure of the decaying parent and of the daughter nuclei, and the phase space factors (PSFs) which taken into account the distortion of the electron wave function by the nuclear Coulomb field. Hence, for a precise calculation of the β -decay half-lives, an accurate computation of both these quantities was needed. The largest uncertainties come from the NME computation. In literature one can find different calculations of the NMEs for β -decays, realized for different types of transitions and final states, and with different theoretical models (e.g. based on gross theory [81], QRPA approaches [44, 54, 79, 82–87] and shell model [88]).

Comparing present results with previous similar calculations employing approximate electron wave functions, several notable differences was noticed, especially for heavier nuclei $52 \leq A \leq 205$ [115]. The new calculation can easily be extended to any arbitrarily heavy nuclei. To include β -decay reactions, new PSF calculations (of positron decay and EC reactions) were extended here. In order to complete the calculation of β -decay half-lives, the set of NMEs was calculated using the proton-neutron quasi-particle random phase approximation model in deformed basis. A schematic separable potential both in particle-particle and particle-hole channels was considered. Other nuclear models and a set of improved input parameters may result in a better calculation of NMEs. Both Gamow-Teller and Fermi transitions to ground and excited states was calculated, for medium and heavy nuclei of

interest.

5.4.1 Parameters used for Calculation

β -decay half-lives could calculate as a sum over all transition probabilities to the daughter nucleus states through excitation energies lying within the Q_β value

$$T_{1/2} = \left(\sum_{0 \leq E_f \leq Q_\beta} 1/t_f \right)^{-1}, \quad (5.25)$$

where the partial half-lives (PHL), t_f , can be calculated using

$$t_f = \frac{C}{(g_A/g_v)^2 F_A(Z, A, E) B_{GT}(E_f) + F_V(Z, A, E) B_F(E_f)}. \quad (5.26)$$

In Eq. (5.26) value of C was taken as 6143 s [51], g_A , g_v were axial-vector and vector coupling constants of the weak interaction, respectively, having $g_A/g_v = -1.2694$ [52], while E_f was the final state energy. $E = Q_\beta - E_f$ where Q_β was the window accessible to either β^+ -, β^- - or EC decay. $F_{A/V}$ were the PSFs. B_{GT} and B_F the reduced transition probabilities for Gamow-Teller and Fermi transitions, respectively, and expressed as

$$B_F(E_f) = \frac{1}{2I_i + 1} |\langle f || M_F || i \rangle|^2, \quad (5.27)$$

$$B_{GT}(E_f) = \frac{1}{2I_i + 1} |\langle f || M_{GT} || i \rangle|^2 \quad (5.28)$$

In Eq. (5.27) and Eq. (5.28), I_i denotes the spin of the parent state, M_F and M_{GT} for the Fermi and Gamow-Teller transition operators, respectively. Detailed calculation of the NMEs within the proton-neutron quasi-particle random phase approximation (pn-QRPA) formalism may be found in Refs. [41, 54]. In this section the NMEs calculation performed using the pn-QRPA model. The Nilsson model [66] was used to calculate single particle energies and wave functions which taken into account the nuclear deformation.

Pairing correlations were tackled using the BCS approach. The proton-neutron residual interaction was considered in two channels, namely the particle-particle and the particle-hole interactions. Separable forms were chosen for these interactions and were characterized by interaction constants χ for particle-particle and κ for particle-hole interactions. Here, the same range for χ and κ was used and discussed in [41, 54]. Deformation parameter values β_2 for all cases were taken from Ref. [117]. For pairing gaps a global approach $\Delta_n = \Delta_p = 12/\sqrt{A}$ [MeV] was employed. A large model space up to $7\hbar\omega$ was incorporated in pn-QRPA to perform half-lives calculations for heavy nuclei considered in present work.

5.4.2 *Comparison between Measured and Calculated Half-lives*

Half-lives were computed using Eq. (5.25) and Eq. (5.26). The NMEs were calculated using Eq. (5.27) (for Fermi transitions) and Eq. (5.28) (for GT transitions) within the pn-QRPA formalism. For the PSFs calculation two different recipes were used in present section. One was newly calculation recipe [115] and the other one was the conventional computation using the prescription of Gove and Martin (*GM*) [97]. It stated again that the same set of NMEs were used in both types of half-life calculations.

Table 5.11 presents a comparison between the measured and calculated half-lives for β^+ /EC-decay of twenty medium and heavy nuclei of interest. Entries in third column were calculated using the pn-QRPA method for the NMEs, while the PSFs were calculated with the method from Ref. [97] and denoted by (*GM*). The fourth column shows the calculated half-lives using new recipe of PSF [115] and labeled (*TW*) (this work). Most of the nuclei shown in this table were the same as those presented in previous section and [115]. All half-lives was given in units of seconds. Q -values for the reaction were taken from [107]. It can seen from Table 5.11 that the newly calculated half-lives were systematically larger than those computed using the PSFs of (*GM*) [97]. The last column displays the percentage deviation (PD) of the two calculated half-lives. The PD between the two computed half-lives was calculated using the formula

Table 5.11: Comparison of measured, calculated half-lives and percentage deviation (PD) for positron decay of selected nuclei.

Nucleus	$T_{1/2}^{(EXP)}$ (s) [107]	$T_{1/2}^{(GM)}$ (s) [97]	$T_{1/2}^{(TW)}$ (s)	PD (%)
⁵² Fe	2.98E+04	1.29E+04	1.30E+04	0.77
⁵⁶ Ni	5.25E+05	4.26E+05	4.44E+05	4.05
⁶² Zn	3.31E+04	9.80E+03	1.01E+04	2.97
⁷⁶ Br	5.83E+04	1.62E+04	1.66E+04	2.41
⁸¹ Rb	1.65E+04	5.00E+03	5.12E+03	2.34
⁸⁸ Y	9.21E+06	1.25E+07	1.27E+07	1.57
⁹⁰ Nb	5.26E+04	4.25E+04	4.32E+04	1.62
¹⁰² Cd	3.30E+02	2.35E+02	2.42E+02	2.89
¹⁰⁵ Ag	3.57E+06	2.45E+04	2.52E+04	2.78
¹⁰⁷ Sb	4.00E+00	3.92E+00	4.04E+00	2.97
¹¹³ Sb	4.00E+02	2.42E+02	2.47E+02	2.02
¹¹³ Te	1.02E+02	9.55E+01	9.77E+01	2.25
¹¹⁵ I	3.48E+02	9.98E+01	1.02E+02	2.16
¹¹⁶ I	2.91E+00	9.49E-01	9.73E-01	2.47
¹¹⁶ Xe	5.90E+01	2.01E+01	2.05E+01	1.95
¹²⁰ Ba	2.40E+01	1.73E+01	1.76E+01	1.70
¹²⁰ Xe	2.76E+03	1.58E+03	1.61E+03	1.86
¹²⁶ Cs	9.84E+01	5.35E+02	5.42E+02	1.29
¹⁸² Re	2.30E+05	3.67E+05	3.80E+05	3.42
²⁰⁵ Bi	1.32E+06	1.47E+06	1.52E+06	3.46

$$PD = \frac{T_{1/2}^{(TW)} - T_{1/2}^{(GM)}}{T_{1/2}^{(TW)}} \times 100(\%) \quad (5.29)$$

Table 5.11 shows that the PD increases to a maximum value of 4.05 % for the ⁵⁶Ni nucleus. In Table 5.11 the biggest PD for β^+ /EC-decay half-lives were recorded for the nucleus ⁵⁶Ni whereas the smallest difference was noted for ⁵²Fe.

Table 5.12 shows the comparison of measured and calculated half-lives for β^- -decay cases. The Q -values were taken from [107].

Table 5.12: Same as Table. 5.6 but for β^- -decaying nuclei.

Nucleus	$T_{1/2}^{EXP}$ (s) [107]	$T_{1/2}^{(GM)}$ (s) [97]	$T_{1/2}^{(TW)}$ (s)	PD (%)
⁹⁸ Sr	6.53E-01	4.45E-01	4.57E-01	2.63
¹⁰⁰ Sr	2.02E-01	2.28E-01	2.37E-01	3.82
¹⁰⁰ Zr	7.10E+00	8.04E+00	8.25E+00	2.55
¹⁰² Zr	2.90E+00	8.45E+00	8.73E+00	3.21
¹⁰² Mo	6.78E+02	1.90E+02	1.94E+02	2.06
¹⁰⁴ Mo	6.00E+00	5.93E+00	6.08E+00	2.47
¹⁰⁶ Mo	8.73E+00	6.35E+00	6.53E+00	2.76
¹⁰⁸ Ru	2.73E+02	5.61E+02	5.74E+02	2.26
¹¹⁰ Ru	1.20E+01	6.27E+01	6.46E+01	2.94
¹¹² Ru	1.75E+00	6.27E+00	6.47E+00	3.09
¹¹² Pd	7.57E+04	3.89E+04	4.00E+04	2.75
¹¹⁴ Pd	1.45E+02	1.00E+02	1.03E+02	2.91
¹¹⁶ Pd	1.18E+01	4.53E+01	4.67E+01	3.00
¹³⁸ Xe	8.44E+02	4.69E+02	4.84E+02	3.10
¹⁴⁰ Xe	1.36E+01	1.36E+00	1.40E+00	2.86
¹⁴² Ba	6.36E+02	7.97E+02	8.19E+02	2.69
¹⁴⁴ Ba	1.15E+01	2.44E+01	2.51E+01	2.79
¹⁴⁶ Ce	8.11E+02	4.74E+01	4.85E+01	2.27
¹⁴⁸ Ce	5.60E+01	7.93E+01	8.13E+01	2.46
¹⁵² Nd	6.84E+02	8.64E+03	8.82E+03	2.04

The difference between the two calculated half-lives as well as their mutual comparison with the experimental data, was done intuitively in a graphical way in Fig. 5.5 for few selected β^+ decay cases. We display the ratio between the experimental half-lives and the theoretical ones, $R = T_{1/2}^{(exp)} / T_{1/2}^{(X)}$, where (X) stands for the calculation recipe, (GM) or (TW) . With solid lines the ratios calculated with (TW) recipe were represented, while with dotted lines the conventional (GM) computations were displayed. We note that systematically our half-lives were larger than the GM , improving the agreement with the measured data for most of the cases. From Fig. 5.5 it can be remarked that the (TW) ratios were in general closer to the value 1 than the (GM) ones. This effect was highlighted in Fig. 5.5 by the link between the dotted line and the solid line. In Fig. 5.6, the ratios corresponding to β^- decays were displayed in the same manner as in Fig. 5.5. It was noted that no appreciable improvement brought in calculation of β^- decay half-lives except for a few cases in which the experimental data were undervalued by calculations, as also evident from Table 5.12. Overall, we note a good agreement of the new theoretical half-lives with the experimental ones. It was again remarked that this comparison could have improved further with a more reliable set of NMEs or choice of better model parameters for the calculation of NMEs (not the subject of current paper).

The differences between the (GM) and the present results can be explained by the use of a more rigorous approach in our case for the free states in the PSF computation, but also were due to the differences between our potential and the one used by (GM) . Regarding only the free states, in the (GM) method the screening correction was introduced empirically, by modifying the solutions of the Dirac equation with a function evaluated at the nuclear surface. This function depends on the difference between the effective potential and the point like nucleus Coulomb interaction. On the other hand, in our calculation the screening was introduced by considering an effective Coulomb potential. The Dirac equation was solved numerically for this effective Coulomb potential up to large values of r , where the wave functions were well approximated by its asymptotic form. Later, the wave functions

were normalized by comparing their value with the asymptotic forms. This normalization determines the value of each wave function on the surface of the nucleus. Further, in the (*GM*) calculation, the nuclear finite size of the nucleus was simulated by additional corrections to the Fermi functions, while in our calculation, the effective Coulomb field was built up from the proton density of the nucleus, as also mentioned before. Regarding the bound states, the (*GM*) method uses tabulated values of the energies and of the radial densities that were obtained by solving the Dirac equation within a more sophisticated self-consistent Coulomb potential.

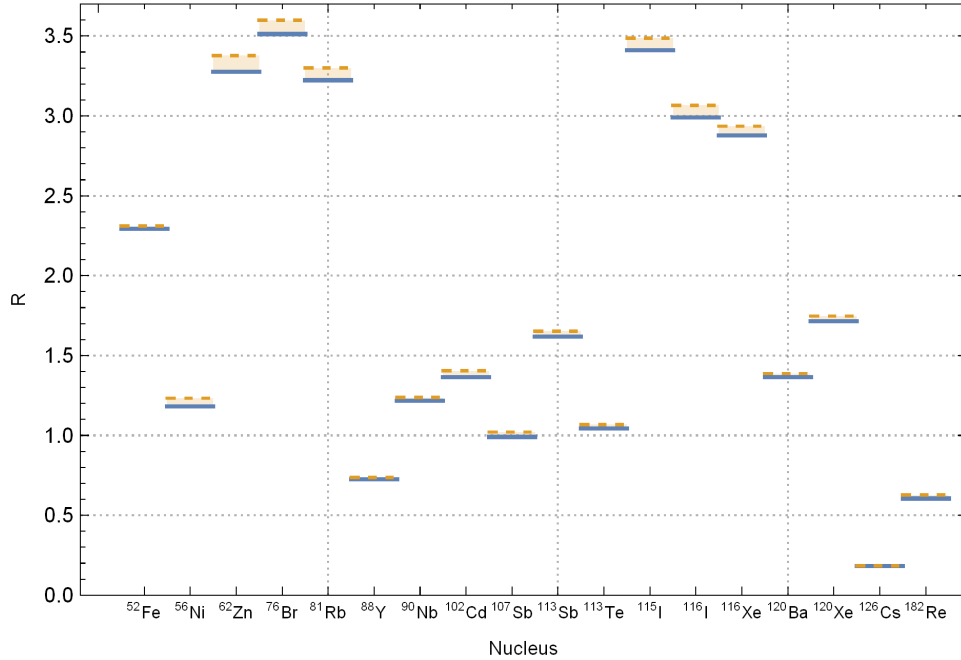


Figure 5.5: Ratios R between experimental [107] and calculated half-lives undergoing β^+ decay for selected cases. Full lines: theoretical half-lives calculated within the (*TW*) recipe. Dotted lines: theoretical half-lives calculated with the (*GM*) recipe of Ref. [97].

5.5 Summary

In present work a new code for computing PSF values for positron decays and EC processes was constructed. In this approach positron free and electron bound w.f. by solving

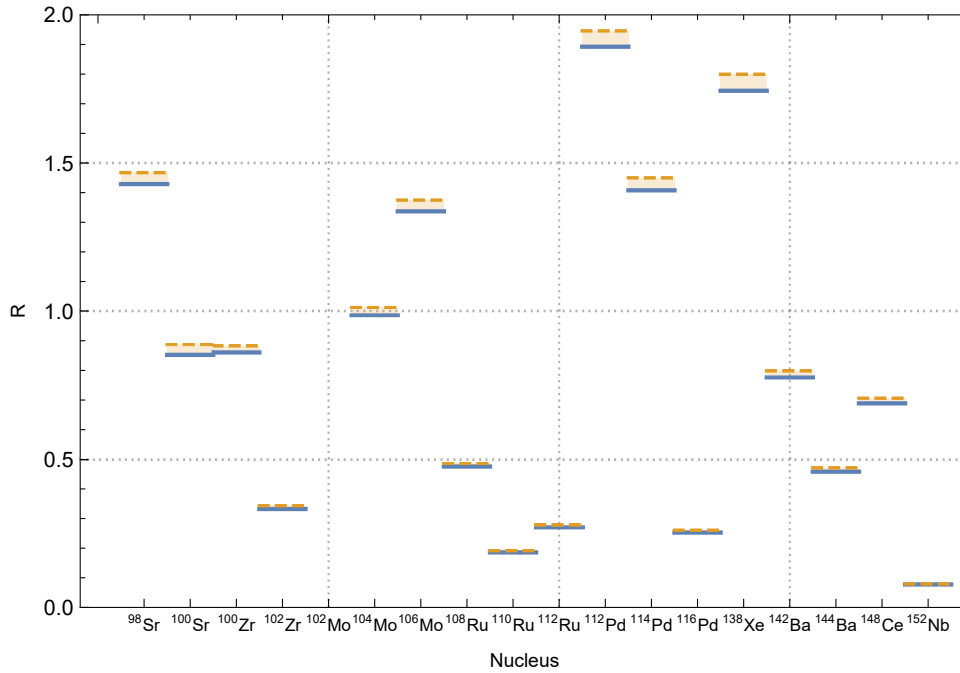


Figure 5.6: Same as Fig. 5.5 but for selected β^- decay cases.

a Dirac equation with a Coulomb-type potential were obtained from a realistic distribution of protons in the daughter nuclei. The FNS and screening effects were addressed as well by new recipe. Using the same Q-values, comparison of present work results with previous calculations where electron/positron w.f. were obtained in an approximate way. For positron decays the agreement with older results was quite good, while for EC processes the differences between "new" and "old" PSF values was as big as 35%. Further it was realized that the screening effect was important for EC processes, specially for light nuclei, having an impact up to 10-15% on the calculated PSF values. Finally, using new method, re-computed the PSF for all nuclei using up-dated Q-values.

The aim of present work was to investigate the effect of the incorporation of new PSF values, computed with a more precise and rigorous method, on the theoretical half-lives for β^\pm and EC decays of unstable nuclei. The newly calculated β -decay half-lives were systematically larger than those given in the previous calculations. The mean percentage

deviation was larger for the β^- decay (2.73%) as compared to the β^+ /EC decay rates (2.35%). For the adopted set of NMEs, in general the half-lives computed with newly PSFs were closer to the measured ones than the half-lives calculated with PSFs with approximate method (i.e., using approximate electron wave functions) [97] for free states. Although the largest uncertainty in the computation of β -decay half-lives comes from the NMEs, introduction of the newly PSF values may improve the comparison with experiment and should be taken into account for accurate predictions.

5.6 Gamow-Teller Strength Distributions and Stellar Rates for ^{76}Ge , ^{82}Se

Important information about the Gamow-Teller (GT) strength and associated weak rates about some important medium heavy nuclei ^{76}Ge , ^{82}Se in stellar environment will be discussed in present section. The GT strength response in astrophysical environment has crucial importance for many nuclides. The lepton fraction is one important factor responsible for late evolution phases in stellar core and beginning of the stellar core collapsing of massive stars towards Type-I and Type-II supernovae [118–120]. The weak interaction rate controls the said lepton fraction, while key contribution in the weak interaction rates is due to GT strength distribution. Modern research present improvements in the field of nuclear structure, transforming the GT strength distribution role. One of these developments state if iron core exceeds the limit of Chandrasekhar mass then relativistic degenerate pressure of the electron gas cannot repel against the gravitational force. In return stellar core begins collapsing leading to the start of Type-II supernovae. The SNe Ia were considered as outbursts of white dwarfs which accrete matter from the binary associates/allies. In white dwarfs very high Fermi energy of degenerate electron gas, lessens the electron fraction considerably, and in turn it controls the ejection of isotopic identities in result of these bursts. Strengths of Gamow-Teller transitions have crucial implications in such scenario's,

for example nucleosynthesis in O-Ne-Mg white dwarfs [121,122]. The results which will be discussed in this section would be concerned on the GT strength for beta decay of medium mass nuclei and its dynamics on supernovae core collapse. Such weak interaction stellar rates need the calculations about GT and Fermi transition strength distribution. Only allowed GT transitions were taken into account for the above mentioned cases. The calculated GT strength distribution, stellar weak rates employing deformed pn-QRPA formalism will be presented in the succeeding section compared with shell model and experimentally extracted GT strengths.

5.6.1 *Parameters used for the Calculation of Gamow-Teller Strength and Stellar Rates*

This section briefly describes the parameters and model framework employed for this work calculation in comparison with those done by Ha and Cheoun [123]. Present work calculations were based on deformed pn-QRPA model which differ in two ways from deformed pn-QRPA calculations performed by Ha and Cheoun [123]. A deformed Nilsson single particle basis was considered in present work whereas Ha and Cheoun uses a deformed, axially symmetric Woods-Saxon potential. The interaction choice was the next main difference. Ha and Cheoun took the Brueckner G-matrix based on the CD Bonn potential while this work considered a schematic separable interaction [41, 49, 54, 68]. The main edge of employing the separable GT forces was that QRPA matrix equation reduces to an algebraic equation of 4th order, that was much easier to solve in comparison with full diagonalization of the non-Hermitian matrix of large dimensionality. Solution of algebraic equation saves order of magnitude in CPU time and allows a microscopic calculation of GT strength off parent excited states. The model used in present calculations, proton-neutron (p-n) residual interactions occur as particle-hole (p.h) (characterized by interaction constant χ) and (p.p) (characterized by interaction constant κ) interactions. The (p.p) interaction was commonly neglected in previous β^- -decay calculations [41, 42, 46, 47]. However it was

later found to be important, specially for the calculation of β^+ -decay [41, 48, 54, 92]. The incorporation of particle-particle force leads to a redistribution of the calculated β strength, which was commonly shifted toward lower excitation energies [54]. Other variations of the deformed pn-QRPA formalism also exists in literature. One such example includes residual spin-isospin forces in the particle-hole and particle-particle channels based on a deformed Hartree-Fock calculation with density-dependent Skyrme forces [124].

In order to reproduce the GT strength the interaction strength parameters value for χ and κ were adjusted as 0.01 MeV for χ and 0.0955 MeV for κ in this calculation. A detailed description of the formalism can be found in [49]. The deformation parameter (β) value was adopted experimentally for ^{76}Ge (0.26) and ^{82}Se (0.19), extracted by relating the measured energy of the first 2^+ excited state with the quadrupole deformation, was taken from [125]. Q -values were taken from the mass compilation of [107]. Further the results of pn-QRPA calculated GT strength was multiplied by a quenching factor of $f_q^2 = (0.55)^2$ [126] in order to compare them with experimental data and prior calculations, and to later use them in for the calculation of astrophysical reaction rates. The total capture/ β^- -decay rate per unit time per nucleus was finally given by

$$\lambda^{bd(pc)} = \sum_{ij} P_i \lambda_{ij}^{bd(pc)}. \quad (5.30)$$

GT transitions properties of two even-even (^{76}Ge and ^{82}Se) nuclei playing vital role in r-process, Germanium (^{76}Ge) and Selenium (^{82}Se) will be discussed in this section. GT transitions on these particular isotopes have a special mention as per simulation results of presupernova evolution of heavy mass stars. Weak interactions in presupernova stars were known to be dominated by allowed Fermi (vector-type) and GT (axial-vector-type) transitions. The calculation of weak interaction rates was very sensitive to the distribution of the GT_{\pm} strength function. In the GT_+ strength a proton was changed into a neutron whereas the GT_- strength was responsible for transforming a neutron into a proton. The electron-to

baryon ratio Y_e reduces due to the electron capture process and as a result, the nuclear configuration was moved to more neutron-rich and heavier nuclei [118]. The first-ever extensive calculation of stellar weak rates was carried by employing the Independent Particle Model for iron group nuclei [119, 120]. During the supernova and presupernova phases of a massive star, a reasonable probability of occupation of parent excited states (because of the prevailing high temperatures and densities) and the total weak interaction rates have a finite contribution from these excited states. Brink-Axel hypothesis [127] was adopted by former calculations of stellar weak-interaction rates (e.g. [119, 128]) to approximate the contribution of partial rates from high-lying excited states. By using this hypothesis it was assumed that the excited state GT strength distributions were same as the calculated ground-state distribution. However, there was mounting evidence that the Brink-Axel hypothesis was a poor approximation to GT strength functions off excited parent states. Nabi and collaborators ([122, 129–135]) calculated GT strength distributions off parent excited states in a microscopic fashion for hundreds of nuclei of astrophysical importance and found out that Brink-Axel hypothesis was a poor approximation for GT of excited states. [136, 137] also advocated for the failure of Brink-Axel hypothesis in GT transitions. Thus, whenever it was computationally feasible, one should avoid use of the GT Brink-Axel hypothesis. The proton neutron quasiparticle random phase approximation (pn-QRPA) theory was an efficient and convenient way to generate the GT transitions [138, 139]. There were two main advantages of using the pn-QRPA theory. The first big advantage was that the pn-QRPA model gets rid of the poor Brink's hypothesis and calculates ground as well as excited state GT strength distributions in a microscopic fashion. Secondly the model can carry reliable calculation of stellar weak rates for any arbitrary heavy system of nucleons (as calculations were performed in a model space of up to seven major oscillator shells).

This section explains the performance in ground and excited states GT calculation for two nuclei having energetically allowed $\beta\beta$ -channels available. Only few nuclei in nature undergo allowed $\beta\beta$ -decay which was a two-step second-order weak process. The intermediate β -

decay state was energetically inaccessible and passed through as a virtual intermediate state. Earlier Madey and collaborators [140] studied the excitation-energy distributions of transition strength to 1^+ states excited via the (p, n) reaction at 134.4 MeV on targets of ^{76}Ge and ^{82}Se (along with two heavy isotopes of Te) for excitation energies up to 25 MeV. A better understanding of the low-lying part of the GT strength distribution (theoretical as well as experimental) of ^{76}Ge and ^{82}Se was in order to improve the predictions of $\beta\beta$ -decay rates. Recently Ha and Cheoun [123] employed a deformed pn-QRPA model to calculate ground-state GT strength distributions of these nuclei. However there was a need to also calculate excited state GT strength distributions and associated stellar weak rates for these nuclei. It was decided to chose a deformed pn-QRPA model with schematic separable interaction to calculate ground and excited-states GT_- transitions, β -decay & positron capture rates, energy rates of emitted neutrons from daughter nuclei and probabilities of β -delayed neutron emissions for ^{76}Ge and ^{82}Se . All weak interaction rate calculations were performed in stellar environment.

Farther away from line of stability, with decreasing neutron separation energy, β -delayed neutron emission occurs as a competitive decay mode to the common γ de-excitation. Thus, β -delayed neutron emission may strongly affect the prediction of mean γ energies. Information on probabilities of β -delayed neutron emission (P_n) was even more scarce than that for mean energies. P_n values were also of interest in astrophysics since they influence the final abundance of heavy elements synthesized in the r-process. Despite their importance, β -delayed neutron emission was often treated in rather crude approximations. A reliable prediction of P_n values requires particularly accurate information about the shape of the β strength function, thus underlining the necessity of microscopic calculations [141].

The cumulative GT_- strength for ground state of ^{76}Ge was shown in Fig. 5.7. Here the abscissa represents daughter excitation energy in units of MeV. The GT_- strength has been calculated in the energy interval 0 – 12 MeV. The GT strength calculation by Ha & Cheoun [123] has also been shown in Fig. 5.7. Excitation-energy distributions of

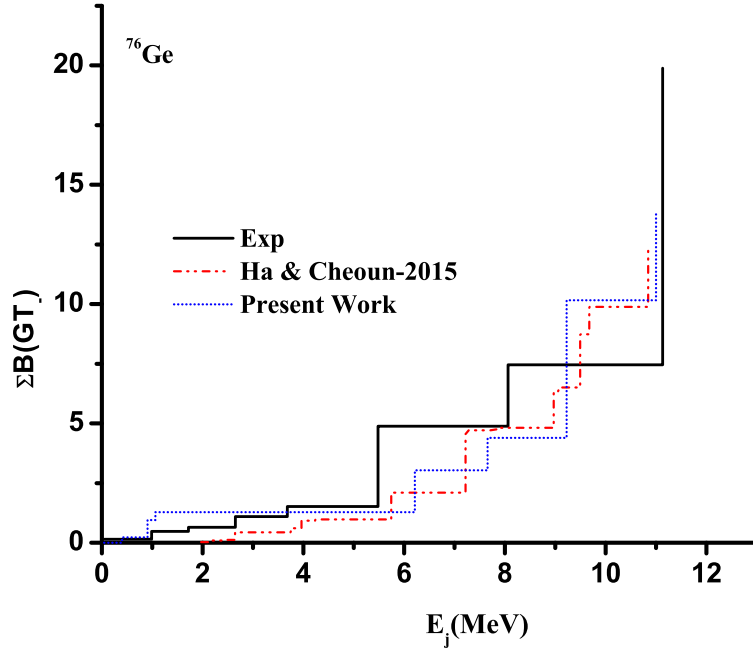


Figure 5.7: Present calculated cumulative $B(GT_-)$ distribution for the ground state of ^{76}Ge compared with experimental data [140] and the Ha and Cheoun [123] calculation.

transition strength to 1^+ states at 134.4 MeV on various targets (including ^{76}Ge and ^{82}Se) were measured for excitation energies up to 25 MeV via the (p, n) reaction by Madey and collaborators [140]. The measured data was also shown in Fig. 5.7 for comparison with present and former calculations. It was clear from Fig. 5.7 that the two calculations were in decent agreement with the measured total strength. Table 5.13 shows that the pn-QRPA model places the GT centroid at 8.66 MeV energy in daughter which was in good agreement with the measured centroid energy placed at 9.10 MeV. The Ha & Cheoun calculation leads to a much higher centroid. The pn-QRPA calculated total GT_- strength of 16.30 was also in better comparison with measured strength value of 19.89. Ha & Cheoun calculated strength was also higher. It could be noted that the Ha & Cheoun calculation did not employ any quenching factor in their calculation.

Similarly Fig. 5.8 displays calculated and measured GT_- strength for ground state of ^{82}Se . Measured data was taken from the same (p, n) experiment [140]. The experimental GT_- strength was observed between 0 – 12 MeV in daughter. The Ha & Cheoun model calculates strength in the range 3 – 19 MeV. The pn-QRPA model calculates GT strength for ^{82}Se between energy range of 0 – 12 MeV as also supported by measurements [140].

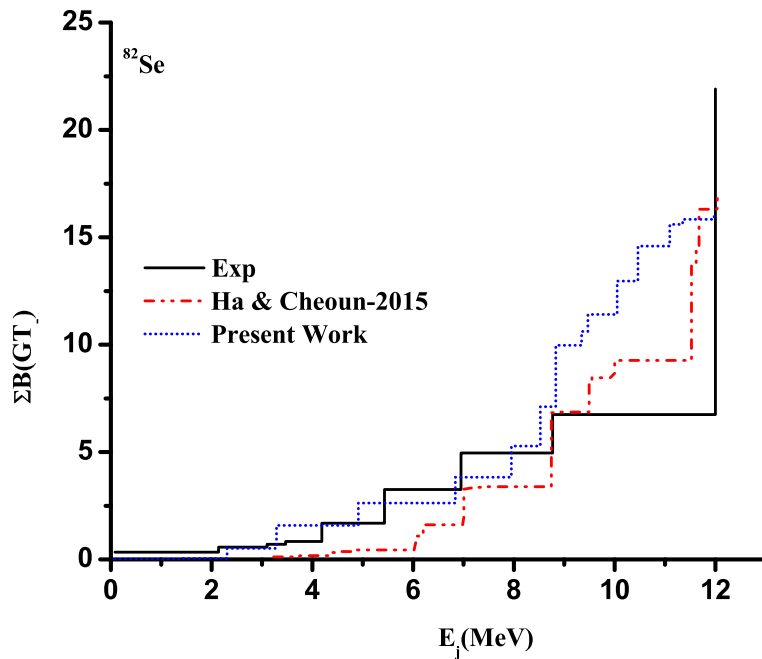


Figure 5.8: Same as Fig. 1 but for ^{82}Se .

Table 5.13 once again shows that present calculated results for GT_- strength and centroid placement agrees well with the measured data. After achieving decent agreement with experimental data this work has been proceed to calculate weak-interaction mediated rates for ^{76}Ge and ^{82}Se in stellar environment.

Table 5.13: Measured and calculated total GT strength and centroid values for ^{76}Ge and ^{82}Se along β -decay direction. For references see text.

Nucleus	Model	$\sum B(\text{GT}_-)$	E_- (MeV)	Cut off energy(MeV)
^{76}Ge	EXP	19.89	9.10	11.13
	Ha & Cheoun 2015	24.28	10.20	16.90
	This work	16.30	8.66	26.50
^{82}Se	EXP	21.91	10.17	12.00
	Ha & Cheoun 2015	32.46	11.61	19.19
	This work	18.4	9.04	26.60

5.6.2 Results and Discussion

Fig. 5.9 and Fig. 5.10 depicts (pn-QRPA) calculated (in present project) sum of stellar β -decay and positron capture rates as a function of stellar temperature at a fixed stellar density of $10^{9.6} \text{ g cm}^{-3}$ for ^{76}Ge and ^{82}Se , respectively. The ordinate shows weak rates in logarithmic scale (to base 10) in units of s^{-1} . In these graphs this work calculated rates with contribution only from parent ground state (shown as (G)) and those with contributions from all 200 parent excited states (shown as (T)) has been demonstrated. The recalculation of weak rates from the the measured GT distribution [140] and the calculated GT distribution of Ha & Cheoun [123] has also been done. The later two rates were calculated on the basis of ground state GT_- strength distributions alone. In other words for "This work(G)", "Ha and Cheoun 2015" and "EXP" rates shown in the figures, all parent excited state GT strength functions were taken to be zero (i.e. in Eq. 5.30 summation was performed only on the parent ground state). It can be seen from Fig. 5.9 that present work rates with only ground state contribution are in excellent agreement with measured data rates.

This was attributed to the decent comparison of calculated GT distribution (this work) with the measured GT distribution (see Fig. 5.7). The Ha & Cheoun model calculated rates were smaller than the rates calculated using the measured data. This was primarily because of the higher centroid placement in their model. Present work calculated stellar rates, with contributions from all 200 parent excited states, were enhanced by orders of magnitude as compared to other three rates because of finite contribution to the total weak rates from

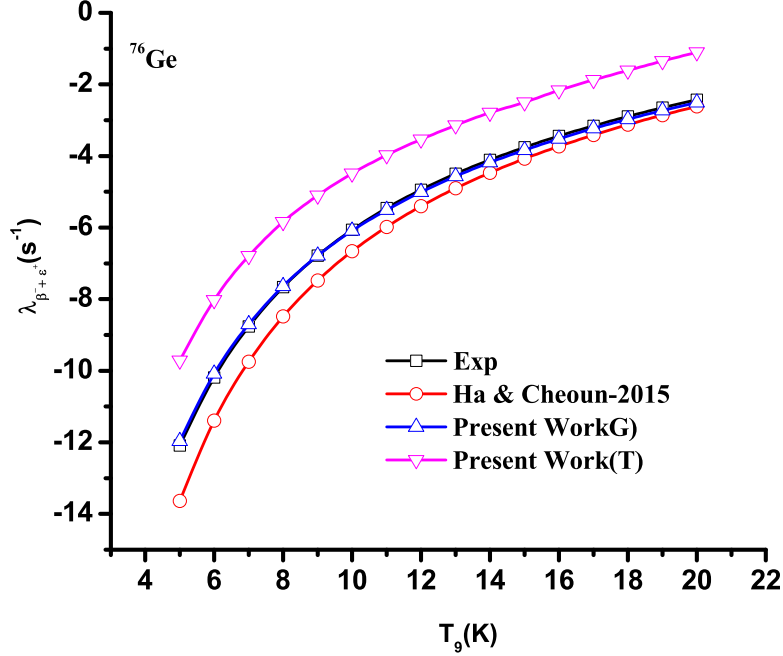


Figure 5.9: This work calculated β -decay and positron capture rates for ^{76}Ge compared with other calculations as a function of stellar temperatures for a fixed stellar density $\rho = 10^{9.6} \text{ g cm}^{-3}$. For explanation of legends see text.

excited state GT strength distributions. A more or less similar behavior was witnessed for the case of ^{82}Se in Fig. 5.10.

After showing dependence of calculated weak rates on stellar temperature, next was their dependence on stellar density. Fig. 5.11 and Fig. 5.12 show the calculated rates at a fixed stellar temperature of T_9 (K)=10 as the stellar core stiffens from $10^{8.5} - 10^{11} \text{ g cm}^{-3}$ for the nuclei ^{76}Ge and ^{82}Se , respectively. Fig. 5.11 shows that the Ha & Cheoun and present calculated rates (with only ground state contribution) were in excellent agreement with the experimental rates.

This was because at high densities and temperatures, the electron chemical potential appreciably exceeds the Q -value, and in this phase, weak rates were largely dictated by the total GT strength and its centroid energy (the low-lying individual transitions does not

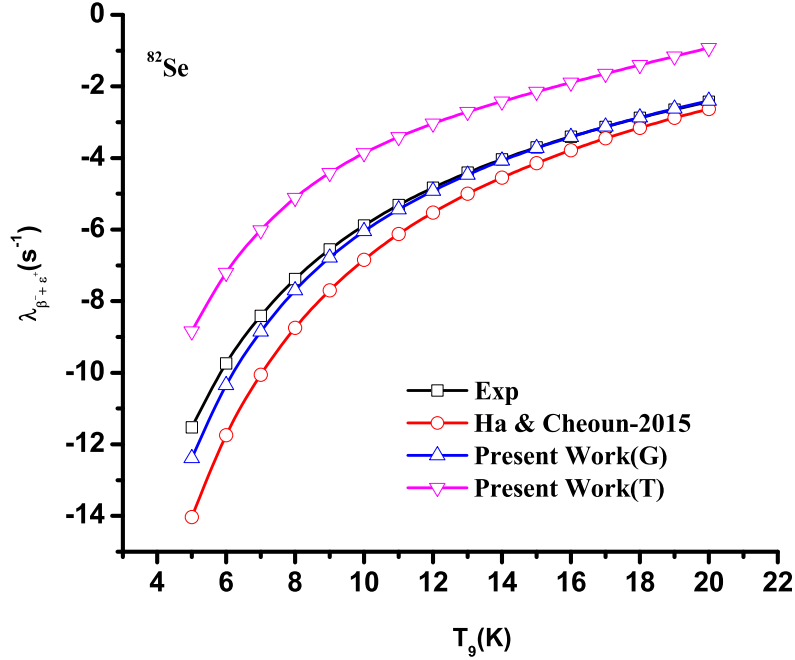


Figure 5.10: Same as Fig. 5.9 but for ^{82}Se .

matter as much). Table 5.13 shows a decent comparison of calculated and measured data for ^{76}Ge . Once again calculated rates (this work) with contributions from all parent excited states were bigger because of finite contribution of excited state GT strength distributions (missing in the experimental data and other calculations). Fig. 5.12 depicts the density dependence of calculated rates for the case of ^{82}Se . Here it can be seen that the calculated rates for ^{82}Se show a similar behavior as for the case of ^{76}Ge . The Ha & Cheoun calculated rates were smaller compared to the experimental rates. Ha & Cheoun placed the centroid at roughly 1.5 MeV higher than the centroid placement of the measured data which resulted in decrement of their calculated rates.

Table 5.14 shows the relative contribution of present calculated stellar positron capture and β -decay rates to the total calculated rates for the two nuclei. For the case of ^{76}Ge the calculated β -decay rates were 2 – 4 orders of magnitude bigger than the competing positron

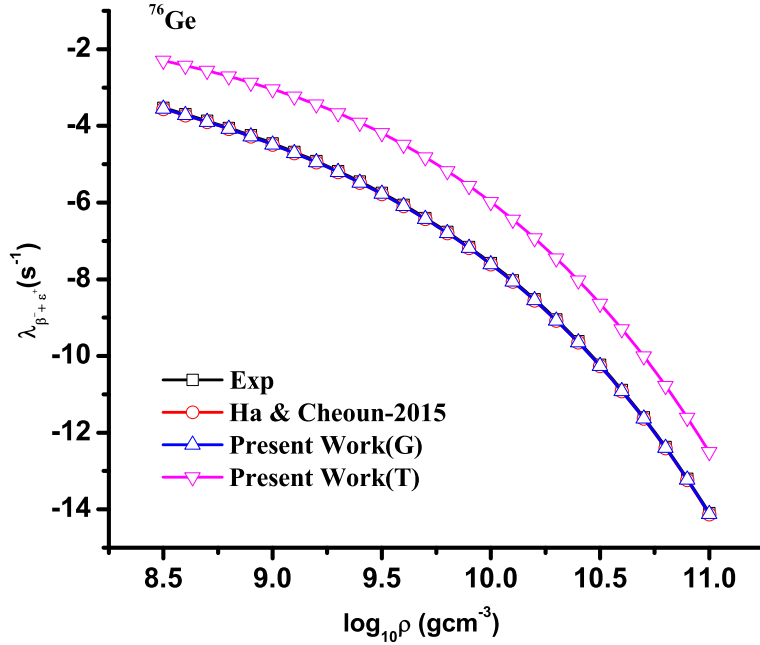
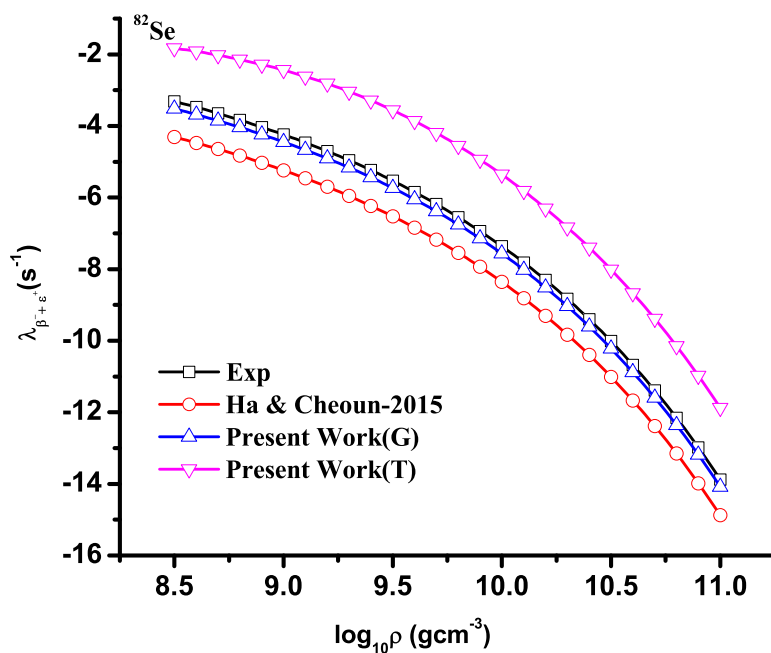


Figure 5.11: Same as Fig. 5.9 but as a function of stellar density at a fixed temperature of $T_9(K) = 10$.

capture rates at low stellar temperatures ($T_9(K) \leq 10$). The positron capture rates compete well with the β -decay rates at $T_9(K) = 10$. The positron capture rates were bigger by one (two) order(s) of magnitude at $T_9(K) = 20$ ($T_9(K) = 30$). For the case of ^{82}Se once again the β -decay rates command the total rates at low stellar temperatures. The positron capture rates were 1–2 orders of magnitude bigger at higher T_9 values. At high temperatures ($kT > 1$ MeV), positrons appear via electron-positron pair creation and their capture rates exceed the competing β -decay rates.

Figure 5.12: Same as Fig. 5.11 but for ^{82}Se .Table 5.14: Ratio of calculated positron capture to β -decay rates as a function of stellar temperature and density.

Nucleus	ρ Y_e	$R(pc/bd)$				
		$T_9=01$	$T_9=05$	$T_9=10$	$T_9=20$	$T_9=30$
^{76}Ge	8.50	1.28E-03	2.40E-02	1.94E+00	3.90E+01	3.45E+02
	9.50	2.22E-04	4.78E-02	4.48E+00	1.08E+01	1.47E+02
	10.50	2.00E-04	4.19E-02	3.90E-01	8.13E+00	9.25E+01
^{82}Se	8.50	7.52E-06	5.95E-03	1.20E-01	9.04E+00	1.79E+02
	9.50	2.40E-07	1.47E-03	3.55E-02	2.77E+00	7.79E+01
	10.50	1.82E-07	1.29E-03	3.18E-02	2.19E+00	5.01E+01

5.7 Summary

Present work calculations showed that at low stellar temperatures ($T_9(K) \leq 5$), the positron capture rates on ^{76}Ge and ^{82}Se can easily be neglected in comparison to the competing β -decay rates. At high stellar temperatures ($T_9(K) > 10$), the positron capture rates command the total weak rates. The microscopically calculated P_n values, presented in this work, may influence the final abundance of heavy elements synthesized in the r-process. It was well known that a smaller lepton fraction disfavors the outward propagation of the post-bounce shock waves, as more overlying iron core has to be photo-dissociated. The β -decay rates for medium-heavy nuclei presented in this work, can assist in a more vigorous URCA process and may lead to cooler presupernova cores consisting of lesser neutron-rich matter than in presently assumed simulations.

Chapter 6

Summary, Conclusions and Future Work

6.1 Conclusions and Summary

- The aim of this thesis was to suggest improvements in the theoretical and experimental regimes about the β -decay half-life calculations. The experimental approach employed in current investigation produces decent half-life result in comparison with the literature data. Certain progresses about half-life calculations has been explored with the help of pn-QRPA theory i.e, reliable calculation of half-life, pairing correlations effect, development of new code for the calculation of PSFs and then implementing new values of PSFs to check the effect on the value of calculated half-life in comparison with available literature data as well as previous results.

- The spectra for half-life of ^{44}Sc obtained by photon activation analysis (PAA) has been analyzed by MAESTRO and ROOT packages. The photonuclear reaction was produced using a cLINACs which generate bremsstrahlung photon beam to activate the desired sample. One novelty of the present work was the comparison of measured results by PAA with the calculated β -decay half-life using the pn-QRPA model. A decent comparison was ob-

served between measured, another uniqueness was the successful implementation of medical cLINACs for research purpose in the field of nuclear physics.

- β^+ -decay terrestrial half-lives using the pn-QRPA model for neutron deficient fp-shell nuclei has been investigated. The implications of pairing correlations on the calculation of terrestrial β decay half-lives for a set of even-even medium mass neutron deficient nuclei in the range of $Z= 24-34$ has been investigated with the help of pn-QRPA theory. Two different empirical formulas for the calculation of pairing gaps were used and the effect of two pairing gaps on the β -decay half-life were studied. It was concluded that a reasonable choice of interaction constant parameters in the particle particle and particle hole improved the beta decay half-life. It was further demonstrated that Emp-1 formula for calculation of pairing gaps resulted in better prediction of calculated half-life values than by using Emp-2 scheme.

- A new code for computing phase space factor (PSF) values for calculation of beta decay half-lives was developed in collaboration with Romanian collaborators. In this approach electron/positron free and bound wave function were constructed by solving a Dirac equation with a Coulomb-type potential obtained from a realistic distribution of protons in the daughter nuclei. The impact of newly calculated PSF on computed beta decay half life was later studied. β^\pm and EC half-lives were calculated using the new recipe and compared with measured data and previous calculations. It was concluded that the new PSF led to a better agreement of calculated beta decay half-lives with measured data. The mean percentage deviation of calculated with experimental half-life at most was found larger for the β^- -decay (2.73%) as compared to the β^+ /EC decay rates (2.35%).

- The calculation of ground and excited state GT strength distributions for medium-heavy nuclei, ^{76}Ge and ^{82}Se , using the pn-QRPA model with deformed Nilsson basis states was performed. These nuclei were selected to study the low-lying part of the GT distribution and also for calculation of β -decay and positron capture weak interaction rates in stellar matter. It was concluded that at low stellar temperatures ($T_9(\text{K}) = 5$), the positron capture

rates for ^{76}Ge and ^{82}Se can easily be neglected in comparison to the competing β -decay rates. At high stellar temperatures ($T_9(\text{K}) > 10$), the positron capture rates command the total weak rates. The microscopically calculated β -delayed neutron emission (P_n) values, may influence the final abundance of heavy elements synthesized in the r-process. It is well known that a smaller lepton fraction disfavors the outward propagation of the post-bounce shock waves, as more overlying iron core has to be photo-dissociated.

6.2 Future Work

In future I plan to study and analyze the following:

The study of effect by various theoretical approaches and experimental methods on the measured value of nuclear β -decay half-lives such as co-incidence technique along fully digitizing setup for the results analysis will be performed. The investigation circle about the implications of pairing correlations impact on half-life will be extended to the medium and heavy masses nuclei. I am interested to check the contribution for β^- -decay half-lives by employing Emp-1 formula for the pairing correlations. The effect and significant improvement by employing newly introduced recipe for phase space factors has been elaborated and further we hope to investigate the stellar weak rates using the present half-life results.

Bibliography

- [1] B. Povh, K. Rith, and F. Zetsche, "Particles and Nuclei," vol. 4, Springer, 1995.
- [2] A. Bohr and B. R. Mottelson, "Nuclear Structure Vol. IWA Benjamin," Inc, New York, 1969.
- [3] K. Grotz and H. Klapdor, "The Weak Interaction in Nuclear," Part. Astrophys, (Adam Hilger: Bristol, Philadelphia), 1990.
- [4] C. Fransson and C. Kozma, "Radioactivities and nucleosynthesis in SN 1987A," New. Astro. Rev, vol. 46, pp. 487-492, 2002.
- [5] K. Heyde, "Basic ideas and concepts in nuclear physics: an introductory approach," CRC Press, 2004.
- [6] E. Fermi, "An attempt of a theory of beta radiation. 1," Z. Phys, vol. 88, pp. 161-177, 1934.
- [7] J. Suhonen, "From nucleons to nucleus: concepts of microscopic nuclear theory," Springer Science and Business Media, 2007.
- [8] K. S. Krane, "Radioactive Decay, Introductory Nuclear Physics," New York: John Wiley and Sons, pp. 161, 1988.
- [9] J. A. Halbleib and R. A. Sorensen, "Gamow-Teller beta decay in heavy spherical nuclei and the unlike particle-hole rpa," Nucl. Phys. A, vol. 98, pp. 542, 1967.

-
- [10] J. C. Hardy, I. S. Towner, V. T. Koslowsky, E. Hagberg, and H. Schmeing, "Superaligned $0^+ \rightarrow 0^+$ nuclear β -decays: A critical survey with tests of CVC and the standard model," Nucl. Phys. A, vol. 509, pp. 429, 1990.
- [11] J. M. Blatt and V. F. Weisskopf, "Theoretical nuclear physics," Springer New York, pp. 330, 1979.
- [12] H. F. Schopper, "Weak interactions and nuclear beta decay," North-Holland, pp. 427, 1966.
- [13] H. Behrens and W. Buhring, "Electron radial wave functions and nuclear beta-decay," vol. 67, Oxford University Press, United State of America, 1982.
- [14] G. Gamow and E. Teller, "Selection Rules for the β -Disintegration," Phys. Rev, vol. 49, pp. 895, 1936.
- [15] H. Primakoff and S. P. Rosen, "Double beta decay," Rep. Prog. Phys, vol. 22, pp. 121, 1959.
- [16] J. Byrne, "An overview of neutron decay," Heidelberg Germany, pp. 21, 2002.
- [17] R. Daudel, M. Jean, and M. Lecoïn, "Sur la possibilite d existence dun type particulier de radioactivite phenomene de creation e," Journal de Physique et le Radium, vol. 8, pp. 238-243, 1947.
- [18] M. Jung, F. Bosch, K. Beckert, H. Eickhoff, H. Folger and B. Franzke, "First observation of bound-state β decay," Phys. Rev. Lett, vol. 69, pp. 2164, 1992.
- [19] F. Bosch, T. Faestermann, J. Friese, F. Heine, P. Kienle and E. Wefers, "Observation of bound-state β decay of fully ionized ^{187}Re : ^{187}Re ^{187}Os cosmochronometry," Phys. Rev. Lett, vol. 77, pp. 5190, 1996.
- [20] S. Bilenky, "Neutrinoless double beta-decay," Phys. Part. Nucl, vol. 41, pp. 690-715, 2010.

-
- [21] A. Vertes, "Szemelvények a nukleáris tudomány történetéből: gondolkodok, gondolatok, eredmények," Akadémiai Kiadó, 2009.
- [22] J. Chadwick and M. Goldhaber, "A nuclear photo-effect: disintegration of the deuteron by γ -rays," *Nature*, vol. 134, pp. 237, 1934.
- [23] A. Gaudin and J. H. Pannell, "Determination of beryllium by photodisintegration," *Anal. Chem.*, vol. 23, pp. 1261-1265, 1951.
- [24] R. Basile, J. Hure, P. Leveque, and C. Schuhl, "The Possibility of Determining Oxygen by the (γ, n) Reaction using a Betatron," *Comp. Rend. Acad. Sci.*, vol. 239, pp. 422-424, 1954.
- [25] R. Hofstadter and J. A. McIntyre, "Measurement of gamma-ray energies with two crystals in coincidence," *Phys. Rev.*, vol. 78, pp. 619, 1950.
- [26] C. Segebade, H.-P. Weise, and G. J. Lutz, "Photon activation analysis," Walter de Gruyter, 2011.
- [27] A. Tavendale, "Large germanium lithium-drift pin diodes for gamma-ray spectroscopy," *IEEE. Transac. Nucl. Sci.*, vol. 12, pp. 255-264, 1965.
- [28] G. Westphal, K. Jostl, P. Schroder, and W. Winkelbauer, "Adaptive digital filter for high-rate high-resolution gamma spectrometry," *IEEE. Transac. Nucl. Sci.*, vol. 48, pp. 461-465, 2001.
- [29] N. Reguigui, "Gamma ray spectrometry practical information," pp. 60-69, 2006.
- [30] G. F. Knoll, "Radiation Detection and Measurement, John Wiley and Sons," Inc, New York, vol. 2000, 2000.
- [31] C. F. Delaney and E. Finch, "Radiation detectors: physical principles and applications," Oxford Science Publications, 1992.

-
- [32] V. De Smet, "Study of a GEM tracker of charged particles for the Hall A high luminosity spectrometers at Jefferson Lab," Master Thesis, 2011.
- [33] S. Sahoo, A. Rath, R. Mukharjee, and B. Mallick, "Commissioning of a Modern LINAC for Clinical Treatment and Material Research," *Int. J. Tren. Interdiscip. Stud*, vol. 1, 2012.
- [34] Elekta Digital Accelerator, Technical Training Guide (unpublished), 2003.
- [35] P. Mohr, S. Brieger, G. Witucki, and M. Maetz, "Photoactivation at a clinical LINAC: The Au (γ , n) $^{196-197}\text{Au}$ reaction slightly above threshold," *Nucl. Inst. Meth. Phys. Res. Sec. A: Accel, Spect, Detec. Assoc. Equip*, vol. 580, pp. 1201-1208, 2007.
- [36] M. U. Khandaker, "High purity germanium detector in gamma-ray spectrometry," *Int. J. Fund. Phys. Sci*, vol. 1, pp. 42-46, 2011.
- [37] E. Haller, "Detector materials: germanium and silicon," *IEEE. Transac. Nucl. Sci*, vol. 29, pp. 1109-1118, 1982.
- [38] D. Cha, " $\sigma\tau^+$ strength in nuclei," *Phys. Rev. C*, vol. 27, pp. 2269, 1983.
- [39] V. Soloviev, "Fragmentation of single-particle and collective motions in the quasiparticle-phonon nuclear model," *Prog. Part. Nucl. Phys*, vol. 19, pp. 107-165, 1987.
- [40] V. Kuz-Min and V. Soloviev, "Gamow-Teller β^+ decays and strength functions of (n, p) transitions in spherical nuclei," *Nucl. Phys. A*, vol. 486, pp. 118-132, 1988.
- [41] A. Staudt, E. Bender, K. Muto, and H. V. Klapdor, "Second-generation microscopic predictions of beta-decay half-lives of neutron-rich nuclei," *At. Data Nucl. Data Tables*, vol. 44, pp. 79, 1990.
- [42] E. Bender, K. Muto and H. V. Klapdor, "Calculation of β^- -decay half-lives with the proton-neutron quasiparticle RPA," *Phys. Lett*, vol. 208, pp. 53, 1988.

-
- [43] H. V. Klapdor, "Nuclear beta strength, neutrino mass and cosmology," Prog. Part. Nucl. Phys, vol. 17, pp. 419, 1986.
- [44] J.-U. Nabi and H. V. Klapdor, "Microscopic calculations of weak interaction rates of nuclei in stellar environment for $A= 18$ to 100 ," Eur. Phys. J. A, vol. 5, pp. 337-339, 1999.
- [45] J. -U. Nabi, "Microscopic Calculations of Weak Interaction Rates in Stellar Environment" Ph.D. Thesis, University of Heidelberg, Germany 1999.
- [46] J. Krumlinde and P. Moller, "Calculation of Gamow-Teller β -strength functions in the rubidium region in the RPA approximation with Nilsson-model wave functions," Nucl. Phys., vol. 417, pp. 419, 1984.
- [47] P. Moller and J. Randrup, "New developments in the calculation of β -strength functions," Nucl. Phys. A, vol. 514, pp. 1, 1990.
- [48] J. Suhonen, T. Taigel, and A. Faessler, "pn-QRPA calculation of the β^+ /EC quenching for several neutron-deficient nuclei in mass regions $A= 94$ 110 and $A= 146$ 156 ," Nucl. Phys. A, vol. 486, pp. 91, 1988.
- [49] K. Muto, E. Bender, T. Oda, and H. V. Klapdor, "Proton-neutron quasiparticle RPA with separable Gamow-Teller forces," Z. Phys, vol. 341, pp. 407, 1992.
- [50] K. Muto, E. Bender, and H. Klapdor, "Nuclear structure effects on the neutrinoless double beta decay," Z. Phys, vol. 334, pp. 187-194, 1989.
- [51] J. C. Hardy and I. Towner, "Superallowed $0^+ \rightarrow 0^+$ nuclear β decays: A new survey with precision tests of the conserved vector current hypothesis and the standard model," Phys. Rev, vol. 79, pp. 055502, 2009.
- [52] K. Nakamura, "Review of particle physics," J. Phys. G, vol. 37, pp. 075021, 2010.

-
- [53] E. Rutherford and B. Boltwood, "ART. I. The Relative Proportion of Radium and Uranium in Radio-Active Minerals," *Amer. J. Sci.*, (1880-1910), vol. 22, pp. 1, 1906.
- [54] M. Hirsch, A. Staudt, K. Muto, and H. V. Klapdor, "Microscopic predictions of β^+ /EC-decay half-lives," *At. Data Nucl. Data Tables*, vol. 53, pp. 165, 1993.
- [55] V. Kumar, P. Srivastava, and H. Li, "Nuclear β^- -decay half-lives for and shell nuclei," *J. Phys. G*, vol. 43, pp. 105104, 2016.
- [56] I. Panov, Y. S. Lutostansky, and F.-K. Thielemann, "Beta-decay half-lives for the r-process nuclei," *Nucl. Phys. A*, vol. 947, pp. 1-11, 2016.
- [57] I. Boztosun, H. Dapo, M. Karakoc, S. Ozmen, Y. Cecen, A. Coban, "Photonuclear reactions induced by a clinical linac," *J. Phys: Conference Series*, pp. 012024, 2015.
- [58] M. Aygun, A. Cesur, M. Dogru, I. Boztosun, H. Dapo, M. Kanarya, "Using a clinical linac to determine the energy levels of ^{92m}Nb via the photonuclear reaction," *Appl. Rad. Iso*, vol. 115, pp. 97-99, 2016.
- [59] C. Eke, I. Boztosun, H. Dapo, C. Segebade, and E. Bayram, "Determination of gamma-ray energies and half lives of platinum radio-isotopes by photon activation using a medical electron linear accelerator: a feasibility study," *J. Rad. Anal. Nucl. Chem*, vol. 309, pp. 79-83, 2016.
- [60] J. Rapaport, T. A. Belote, D. E. Bainum, and W. E. Dorenbusch, "Levels of ^{44}Sc by the (^3He , a) reaction on ^{45}Sc ," *Nucl. Phys. A*, vol. 168, pp. 177, 1971.
- [61] C. Grignon, J. Barbet, M. Bardies, T. Carlier, J. Chatal and O. Couturier, "Nuclear medical imaging using $\beta+\gamma$ coincidences from ^{44}Sc radio-nuclide with liquid xenon as detection medium," *Nucl. Inst. Meth. Phys. Res. Section A: Accel. Spect, Detec and Assoc. Equipment*, vol. 571, pp. 142-145, 2007.

-
- [62] R. Chakravarty, S. Goel, H. F. Valdovinos, R. Hernandez, H. Hong and R. J. Nickles, "Matching the decay half-life with the biological half-life: Immuno PET imaging with ^{44}Sc -labeled cetuximab Fab fragment," *Bioconj. Chem*, vol. 25, pp. 2197-2204, 2014.
- [63] E. Garcia-Torano, V. Peyres, M. Roteta, A. Sanchez-Cabezudo, E. Romero, and O. A. Martinez, "Corrigendum to standardization and precise determination of the half-life of ^{44}Sc ," *Appl. Radiat. Iso*, vol. 109, pp. 314-318, 2016.
- [64] K. Kolsky, V. Joshi, L. Mausner, and S. Srivastava, "Radiochemical purification of no-carrier-added scandium-47 for radio-immuno-therapy," *Appl. Radiat. Iso*, vol. 49, pp. 1541-1549, 1998.
- [65] E. Koumarianou, N. Loktionova, M. Fellner, F. Roesch, O. Thews and D. Pawlak, " ^{44}Sc -DOTA-BN [2-14] NH₂ in comparison to ^{68}Ga -DOTA-BN [2-14] NH₂ in pre-clinical investigation. Is ^{44}Sc a potential radionuclide for PET," *Appl. Radiat. Iso*, vol. 70, pp. 2669-2676, 2012.
- [66] S. G. Nilsson, "Binding states of individual nucleons in strongly deformed nuclei," *Mat. Fys. Medd. K. Dan. Vidensk. Selsk*, vol. 29, pp. 16, 1955.
- [67] M. Majid, J.-U. Nabi, G. Daraz, "Allowed and unique first-forbidden stellar electron emission rates of neutron-rich copper isotopes," *Astrophys. Spa. Sci*, vol. 362(108), pp. 1, 2017.
- [68] H. Homma, E. Bender, M. Hirsch, K. Muto, H. V. Klapdor, and T. Oda, "Systematic study of nuclear β -decay," *Phys. Rev. C*, vol. 54, pp. 2972, 1996.
- [69] J.-U. Nabi, N. Cakmak, S. Stoica, and Z. Iftikhar, "First-forbidden transitions and stellar β -decay rates of Zn and Ge isotopes," *Phys. Scri*, vol. 90, pp. 115301, 2015.
- [70] J.-U. Nabi, N. Cakmak, and Z. Iftikhar, "First-forbidden β -decay rates, energy rates of β -delayed neutrons and probability of β -delayed neutron emissions for neutron-rich nickel isotopes," *Eur. Phys. J. A*, vol. 52, pp. 5, 2016.

-
- [71] J.-U. Nabi, N. Cakmak, M. Majid, and C. Selam, "Unique first-forbidden β -decay transitions in odd-odd and even-even heavy nuclei," Nucl. Phys. A, vol. 957, pp. 1-21, 2017.
- [72] P. Moller and J. R. Nix, "Atomic masses and nuclear ground-state deformations calculated with a new macroscopic-microscopic model," At. Data Nucl. Data Tables, vol. 26, pp. 165, 1981.
- [73] G. Audi, F. Kondev, M. Wang, W. Huang, and S. Naimi, "The NUBASE2016 evaluation of nuclear properties," Chin. Phys. C, vol. 41, pp. 030001, 2017.
- [74] <https://www.nndc.bnl.gov/nudat2>
- [75] D. Radford, "ESCL8R and LEVIT8R: Software for interactive graphical analysis of HPGe coincidence data sets," Nucl. Inst. Meth. Phys. Res. Sec. A: Accel. Spect. Det. Assoc. Equipment, vol. 361, pp. 297-305, 1995.
- [76] R. Brun and F. Rademakers, "ROOT-an object oriented data analysis framework," Nucl. Inst. Meth. Phys. Res. Sec. A: Accel. Spect. Det. Assoc. Equipment, vol. 389, pp. 81-86, 1997.
- [77] A. Gun, K. Gupta, B. Dasgupta, "Fundamentals Of Statistics (World Press)", ISBN, 9788187567813, 2008.
- [78] J. Chen, B. Singh, and J. A. Cameron, "Nuclear data sheets for A= 44," Nucl. Data. Sheets, vol. 112, pp. 2357, 2011.
- [79] W. Tan, D. Ni, and Z. Ren, "Calculations of the β -decay half-lives of neutron-deficient nuclei," Chin. Phys. C, vol. 41, pp. 054103, 2017.
- [80] P. Sarriguren, R. Alvarez-Rodriguez, and E. Moya de Guerra, "Half-lives of rp-process waiting point nuclei," Eur. Phys. J. A, vol. 24, pp. 193, 2005.

-
- [81] K. Takahashi, M. Yamada, and T. Kondoh, "Beta-decay half-lives calculated on the gross theory," *At. Data Nucl. Data Tables*, vol. 12, pp. 101-142, 1973.
- [82] Z. Y. Wang, Y. F. Niu, Z. M. Niu, and J. Y. Guo, "Nuclear β -decay half-lives in the relativistic point-coupling model," *J. Phys. G*, vol. 43, pp. 045108, 2016.
- [83] D. Ni and Z. Ren, " β -decay rates of r-process waiting-point nuclei in the extended quasiparticle random-phase approximation," *J. Phys. G*, vol. 41, pp. 025107, 2014.
- [84] T. Niksic, T. Marketin, D. Vretenar, N. Paar, and P. Ring, " β -decay rates of r-process nuclei in the relativistic quasiparticle random phase approximation," *Phys. Rev. C*, vol. 71, pp. 014308, 2005.
- [85] T. Marketin, D. Vretenar, and P. Ring, "Calculation of β -decay rates in a relativistic model with momentum-dependent self-energies," *Phys. Rev. C*, vol. 75, pp. 024304, 2007.
- [86] H. Liang, N. Van Giai, and J. Meng, "Spin-isospin resonances: A self-consistent covariant description," *Phys. Rev. Lett*, vol. 101, pp. 122502, 2008.
- [87] Z. M. Niu, Y. F. Niu, H. Z. Liang, W. H. Long, T. Niksic, D. Vretenar, and J. Meng, " β -decay half-lives of neutron-rich nuclei and matter flow in the r-process," *Phys. Lett. B*, vol. 723, pp. 172, 2013.
- [88] G. Martinez-Pinedo and K. Langanke, "Shell-model half-lives for $N=82$ nuclei and their implications for the r process," *Phys. Rev. Lett*, vol. 83, pp. 4502, 1999.
- [89] P. Moller, J. R. Nix, and K.-L. Kratz, "Nuclear properties for astrophysical and radioactive-ion-beam applications," *At. Data Nucl. Data Tables*, vol. 66, pp. 131, 1997.
- [90] G. Pantis, F. Simkovic, J. D. Vergados, and A. Faessler, "Neutrinoless double beta decay within the quasiparticle random-phase approximation with proton-neutron pairing," *Phys. Rev. C*, vol. 53, pp. 695, 1996.

-
- [91] P. Moller, A. J. Sierk, T. Ichikawa, and H. Sagawa, "Nuclear ground-state masses and deformations: FRDM," *At. Data Nucl. Data Tables*, vol. 109, pp. 1-204, 2016.
- [92] M. Hirsch, A. Staudt, K. Muto, and H. V. Klapdor-Kleingrothaus, "Microscopic calculation of β^+ /EC decay half-lives with atomic numbers $Z = 10-30$," *Nucl. Phys. A*, vol. 535, p. 62, 1991.
- [93] A. H. Wapstra, G. Audi and R. Hoekstra, "Atomic masses from (mainly) experimental data," *At. Data Nucl. Data Tables*, vol. 39, pp. 281, 1988.
- [94] E. I. Hilf, H. von Groote, and K. Takahashi, "Proceedings of the Third International Conference on Nuclei Far from Stability," CERN Report No. 76-13, 1976.
- [95] H. V. Groote, E. R. Hilf, and K. Takahashi, "A new semiempirical shell correction to the droplet model: Gross theory of nuclear magics," *At. Data Nucl. Data Tables*, vol. 17, pp. 418, 1976.
- [96] M. J. Martin and P. H. Blichert-Toft, "Radioactive atoms: Auger-electron, α^- , β , γ^- , and X-ray data," *Nucl. Data*, vol. 8, pp. 1, 1970.
- [97] N. B. Gove and M. J. Martin, "Log-f tables for beta decay," *At. Data Nucl. Data Tables*, vol. 10, pp. 205, 1971.
- [98] M. Rose, "A note on the possible effect of screening in the theory of beta-disintegration," *Phys. Rev.*, vol. 49, pp. 727, 1936.
- [99] R. Good, "Effect of atomic electron screening on the shape of forbidden beta spectra," *Phys. Rev.*, vol. 94, pp. 931, 1954.
- [100] M. E. Rose and D. K. Holmes, "The effect of finite nuclear size in beta-decay," *Phys. Rev.*, vol. 83, pp. 190, 1951.
- [101] M. E. Rose, D. K. Holmes, "The Effect of the Finite Size of the Nucleus in Beta-Decay," ORNL-I022 1957.

-
- [102] L. R. B. Elton, "Nuclear sizes," vol. 561: Oxford University Press London, 1961.
- [103] W. Burhing, "Computational improvements in phase shift calculations of elastic electron scattering," *Z. Phys*, vol. 187, pp. 180-196, 1965.
- [104] F. Salvat and R. Mayol, "Accurate numerical solution of the Schrodinger and Dirac wave equations for central fields," *Comput. Phys. Commun*, vol. 62, pp. 65, 1991.
- [105] F. Salvat, J. Fernandez-Varea, and W. Williamson Jr, "Accurate numerical solution of the radial Schrodinger and Dirac wave equations," *Comput. Phys. Commun*, vol. 90, pp. 151-168, 1995.
- [106] S. Esposito, "Majorana solution of the Thomas-Fermi equation," *Amer. J. Phys*, vol. 70, pp. 852-856, 2002.
- [107] G. Audi, M. Wang, A. H. Wapstra, F. G. Kondev, M. MacCormick, X. Xu, and B. Pfeiffer, "The Ame2012 atomic mass evaluation (I)," *Chin. Phys. C*, vol. 36, pp. 1287, 2012.
- [108] D. H. Wilkinson and BEF Macefield, "A parametrization of the phase space factor for allowed β -decay," *Nucl. Phys. A*, vol. 232, pp. 58, 1974.
- [109] M. Wang, G. Audi, A. H. Wapstra, F. G. Kondev, M. MacCormick, X. Xu, and B. Pfeiffer, "The Ame2012 atomic mass evaluation," *Chin. Phys. C*, vol. 36, pp. 1603, 2012.
- [110] I. S. Towner and J. C. Hardy, "Superallowed $0+ \rightarrow 0+$ nuclear β -decays," *Nucl. Phys. A*, vol. 205, pp. 33, 1973.
- [111] S. Stoica and M. Mirea, "New calculations for phase space factors involved in double- β decay," *Phys. Rev. C*, vol. 88, pp. 037303, 2013.
- [112] M. Mirea, T. Pahomi, and S. Stoica, "Values of the phase space factors involved in double beta decay," *Rom. Rep. Phys*, vol. 67, pp. 872, 2015.

-
- [113] G. Audi and A. H. Wapstra, "The 1995 update to the atomic mass evaluation," Nucl. Phys. A, vol. 595, pp. 409, 1995.
- [114] J. N. Bahcall, "Exchange and overlap effects in electron capture and in related phenomena," Phys. Rev, vol. 132, pp. 362, 1963.
- [115] S. Stoica, M. Mirea, O. Niuescu, J.-U. Nabi and M. Ishfaq, "New phase space calculations for β decay half lives," Adv. H. Ener. Phys, vol. 2016, 8729893, 2016.
- [116] Q. Zhi, E. Caurier, J. J. Cuenca-Garcia, K. Langanke, G. Martinez-Pinedo, and K. Sieja, "Shell-model half-lives including first-forbidden contributions for r-process waiting-point nucle," Phys. Rev. C, vol. 87, pp. 025803, 2013.
- [117] S. Raman, C. W. Nestor, Jr., and P. Tikkanen, "Transition probability from the ground to the first excited 2+ state of even even nuclides," At. Data Nucl. Data Tables, vol. 78, pp. 1, 2001.
- [118] H. A. Bethe, G. E. Brown, J. Applegate, and J. M. Lattimer, "Equation of state in the gravitational collapse of stars," Nucl. Phys. A, vol. 324, pp. 487, 1979.
- [119] G. M. Fuller, W. A. Fowler, and M. J. Newman, "Stellar weak interaction rates for intermediate-mass nuclei. II-A= 21 to A= 60," Astrophys. J, vol. 252, pp. 715, 1982.
- [120] G. M. Fuller, W. A. Fowler, and M. J. Newman, "Stellar weak interaction rates for intermediate-mass nuclei. IV-Interpolation procedures for rapidly varying lepton capture rates using effective log (ft)-values," Astrophys. J, vol. 293, pp. 1, 1985.
- [121] T. Oda, M. Hino, K. Muto, M. Takahara, and K. Sato, "Rate tables for the weak processes of sd-shell nuclei in stellar matter," At. Data Nucl. Data Tables, vol. 56, pp. 231, 1994.
- [122] J.-U. Nabi and M.-U. Rahman, "Gamow-Teller transitions from ^{24}Mg and their impact on the electron capture rates in the O+ Ne+ Mg cores of stars," Phys. Rev. C, vol. 75, pp. 035803, 2007.

-
- [123] E. Ha and M. -K. Cheoun, "Gamow Teller strength distributions in ^{76}Ge , $^{76,82}\text{Se}$, and $^{90,92}\text{Zr}$ by the deformed proton neutron QRPA," Nucl. Phys. A, vol. 934, pp. 73, 2015.
- [124] P. Sarriguren, E. Moya de Guerra, L. Pacearescu, A. Faessler, F. Simkovic, and A. A. Raduta, "Gamow-Teller strength distributions in ^{76}Ge and ^{76}Se from deformed quasi-particle random-phase approximation," Phys. Rev. C, vol. 67, pp. 044313, 2003.
- [125] S. Raman, C. H. Malarkey, W. T. Milner, C. W. Nestor, Jr., and P. H. Stelson, "Transition probability, $B(E2)$, from the ground to the first-excited $2+$ state of even-even nuclides," At. Data Nucl. Data Tables, vol. 36, pp. 1, 1987.
- [126] S. Cakmak, J.-U. Nabi, T. Babacan, and I. Maras, "Spin-isospin transitions in chromium isotopes within the quasiparticle random phase approximation," Adv. Spa. Res, vol. 55, pp. 440-453, 2015.
- [127] P. Axel, "Electric dipole ground-state transition width strength function and 7-MeV photon interactions," Phys. Rev, vol. 126, pp. 671, 1962.
- [128] K. Langanke and G. Martinez-Pinedo, "Shell-model calculations of stellar weak interaction rates: II. Weak rates for nuclei in the mass range $A= 45- 65$ in supernovae environments," Nucl. Phys. A, vol. 673, pp. 481, 2000.
- [129] J.-U. Nabi and M.-U. Rahman, "Gamow-Teller strength distributions and electron capture rates for ^{55}Co and ^{56}Ni ," Phys. Lett. B, vol. 612, pp. 190-196, 2005.
- [130] J.-U. Nabi and M. Sajjad, "Comparative study of Gamow-Teller strength distributions in the odd-odd nucleus ^{50}V and its impact on electron capture rates in astrophysical environments," Phys. Rev. C, vol. 76, pp. 055803, 2007.
- [131] J.-U. Nabi, "Stellar neutrino energy loss rates due to ^{24}Mg suitable for O+ Ne+ Mg core simulations," Phys. Rev. C, vol. 78, pp. 045801, 2008.
- [132] J.-U. Nabi, "Weak-interaction-mediated rates on iron isotopes for presupernova evolution of massive stars," Euro. Phys. J. A, vol. 40, pp. 223-230, 2009.

-
- [133] J.-U. Nabi, "Stellar $\beta\pm$ decay rates of iron isotopes and its implications in astrophysics," *Adv. Spa. Res.*, vol. 46, pp. 1191-1207, 2010.
- [134] J.-U. Nabi, "Ground and excited states Gamow-Teller strength distributions of iron isotopes and associated capture rates for core-collapse simulations," *Astrophys. Spa. Sci.*, vol. 331, pp. 537-554, 2011.
- [135] J.-U. Nabi, "Nickel isotopes in stellar matter," *Euro. Phys. J. A*, vol. 48, pp. 84, 2012.
- [136] G. W. Misch, G. M. Fuller, and B. A. Brown, "Modification of the Brink-Axel hypothesis for high-temperature nuclear weak interactions," *Phys. Rev. C*, vol. 90, pp. 065808, 2014.
- [137] N. Frazier, B. A. Brown, D. Millener, and V. Zelevinsky, "Gamow-Teller strength as a function of excitation energy," *Phys. Lett. B*, vol. 414, pp. 7-12, 1997.
- [138] P. Vogel and M. R. Zirnbauer, "Suppression of the two-neutrino double-beta decay by nuclear-structure effects," *Phys. Rev. Lett.*, vol. 57, pp. 3148, 1986.
- [139] J. Engel, P. Vogel, and M. R. Zirnbauer, "Nuclear structure effects in double-beta decay," *Phys. Rev. C*, vol. 37, pp. 731, 1988.
- [140] R. Madey, B. S. Flanders, B. D. Anderson, A. R. Baldwin, J. W. Watson, S. M. Austin, C. C. Foster, H. V. Klapdor, and K. Grotz, "Low-lying structures in the Gamow-Teller strength functions for the double-beta-decaying nuclei ^{76}Ge , ^{82}Se , ^{128}Te , and ^{130}Te ," *Phys. Rev. C*, vol. 40, pp. 540, 1989.
- [141] M. Hirsch, A. Staudt, and H. V. Klapdor, "Prediction of average β and γ energies and probabilities of β -delayed neutron emission in the region of fission products," *At. Data Nucl. Data Tables*, vol. 51, pp. 244, 1992.